DESIGN AND SIMULATION OF HIGH-FREQUENCY TRANSMISSION LINES EXPERIMENTATION SYSTEM (HF-TEST) ON A 6-LAYER PCB USING FR4 SUBSTRATE, FOR SUB-2 GHZ APPLICATIONS

October 2025

Project Report

Design And Simulation Of High-Frequency Transmission Lines Experimentation System (HF-Test) On A 6-Layer PCB Using FR4 Substrate, For Sub-2 GHz Applications

Department of Electrical/Electronic Engineering

University of Benin, Benin City, Edo State.

Supervisor: Dr. NOSA BELLO

November 13, 2025

RESEARCHERS

Ndubuisi-Okolie Ezinne Mirabel	ENG2002272
Ukhuakhua Osemudiamen Best	ENG2002329
Edionweme Awesome Osahumense	ENG2008341
Odiase Emwinghama Anthonet	ENG2002281

CERTIFICATION

This is to certify that this project work was carried out by **Ndubuisi-Okolie Ezinne Mirabel**, **Ukhuakhua Osemudiamen Best**, **Edionweme Awesome Osahumense**, and **Odiase Emwinghama Anthonet**, in partial fulfillment of the requirements for the award of the degree of Bachelor of Electrical/Electronic Engineering in the Department of Electrical/Electronic Engineering, Faculty of Engineering, University of Benin, Benin City, Edo State.

Dr. N. Bello	Date
(Project Supervisor)	
Engr. Dr. O.S Omorogiuwa	Date
(Head of Department)	

CERTIFICATION OF THESIS ON PLAGIARISM

We the undersigned declare that this project report by, **Ndubuisi-Okolie Ezinne Mirabel**, **Ukhuakhua Osemudiamen Best**, **Edionweme Awesome Osahumense**, and **Odiase Emwinghama Anthonet**, on Design And Simulation Of High-Frequency Transmission Lines Experimentation System (HF-Test) On A 6-Layer PCB Using FR4 Substrate, For Sub-2 GHz Applications has successfully passed the anti-plagiarism test and does not violate any copywrite regulations.

Dr. N. Bello	Date
(Project Supervisor)	
Engr. Dr. O.S Omorogiuwa	Date
(Head of Department)	

DEDICATION

This work is dedicated to God Almighty and to the Edionweme family, the Ndubuisi-Okolie family, the Ukhuakhua family, and the Odiase family for their continuous support throughout our stay at the University of Benin.

ACKNOWLEDGEMENT

Firstly, we thank the Almighty God for the strength, wisdom, and opportunity to undertake this project. We extend our heartfelt gratitude to our families: Edionweme, Ndubuisi-Okolie, Ukhuakhua, and Odiase, whose constant moral and financial encouragement helped see us through this journey. We also extend our gratitude to our friends and closest companions for their unwavering support throughout the challenges of our academic pursuits.

Our sincere appreciation goes to Engr. (Dr.) N. Bello, our Project supervisor, for his patience, valuable advice, and continuous guidance, which were crucial to the success of our project. His dedication to reviewing this work and emphasis on discipline, excellence, and standards have been instrumental throughout this project, and we're extremely grateful for it.

Abstract

The comprehensive study of high-frequency transmission lines, including stripline, microstripline, differential microstriplines and differential striplines configuration is critical for advanced RF and microwave engineering education. Fundamentals of some transmission line phenomenon such as impedance matching, reflection coefficient and the effect of open and short circuits, relies greatly on practical hands-on experience alongside theoretical tools like the Smith chart. Furthermore, many academic institutions face challenges in providing laboratory systems that accurately represent high-frequency transmission line structures on common PCB substrates such as FR4. The absence of versatile and cost-effective experimental circuits limits students' opportunities to explore and solve real-world transmission line problems, thereby hindering the development of essential engineering skills.

This project aims to develop an integrated high-frequency transmission line experimentation systems for university laboratories, incorporating stripline, microstripline, differential microstriplines and differential striplines configuration on FR4 substrates. The system will facilitate direct measurement and analysis of transmission line behavior, enabling students to visualize various experiments, and investigate the proposed applications (e.g. open and short circuit effects, s-parameters, transmission line as a filter etc.) within a controlled environment.

By linking theoretical concepts with practical experiments, specifically through the application of Smith chart and transmission line theory, this system will enhance RF engineering education, equipping students with the competence needed to address modern communication system challenges effectively.

Contents

List of Figures

List of Tables

Chapter One

Introduction

1.1 Background of the Study

The development of high-frequency transmission lines began in the late 19th century, driven by the need to improve telegraph and early radio systems. Oliver Heaviside's telegrapher's equations (1880s), built on Maxwell's electromagnetic theory (1861–1862), modeled signal propagation as waves, addressing losses in long cables (Pozar, 2012). The 20th century witnessed rapid progress in electromagnetic communication. Marconi's successful transatlantic radio transmission in 1901 demonstrated long-distance wireless communication and inspired further research into high-frequency systems. By the 1930s, the introduction of coaxial cables improved signal transmission for telephone and broadcasting networks. During World War II, radar research accelerated the development of microwave engineering, where operating frequencies above 1 GHz required low-loss transmission lines and precise impedance control (Collin, 2001). By the 1950s, printed circuit boards (PCBs) had become commercially viable, marking a shift from point-to-point wiring to planar circuit interconnections. Around the same period, researchers such as Robert Barrett pioneered the concept of microwave printed circuits, which later evolved into microstrip and stripline technologies for RF applications. The adoption of FR-4 substrates in the 1960s and 1970s further enabled cost-effective RF and high-frequency circuit fabrication (Bahl, 2003 and Coombs, 2008). The emergence of modern wireless technologies such as 5G and IoT has increased the need for engineers who understand high-frequency transmission concepts.

Even with significant progress in wireless communication technologies, there remains a considerable deficiency in education related to RF and microwave. Although various teaching resources are available for learning RF concepts, many are tailored

for extremely high frequencies and require advanced laboratory equipment. As a result, there are only a limited number of systems that concentrate on the more achievable sub-2 GHz range, where technologies like GSM, LTE, and Wi-Fi function, and where students can practically explore real transmission-line behavior using affordable resources.

This project addresses that gap by designing and simulating a modular FR-4-based printed circuit board (PCB) system intended for teaching fundamental transmission-line principles including microstrip, stripline, stubs, and resonators. The virtual platform allows students and researchers to analyze and visualize wave propagation, impedance matching, and S-parameter behavior within a controlled simulation environment.

By leveraging the cost-effectiveness and wide availability of FR-4 substrates in PCB design, the proposed system serves as a low-cost, simulation-driven educational model that bridges theoretical electromagnetics with practical RF design concepts. It aligns with the growing demand for accessible, practice-oriented engineering education across Africa, where advanced RF laboratory facilities remain limited due to financial and infrastructural constraints.

1.2 Problem Statement

At high frequencies, electrical interconnections behave as transmission lines, where parameters such as impedance, reflection, and attenuation significantly affect signal behavior. Understanding these principles is critical for engineers working in modern communication and electronic systems. However, in many developing countries and academic institutions, the practical study of high-frequency transmission lines remains limited due to the high cost of RF laboratory equipment and the complexity of experimental setups.

Existing instructional systems for RF and microwave education are often designed for very high frequencies (above 3 GHz) or require specialized instruments such as vector network analyzers, spectrum analyzers, and precision calibration kits. These systems are often beyond the financial reach of most institutions especially those in underdeveloped countries and thus unavailable for routine undergraduate

training. As a result, students are typically exposed to these topics only through theory, memorizing transmissionline equations without the opportunity to visualize or analyze real electromagnetic behavior.

1.3 Aim and Objectives of the Study

Aim: To design and simulate a six-layer FR4-based high-frequency transmission experimentation system that serves as a virtual educational platform for studying and demonstrating key transmission-line concepts below 2 GHz.

Specific Objectives:

1. To develop a standard six-layer PCB stack-up suitable for high-frequency signal routing and impedance control using FR-4 substrate material.
2. To design and simulate transmission line structures including microstrip, stripline, differential microstrip,differential stripline, series and shunt stubs, and resonance circuits.
3. To analyze the electromagnetic field distribution, reflection coefficient, and impedance behavior of the designed structures using 3D EM simulation tools.
4. To evaluate key RF parameters such as return loss and insertion loss (S-parameters), crosstalk and reflection analysis to understand performance under sub-2 GHz operation.
5. To provide a low cost, simulation-based teaching model that bridges theoretical understanding and practical insight into high-frequency circuit behavior for educational institutions in developing regions.

1.4 Significance of the Study

This project provides a cost-effective and accessible learning platform for understanding high-frequency transmission line behavior without the need for expensive laboratory equipment. By using simulation-based analysis, it allows students and researchers to visualize wave propagation, impedance matching, and S-parameter performance in a controlled environment.

The study supports engineering education by bridging the gap between theoretical electromagnetics and practical RF concepts, helping learners develop stronger analytical and design skills. It also demonstrates how a standard six-layer FR-4 PCB configuration can be effectively designed for teaching transmission-line principles under 2 GHz, making it adaptable for institutions with limited laboratory resources in developing regions.

1.5 Scope of the Study

This project focuses on the design and simulation of a six-layer FR4-based high-frequency transmission experimentation system for educational and research purposes. It covers the modeling of key transmission line structures such as microstrip, stripline, differential pairs, stubs, and resonators, operating below 2 GHz.

All analyses are performed using electromagnetic simulation tools to study wave propagation, impedance characteristics, and S-parameter behavior. The study does not include hardware fabrication or laboratory testing, as it is entirely simulation-based.

Chapter Two

Literature Review

2.1 Overview

As the demand for high-speed communication systems and compact RF circuits grows, so does the importance of properly designed transmission lines in printed circuit boards (PCBs). As signal frequencies reach the GHz range, traditional lumped circuit models become insufficient due to increasingly complex signal behavior that defies simple circuit approximations. As such, distributed transmission line theory must be applied (Pozar, 2012).

Using simulation tools like *Ansys HFSS* coupled with the *Smith Chart*, this project aims to design and simulate a range of high-frequency transmission lines on a 6-layer PCB using FR4 substrate. FR4 is not only known for its low cost, but also for its higher dielectric loss and signal dispersion due to its high dissipation factor at frequencies above 2 GHz (Rogers, 2020). This makes it a practical choice for schools and colleges, yet a performance-sensitive choice for real-world applications.

This project aims to bridge the gap between theory and practice by providing engineers and students with hands-on learning. It enables the observation of typically invisible concepts such as transmission loss, crosstalk and signal reflection. Furthermore, it helps students understand how design decisions affect signal behavior.

2.2 Printed Circuit Boards (PCBs)

A printed circuit board (PCB) is the platform upon which microelectronic components such as semiconductor chips and capacitors are mounted (Ladou, 2006). It provides the electrical interconnections between components and is found in virtu-

ally all electronics products. These boards are mainly composed of two elements: copper plates to ensure efficient electrical conduction and a dielectric substrate (e.g. FR4) that has several functions, such as providing electrical insulation between copper traces, optimizing the operation of the circuit built on the board, giving the board rigidity and durability (Ulrich, 2008). A well-designed PCB provides signal integrity, reduces production costs, and reduces issues related to noise and heat. A 3D view of a finished PCB layout is shown in figure 2.1.

PCBs play a crucial role particularly in high-speed and high-frequency applications. One of the most critical challenges in PCB design is ensuring Electromagnetic Compatibility (EMC), which involves controlling electromagnetic emissions and susceptibility to maintain system functionality and meet regulatory standards (Rahman, 2025). EMC refers to the ability of an electronic system to operate in its intended electromagnetic environment without introducing intolerable electromagnetic disturbances or being adversely affected by external sources. As devices operate at higher speeds and frequencies, even small design errors can lead to substantial EMC problems.

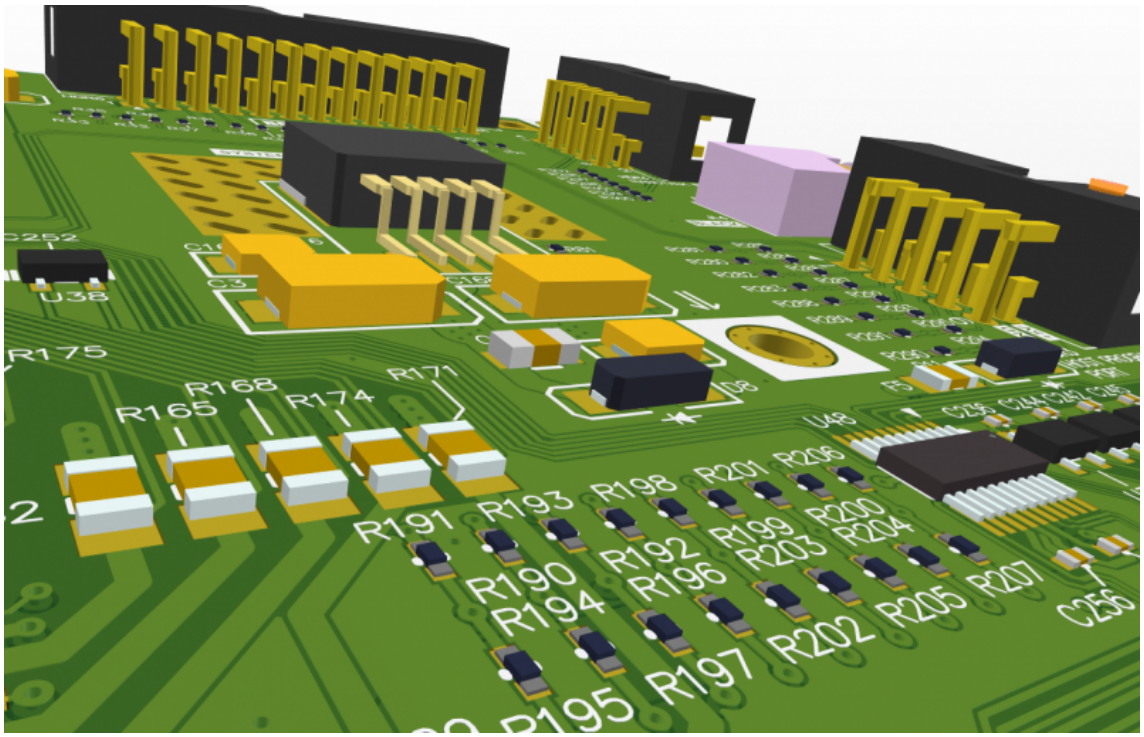

Figure 2.1: 3D view of a finished PCB layout (Altium,2025)

Designing and fabricating a PCB is vital for hands-on training, to guide students

to carry out various experiments. Hence, universities require a perfect trainer PCB. Moreover, this trainer board should be well flexible to handle a vast variety of experiments. The assembly cycle of PCBs with installed dynamic segments requires a few adjustments on the development layer arrangement, including the utilization of more slender layers and heterogeneous composite materials (Prasanna, 2021).

2.2.1 Structure

A basic PCB consists of a flat sheet of insulating material and a layer of copper foil, laminated to the substrate. This substrate, usually a base material like fiberglass-reinforced resin, FR4, is rigid enough to serve as the foundation on which subsequent layers of copper can be built. According to Bosshart (1983), the base material of the PCB must provide strength, low dielectric loss, and stability under temperature variation. Also, it is a double copper layer by default with copper at both the top and the bottom. Hence, to make a 6-layer PCB, PREPREG (a dielectric material) is placed over the top and bottom copper layers in the core, forming this PCB in the order:

Copper Layer (Signal) – Prepreg - Copper Layer (Plane) - FR4 - Copper Layer (Signal) – Prepreg - Copper Layer (Plane) - FR4 - Copper Layer (Plane) - Prepreg - Copper Layer (Signal)

Other possible layers such as 8 and 16-layers can be implemented as well. PCB applications solely depend on the type and thickness of substrate, prepreg and the copper foil used. The thickness of copper in PCB industry is specified in OUNCE (oz). By default, the substrate used to build a PCB is $1oz$ spread out over $1ft$ wide of uniform spread out sheet, equivalent to 0.0348mm thickness. In the 6-layer board for example, we have 6 copper layers sandwiched between 5 dielectrics. The top copper layer, first inner layer, second inner layer, third inner layer, fourth inner layer and the bottom copper layer. To connect from one layer to another, a **VIA** is used. There are various types of transmission lines via. They include:

1. **Thru-hole via:** This is the type of via that is used most often in a circuit board. The holes are drilled all the way through the board with a mechanical drill bit and can get down to 6 mils in size.

2. **Buried via:** This via only connects internal layers of the board and is useful for PCBs with very dense routing.

3. **Blind via:** This via starts on either the top or bottom of the board but doesn't go all the way through it.

4. **Microvia:** For hole sizes smaller than 6 mils, a laser-drilled microvia is used. These vias connect only two adjacent layers of the board and can be on the surface or buried within the board layer stackup. Microvias are extremely versatile and can be stacked together, or on top of a buried via, but have a higher fabrication cost associated with them.

On the copper layer, connections are made from one point to another. These connections are known as **TRACE**. A signal trace or circuit trace on a printed circuit board (PCB) is the equivalent of a wire for conducting signals (Nawazi, 2002). Each trace consists of a flat, narrow part of the copper foil that remains after etching. Signal traces are usually narrower than power or ground traces because the current carrying requirements are usually much less. These traces aid signal propagation from one point to another. A protective layer of tin is mostly applied over the copper in a PCB to prevent short circuit and corrosion. This layer is called the **SOLDERMASK**. Monk (2017) notes that, soldermask is vital not only for protection but also for manufacturability, helping guide automated soldering processes. A layer on the PCB, used to print labels is known as the **SILKSCREEN**. It functions as the visual guide of a PCB, offering human-readable identification marks for components and test points (Sharma, 2013).

2.2.2 The Substrate

The commonly used substrate for PCB core at high frequencies (i.e 2 GHz and below) is the **FR4**. It has a relative permittivity of approximately 4.3 (i.e. $\varepsilon_r \approx 4.3$). At very high frequencies (above 2 GHz), the losses in FR4 become significant and can be measured in form of **loss tangent** ($\tan\delta$) or **dissipation factor** (DF). Table 2.1 shows the comparison between FR4 and other substrate materials:

Table 2.1: Comparison of PCB Substrate Materials (Below 2 GHz)

Substrate Material	**Dielectric Constant (ϵ_r)**	**Cost Effectiveness**	**Electrical Properties (Below 2 GHz)**	**Thermal Stability**	**Common Applications**
FR4 (Epoxy Glass)	4.3 – 4.7 *(Ulrich & Schaper, 2008; IPC-4101)*	low cost	Moderate signal loss *(Johnson & Graham, 2003)*	Tg ≈ 130–140°C *(Ng, 2003)*	Consumer electronics, computers
CEM-1	∼4.5 *(Ladou, 2006)*	very low cost	Higher loss than FR4 *(Bosshart, 1983)*	Tg ≈ 105°C *(Sharma & Jain, 2013)*	Indicators, low-cost appliances
Polyimide	3.2 – 3.5 *(Ng, 2003; IPC-4101/41)*	moderate cost	Excellent low loss *(Ulrich & Schaper, 2008)*	> 200°C *(Anderson, 2010)*	Flex circuits, aerospace
Alumina Ceramic	9.8 – 10.2 *(Said, 2011)*	high cost	Very low loss, high ϵ_r *(Lal & Malhotra, 2010)*	> 300°C *(Said, 2011)*	High-voltage modules
Rogers RO4003C	∼3.55 *(Rogers Corp., 2022)*	high cost	Excellent stability *(Anderson, 2010)*	Tg ≈ 235°C *(Rogers Corp., 2022)*	RF, base stations
PTFE + Ceramic Fillers	∼3.0 – 3.5 *(Rogers Corp., 2022)*	very high cost	Ultra-stable ϵ_r *(Ulrich & Schaper, 2008)*	Excellent *(Lal & Malhotra, 2010)*	Military, satellite, GPS
FR2 / Phenolic Paper	4.5 – 5.0 *(Ladou, 2006)*	very low cost	Very lossy *(Sharma & Jain, 2013)*	< 105°C *(Bosshart, 1983)*	Toys, disposable electronics

2.3 Planar Transmission Lines

Planar transmission lines are those transmission lines implemented on flat 2D surfaces. According to Pozar (2011), Planar transmission lines refer to guided structures where the entire geometry lies in a plane, allowing ease of fabrication and integration with circuit component. The conductors consist of flat strips and typically include one or more ground planes parallel to the flat surface of the conductors. These conductors are separated from the ground planes by a solid dielectric material.

Transmission lines can also be constructed in non-planar formats, such as coaxial lines. However, the principal advantage of planar types is that they can be manufactured using the same processes used in printed circuit board fabrication, particularly through the **Photolithography** process. Planar technologies are thus particularly well suited to mass production of such components (Bhat, 1989).

Making circuit elements out of transmission lines is most useful at microwave frequencies. At lower frequencies the longer wavelength makes these components too bulky. At still higher frequencies dielectric waveguide (e.g optical fibre) becomes the technology of choice, but there are planar types of dielectric waveguide available (Yeh & Shimabukuro, 2008). The most widely used planar transmission lines are stripline, microstrip and coplanar waveguide (Jarry & Beneat, 2009).

2.3.1 Modes: An important parameter of a transmission line

An important parameter for transmission lines is the **mode** of transmission employed. The mode describes the electromagnetic field patterns caused by the geometry of the transmission structure (Flaviis, 2004). It is possible for more than one mode to exist simultaneously on the same line. Usually, steps are taken to suppress all modes except the desired one (Connor, 1972). But some devices, such as the dual-mode filter, rely on the transmission of more than one mode (Hunter, 2001). We will discuss two modes of a transmission line as it relates to our scope of study.

TEM mode

The mode found on ordinary conductive wires and cables is the transverse electromagnetic mode (TEM mode). This is also the dominant mode on some planar transmission lines. In the TEM mode, the field strength vectors for the electric and magnetic field are both transverse to the direction of travel of the wave and orthogonal to each other. An important property of the TEM mode is that it can be used at low frequencies, all the way down to zero (i.e. DC) (Oliner, 2006; Maas, 2014; Becherrawy, 2013).

Another feature of the TEM mode is that on an ideal transmission line there is no change of line transmission parameters (characteristic impedance and signal group velocity) with the frequency of transmission. Because of this, ideal TEM transmission lines do not suffer from dispersion, a form of distortion in which different frequency components travel at different velocities. All other modes suffer from dispersion, which puts a limit on the bandwidth achievable (Oliner, 2006).

Quasi-TEM modes

Some planar types, notably microstrip, do not have a homogeneous dielectric; It is different above and below the line. Such geometries cannot support a true TEM mode. There is some component of the electromagnetic field parallel to the direction of the line, although the transmission can be nearly TEM. Such a mode is referred to as quasi-TEM. A quasi-TEM mode is a transmission mode where the electromagnetic fields closely resemble those of a TEM wave, but with small longitudinal components that arise due to the non-uniform dielectric or geometry of the structure (Pozar, 2011). In a TEM line, discontinuities such as gaps and posts (used to construct filters and other devices) have an impedance that is purely reactive (i.e. they can store energy, but do not dissipate it). In most quasi-TEM lines, these structures additionally have a resistive component to the impedance. This resistance is a result of radiation from the structure and causes the circuit to be lossy. The same problem occurs at bends and corners of the line. Unlike true TEM lines (e.g. coaxial cable, stripline), quasi-TEM modes exhibit dispersion which leads to distortion of broadband signals as different frequencies travel at slightly different speeds (Gupta et al., 1996). Because of the non-ideal field distribution, quasi-TEM line can radiate

energy, especially at bends or discontinuities (Bahl & Trivedi, 2007). Hence, they (quasi-TEM line) often experience greater conductor and dielectric losses than true-TEM lines (Wadell, 1991).

Quasi-TEM structures are widely used because they are easier to fabricate than TEM lines. Microstrip lines, coplanar waveguides (CPW), and slotlines are examples where quasi-TEM propagation is dominant.

2.3.2 Various Planar Transmission Lines

There are several types of planar transmission lines; however, this study will focus only on those that fall within our defined scope. They include;

1. Microstripline
2. Stripline
3. Differential Microstripline
4. Differential Stripline

Microstripline

The microstrip line is one of the most widely used planar transmission line structures in modern RF and microwave circuits. It is particularly popular in printed circuit board (PCB) technology due to its simplicity of construction and ease of integration with other components (Pozar, 2012). Microstrip was developed by ITT laboratories as a competitor to stripline (Grieg & Engelmann, 1952). This line does not support a true TEM wave. At non-zero frequencies, both the E and H fields will have longitudinal components (a hybrid mode)(Denlinger, 1971). The longitudinal components are small however, and so the dominant mode is referred to as quasi-TEM. The line is dispersive. With increasing frequency, the effective dielectric constant gradually climbs towards that of the substrate, so that the phase velocity gradually decreases (Cory, 1981). This is true even with a non-dispersive substrate material (i.e the substrate dielectric constant will usually fall with increasing frequency).

The characteristic impedance of the line changes slightly with frequency (again, even with a non-dispersive substrate material). The characteristic impedance of

non-TEM modes is not uniquely defined, and depending on the precise definition used, the impedance of microstrip either rises, falls, or falls then rises with increasing frequency (Bianco et al., 1978). The low-frequency limit of the characteristic impedance is referred to as the quasi-static characteristic impedance, and is the same for all definitions of characteristic impedance. Also, the wave impedance varies over the cross-section of the line. Microstrip lines radiate and discontinuity elements such as stubs and posts, which would be pure reactances in stripline, have a small resistive component due to the radiation from them (Oliner, 2006).

A microstrip line shown in figure 2.2 consists of a conducting strip of width W, which is separated from a ground plane by a dielectric substrate of thickness h and relative permittivity ε_r. The top of the strip is exposed to air, making the effective dielectric constant ε_{eff} a combination of the dielectric and air. The effective dielectric constant ε_{eff} is less than ε_r because of the field fringing into the air. This affects the propagation velocity and wavelength. These lines are Ideal for mass production of RF boards due to its minimal complexity. A major drawback in this line is that its open structure allows EM radiation, especially at higher frequencies (Montrose 2000) and environmental sensitivity (i.e. impedance can vary with humidity, temperature, and nearby objects due to the exposed top). Compared to striplines, microstrips are more prone to EMI and crosstalk.

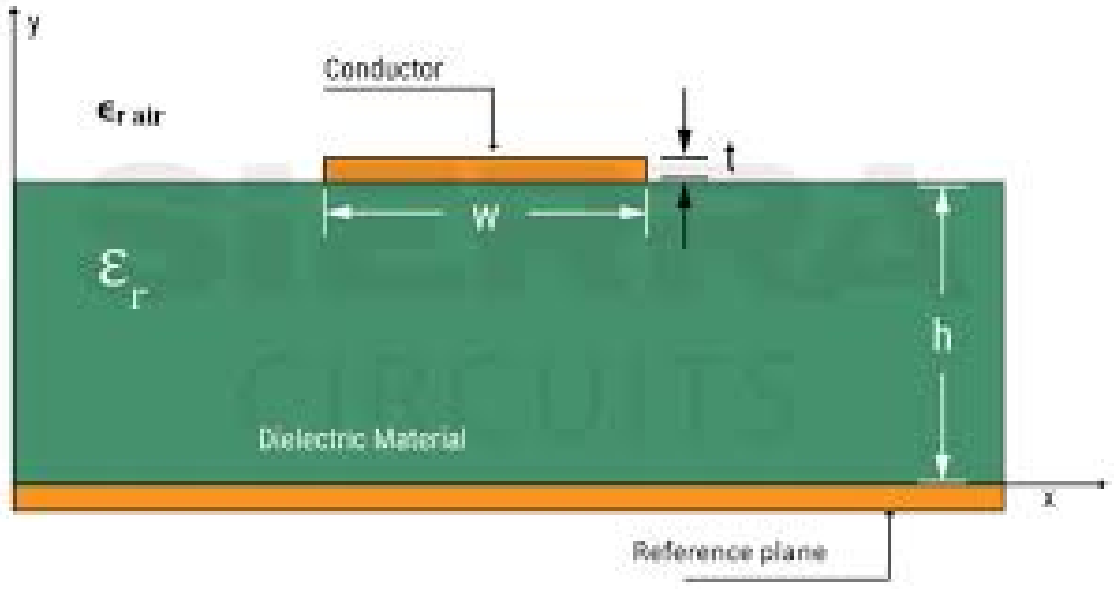

Figure 2.2: Microstripline (Serria Circuits,2019)

Stripline

A **stripline** is a type of transmission line used in high-frequency and microwave circuits. It is a transverse electromagnetic (TEM) transmission line medium invented by Robert M. Barrett of the Air Force Cambridge Research Centre in the 1950s. Stripline is the earliest form of planar transmission line. It consists of a flat, narrow signal conductor embedded symmetrically between two parallel ground planes inside a dielectric substrate which must not be equally spaced between these ground planes. Unlike microstrip, which is open to air on one side, stripline is fully enclosed, offering better shielding and reduced radiation loss. Stripline operates as a distributed transmission line. When high-frequency signals pass through the central strip, they generate electric and magnetic fields confined between the two ground planes. The dielectric ensures all the fields remain within the substrate.Hence, the fields in stripline are completely confined to the dielectric, resulting in true TEM mode propagation (pozar, 2012). A typical stripline shown in figure 2.3 consists of:

1. A central signal conductor (flat copper strip)
2. Dielectric substrate surrounding the strip
3. Top and bottom ground planes

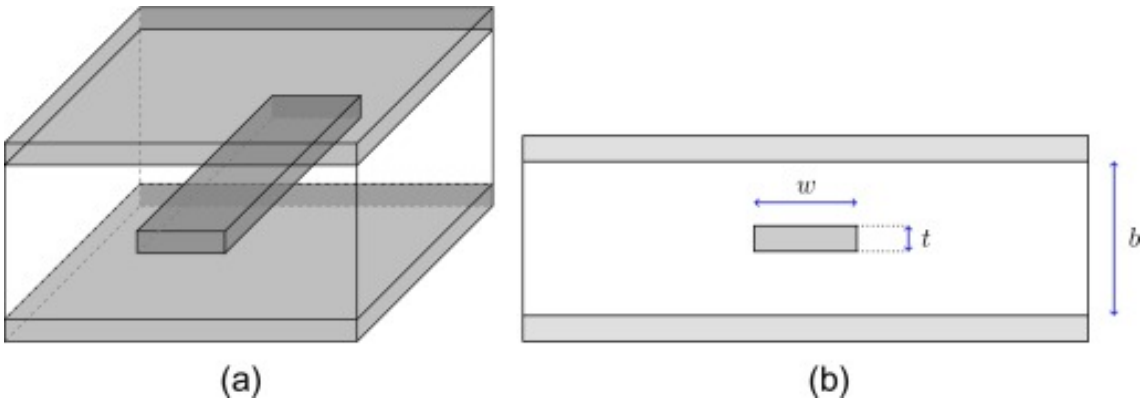

Figure 2.3: Stripline, Jon Varteresian (2002)

Also, this symmetrical configuration allows the propagation of the true TEM (Transverse Electromagnetic) mode signals, similar to coaxial cables in planar form. Like coaxial cable, stripline is non-dispersive (Bhat & Koul, 1989) (provided that

the dielectric of substrate is not itself dispersive), and has no cutoff frequency. Good isolation between adjacent traces can be achieved more easily than with microstrip. Stripline provides for enhanced noise immunity against the propagation of radiated RF emissions, at the expense of slower propagation speeds when compared to microstrip lines. The effective permittivity of striplines equals the relative permittivity of the dielectric substrate because of wave propagation only in the substrate. Hence striplines have higher effective permittivity in comparison to microstrip lines, which in turn reduces wave propagation speed

Stripline possess excellent EMI performance due to full shielding (Bhat & Koul, 1989), true TEM mode propagation for predictable behavior and reduced crosstalk compared to microstrip. They require multilayer PCB making it complex for its fabrication, higher dielectric loss (i.e all the fields travel through the substrate) and it's difficult to probe or modify due to the buried trace. Stripline losses are usually higher than microstrip because all the electromagnetic field is confined within the dielectric, which introduces more loss than air (Gupta, 1996).

Guidelines for a stripline

- Maintain symmetrical geometry for consistent impedance
- Avoid sharp bends in traces to reduce reflections
- Use tight dielectric control in manufacturing
- Implement via stitching to connect ground planes

2.3.3 Comparison between the stripline and microstripline

The main difference between the stripline and microstripline is that a stripline is routed internally between two ground planes, while a microstrip is on an outer layer with a ground plane below it. This means striplines are better shielded and offer higher signal integrity, but are more complex and expensive to make. Microstrips are simpler, cheaper, and easier to fabricate, but have lower shielding and are more susceptible to noise and crosstalk. This comparison is further summarized in Table 2.3 below:

Table 2.3: Comparison between the stripline and microstripline

Feature	**Stripline**	**Microstrip**
Field Propagation	True TEM	Quasi-TEM
Radiation Loss	Very Low	Moderate to High
Shielding	Excellent	Poor
Fabrication	Complex (buried)	Easier (top-layer)
Access	Not accessible	Accessible
Dielectric Loss	Higher	Lower

Differential Stripline

A **differential stripline** (shown in figure 2.4) consists of two signal conductors placed symmetrically between two ground planes within a multilayer PCB. It is similar to a stripline in terms of both its advantages and disadvantages. The electromagnetic (EM) field is entirely contained within the dielectric material, typically FR4 or Rogers, resulting in a well-shielded and balanced transmission medium. Hence, it possess minimized radiation and susceptibility to external noise (Johnson, 2003).

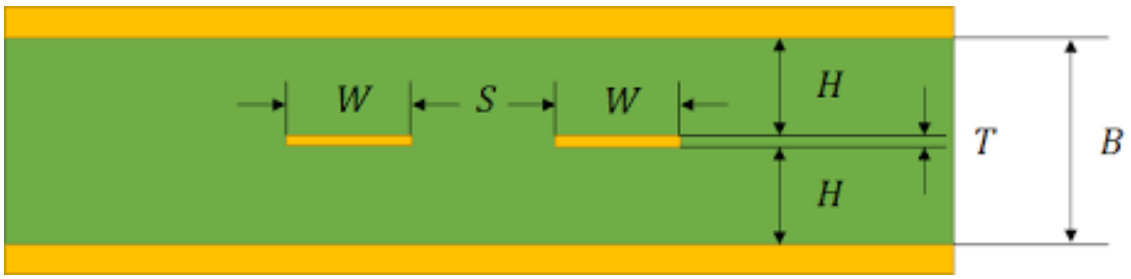

Figure 2.4: Differential Stripline

Differential Microstrip

A **differential microstrip** (shown in figure 2.5) comprises two conductors placed on the outer layer of the PCB, above a single ground plane. The EM field is partly in the dielectric and partly in the surrounding air. It is similar to a microstripline in terms of both its advantages and disadvantages. A differential microstripline is often used for high-speed signals such as DDR2 SDRAM clocks, USB Hi-Speed data lines, PCI Express data lines, LVDS data lines, etc., often all on the same PCB (Olney, 2005).

These transmission line types finds application in:

- High-speed serial buses: USB, HDMI, PCIe, Ethernet.
- Microwave and RF systems: Filters, baluns, antennas.
- Controlled impedance environments for differential signals.

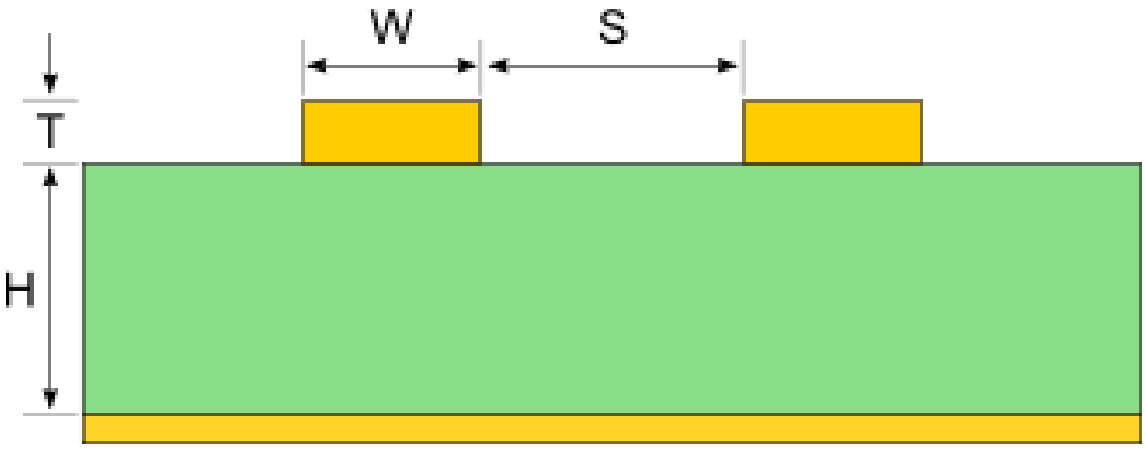

Figure 2.5: Differential Microstrip

2.3.4 Comparison between differential stripline and differential microstripline

The fundamental difference between differential stripline and differential microstripline is in their physical location and surrounding environment within a printed circuit board (PCB) stackup:

- A differential microstripline (figure 2.5) is routed on an external layer (top or bottom) and has a single reference ground plane on the adjacent inner layer below it (or above it). The signal traces are exposed to both the PCB's dielectric material and the air above/below.
- A differential stripline (figure 2.4) is routed on an internal layer and is fully embedded within the dielectric material, sandwiched between two ground planes (one above and one below the signal traces).

The table 2.4 below summarizes the Comparison between differential stripline and differential microstripline:

Table 2.4: Comparison between differential stripline and differential microstripline

Feature	**Differential Stripline**	**Differential Microstrip Line**
Shielding	Excellent (between planes)	Moderate (single plane)
EMI Performance	Very Low Radiation	Higher Radiation
Fabrication	Complex (multilayer PCB)	Simpler (outer layer)
Frequency Range	High (>10 GHz)	Moderate (<10 GHz)
Impedance Control	More Precise	Slightly Less Precise
Dielectric Loss	Higher	Lower
Ease of Access	Difficult (requires vias)	Easy (outer layer)
Environmental Impact	Minimal effect	Moderate effect

2.4 High Frequency Transmission

The transmission of electromagnetic (EM) waves plays a central role in modern communication and high-frequency electronic systems. Unlike low-frequency circuits where interconnects are treated as simple wires, high-frequency signals especially in the RF and microwave engineering require accurate modeling of wave propagation and reflection along distributed structures such as transmission lines (Pozar, 2012). These lines guide EM energy using engineered conductor-dielectric geometries that support transverse electromagnetic (TEM) or quasi-TEM modes, depending on the structure.

Microstrip lines, striplines, and their differential counterparts are among the most widely used transmission media in printed circuit board (PCB) design due to their ease of fabrication and integration. As stated by Edwards and Steer (2000), these structures allow for relatively predictable impedance control and field distribution, making them essential components in filters, matching networks, and resonant circuits. However, the propagation characteristics of EM waves are strongly influenced by the dielectric material properties, conductor geometry, and termination conditions.

At microwave frequencies, even small mismatches in impedance or geometrical discontinuities can cause significant reflections and signal degradation (Collin, 2001). The characteristic impedance, Z_0, propagation constant, γ, and reflection coefficient, Γ, become key parameters in determining transmission efficiency and

signal integrity. According to Gupta et al. (1996), understanding these parameters requires both analytical modeling and full-wave electromagnetic simulations, especially when working with substrates such as FR4.

While substrates like Rogers, RT/duroid offer excellent performance at GHz frequencies, low-cost FR4 remains popular in educational, prototyping, and cost-sensitive applications. The lossy and dispersive nature of FR4 imposes a practical upper limit on usable frequency, typically around 2 GHz (Zurcher and Gardiol, 1995). Recent work continues to explore methods of mitigating these losses and characterizing FR4-based structures using tools like vector network analyzers (VNAs) and time-domain reflectometry (Boesch & Steffen, 2020).

Overall, the study of electromagnetic wave transmission through guided media forms the foundation for efficient RF system design. Bridging theoretical principles with practical measurement and fabrication, especially on affordable substrates, remains a vital area of applied electromagnetic research.

2.4.1 Distributed Modelling of HF Transmission Lines

This model consists of an infinite series of infinitesimal elements, each representing a small segment of the transmission line. These elements include resistance (R), inductance (L), capacitance (C), and conductance (G), all defined per unit length. The model reflects the fact that voltage and current on the line vary continuously along its length and are influenced by these distributed parameters.

These parameters are known as the **Primary Line Constants**, and they form the foundation from which the **Secondary Line Constants** are derived. The secondary constants include:

- Characteristic Impedance (Z_0)
- Propagation Constant (γ)
- Attenuation Constant (α)
- Phase Constant (β)

All of these constants are independent of time, voltage, and current.

Telegrapher's Equations

The Telegrapher's Equations are derived from the distributed element model of transmission lines. They describe how voltage and current vary with distance and time/frequency along the transmission line. These equations are central in transmission line theory and are valid from DC up to the frequency where higher-order (non-TEM) modes start to propagate (Hayt 1989).

Frequency Domain Form (Second Order Form)

The Telegrapher's Equations in the frequency domain are given by:

$$\frac{d^2I}{dx^2} = (G + j\omega C)(R + j\omega L)I \tag{2.1}$$

$$\frac{d^2V}{dx^2} = (R + j\omega L)(G + j\omega C)V \tag{2.2}$$

Where:

- R = resistance per unit length (Ohms/m)
- L = inductance per unit length (Henries/m)
- G = conductance to ground per unit length (Siemens/m)
- C = capacitance to ground per unit length (Farads/m)
- ω = angular frequency in radians/sec

We define the **propagation constant** γ as:

$$\gamma = \sqrt{(R + j\omega L)(G + j\omega C)} \tag{2.3}$$

Hence, the equations simplify to:

$$\frac{d^2V}{dx^2} = \gamma^2 V \tag{2.4}$$

$$\frac{d^2I}{dx^2} = \gamma^2 I \tag{2.5}$$

General Solutions (Travelling Wave Form)

The general solutions for voltage and current are given by:

$$V(x) = V^+ e^{-\gamma x} + V^- e^{\gamma x} \tag{2.6}$$

$$I(x) = I^+ e^{-\gamma x} + I^- e^{\gamma x} \tag{2.7}$$

Here:

- V^+, I^+ represent forward traveling voltage and current waves.
- V^-, I^- represent backward traveling voltage and current waves.

The Complex Quantity, γ

Electromagnetic waves travel in a sinusoidal pattern which can be measured as the current or voltage in the circuit (e.g., the transmission line).

In the section above, we showed that voltage and current are expressed in the form of a complex quantity, γ, known as the **propagation constant**. It is a dimensionless quantity, and it describes how the amplitude and phase of a wave change as it propagates through a medium (Paschotta, 2011). It essentially explains how much the signal weakens (*attenuation*) and how its waveform shifts (*phase shift*) over a certain distance. It's a crucial parameter for understanding wave behavior in various media.

Since the propagation constant is a complex quantity, we can write:

$$\gamma = \alpha + j\beta \tag{2.8}$$

where:

- α, the real part, is called the **attenuation constant**
- β, the imaginary part, is called the **phase constant**

The phase constant is defined as the imaginary part of the propagation constant γ. It is related to the wavelength λ, and the frequency f, and is typically expressed in radians per unit length (i.e., radians/meter) of the wave by the following equation:

$$\beta = \frac{2\pi}{\lambda} = \frac{\omega}{v_p} \tag{2.9}$$

where:

- $\omega = 2\pi f$ is the angular frequency, and
- v_p is the phase velocity of the wave.

A higher phase constant means the waves' phase changes more rapidly with distance, indicating a shorter wavelength and higher frequency (Walter, 1990).

The attenuation constant, also known as the attenuation factor, describes how much the amplitude of a wave decreases as it propagates through a medium. It's typically expressed in *nepers per unit length* (i.e., nepers/meter). A higher attenuation constant means the waves' amplitude decreases more rapidly, indicating a greater loss of energy as it travels.

$$\alpha = \text{Nepers/meter}$$

$$V = |V^+|e^{-\alpha x} \tag{2.10}$$

2.4.2 Characteristic Impedance Z_0 of Various HF Transmission Lines

The characteristic impedance Z_0 of an infinite transmission line at a given angular frequency ω is the ratio of the voltage and current of a pure sinusoidal wave of the same frequency travelling along the line (Lee, 2004). This relation is also the case for finite transmission lines until the wave reaches the end of the line.

Generally, a wave is reflected back along the line in the opposite direction. When the reflected wave reaches the source, it is reflected yet again, adding to the transmitted wave and changing the ratio of the voltage and current at the input, causing the voltage-current ratio to no longer equal the characteristic impedance. This new

ratio including the reflected energy is called the **input impedance** of that particular transmission line and load.

The input impedance of an infinite line is equal to the characteristic impedance since the transmitted wave is never reflected back from the end. Equivalently, the characteristic impedance of a line is that impedance which, when terminating an arbitrary length of line at its output, produces an input impedance of equal value. This is so because there is no reflection on a line terminated in its own characteristic impedance.

Applying the transmission line model based on the telegrapher's equations (Gateece, 2018), the characteristic impedance is given as:

$$\frac{V^+}{I^+} = \sqrt{\frac{R + j\omega L}{G + j\omega C}} \Rightarrow Z_0 = \sqrt{\frac{R + j\omega L}{G + j\omega C}} \tag{2.11}$$

This also applies to the backward traveling wave (V^-, I^-). This expression extends to DC by letting $\omega \to 0$.

Characteristic Impedance of a Microstripline:

The characteristic impedance Z_0 of a symmetric microstripline is given approximately by:

$$Z_0 = \frac{120\pi}{\sqrt{\varepsilon_r}(\frac{w}{h} + 2)} \tag{2.12}$$

Where:

h = distance from strip to ground plane

w = width of the strip

t = thickness of the strip

ε_r = relative dielectric constant

This geometry allows tight control of impedance, critical for high-speed digital and Radio Frequency (RF) signal integrity. (Johnson, 2003)

Characteristic Impedance of a Stripline:

The characteristic impedance Z_0 of a symmetric stripline is given approximately by:

$$Z_0 = \frac{377}{\sqrt{\varepsilon_r \frac{w}{h} + 2}} \tag{2.13}$$

Where:

h = distance from strip to ground plane

w = width of the strip

t = thickness of the strip

ε_r = relative dielectric constant

Most high frequency operation has been standardized and $Z_0 = 50\Omega$. It is observed that the single-ended microstripline is unbalanced compared to the differential microstripline, which is balanced. The same goes for a stripline.‘

A microstripline has its field shielded by the ground plane on one side only. The trace side exposed to the environment radiates field outward that can induce noise into surrounding traces. This is called **Crosstalk**.

In this case, when the microstripline trace is the source of the radiated field that induces noise in a closeby trace, it is called the **Aggressor Trace**. The trace closeby to the aggressor trace that noise voltage gets induced into as a result of the changing magnetic field of the aggressor trace is called the **Victim Trace**. One way to reduce this is to place the victim trace as far as possible from the aggressor trace. A rule of thumb is the victim trace should be placed at $3W$ from the aggressor trace, where W is the width of the aggressor trace.

2.4.3 Intrinsic Impedance

In high-frequency Printed Circuit Board (PCB) design, intrinsic impedance refers to the inherent opposition offered by a medium, typically the dielectric material like Flame Retardant grade 4 (FR4) or Rogers substrate, to the propagation of electromagnetic waves. It is defined as the ratio of the electric field strength (E) to the magnetic field strength (H) in a uniform plane wave traveling through the medium:

$$\eta = \sqrt{\frac{\mu}{\varepsilon}} \tag{2.14}$$

where μ is the permeability and ε is the permittivity of the medium. In free

space, this evaluates to approximately 377 ohms (Pozar, 2012).

When high-speed signals travel through Printed Circuit Board (PCB) traces, such as microstrip or stripline, the dielectric material surrounding the trace alters the waves' intrinsic impedance. This impedance influences the shape and timing of signals. If the trace impedance mismatches the source or load impedance, reflections occur, degrading signal integrity (Johnson & Graham, 2003).

For typical Printed Circuit Board (PCB) materials like Flame Retardant grade 4 (FR4) with a relative permittivity $\varepsilon_r \approx 4.3$, the intrinsic impedance is significantly lower than that in free space. While intrinsic impedance is not directly used in Printed Circuit Board (PCB) layout design, understanding its role is crucial when transitioning between media (e.g., stripline to microstrip), where sudden changes in dielectric affect impedance and may cause reflections (Lee, 2004; Miano & Maffucci, 2001).

2.4.4 Reflection Coefficient

The reflection coefficient quantifies how much of a signal is reflected due to impedance discontinuity. If a Printed Circuit Board (PCB) trace with characteristic impedance Z_0 connects to a load with impedance Z_L, the reflection coefficient Γ is defined as:

$$\Gamma = \frac{Z_L - Z_0}{Z_L + Z_0} \tag{2.15}$$

In Printed Circuit Board (PCB) transmission lines, especially in high-speed or RF circuits, impedance continuity is crucial. Any mismatch, for instance, a 50Ω trace connecting to a 75Ω load, leads to partial reflection ($\Gamma \neq 0$), resulting in signal distortion (Hayt, 1989).

Time Domain Reflectometry (TDR) and Vector Network Analyzers (VNA) are commonly used in Printed Circuit Board (PCB) testing to detect and visualize such reflections. Proper termination techniques (such as resistive loading or matched terminations) are essential to avoid reflections, especially in differential interfaces like Peripheral Component Interconnect (PCIs), High-Definition Multimedia Interface (HDMI), or Universal Serial Bus (USB) (Walter, 1990).

The worst-case scenarios are:

- Short-circuit termination ($Z_L = 0$): $\Gamma = -1$
- Open-circuit termination ($Z_L \to \infty$): $\Gamma = 1$

Both cases lead to 100% reflection and are unacceptable in high-speed Printed Circuit Board (PCB) designs (Pozar, 2012).

2.4.5 Special Cases of a Lossless High-Frequency Transmission Line

In the lossless transmission lines, resistance (R) and conductance (G) are assumed negligible. This approximation is valid at high frequencies where dielectric and conductor losses are minimal. The propagation constant γ becomes:

$$\gamma = j\beta = j\omega\sqrt{LC} \tag{2.16}$$

and the characteristic impedance becomes purely real:

$$Z_0 = \sqrt{\frac{L}{C}} \tag{2.17}$$

This simplification allows efficient modeling of microstrip and stripline transmission lines in PCB CAD tools (e.g., HFSS, ADS) and forms the basis for Radio Frequency (RF) circuit design (Steer, 2019; Pozar, 2012).

Several special terminations arise such as:

Matched Load

When $Z_L = Z_0$, the line is perfectly matched, resulting in $\Gamma = 0$. No reflection occurs, and signal energy is fully absorbed at the load. This is the ideal case in high-speed Printed Circuit Board (PCB) traces, ensuring signal integrity (Lee, 2004).

Open Circuit

An open termination implies $Z_L \to \infty$, yielding $\Gamma = 1$. Voltage is reflected in phase, and a standing wave forms with voltage maxima at the end. This is acceptable in resonator design but must be avoided in digital or analog signal paths (Miano & Maffucci, 2001).

Short Circuit

Here, $Z_L = 0$ and $\Gamma = -1$. Voltage is reflected out-of-phase, resulting in current maxima and voltage minima at the load. Like the open circuit, this is used in specific applications like filters, but is harmful for logic signals (Johnson & Graham, 2003).

Quarter-Wave Transformer

In Printed Circuit Board (PCB) Radio Frequency (RF) design, the quarter-wave transformer provides impedance matching between two mismatched segments. If a trace of length $\lambda/4$ and characteristic impedance $Z_1 = \sqrt{Z_S Z_L}$ is inserted between Z_S (source impedance) and Z_L (load impedance), then reflections are eliminated, and maximum power transfer occurs (Walter, 1990).

Half-Wavelength Transmission Line

A transmission line that is exactly half the wavelength of the signal it carries ($\ell = \frac{\lambda}{2}$) exhibits a unique impedance repetition property. That is, the input impedance of a half-wave line is identical to the load impedance at the other end:

$$Z_{\text{in}} = Z_L \quad \text{if } \ell = \frac{\lambda}{2} \tag{2.18}$$

This occurs because the voltage and current waves realign in phase after traveling a distance of half a wavelength. As a result, the line behaves as a transparent conductor in terms of impedance, regardless of the line's characteristic impedance (Pozar, 2012; Collin, 2001).

In Printed Circuit Board (PCB) applications, this property is used in Radio Frequency (RF) and microwave resonators, delay lines, and impedance repeater structures. For example, at 2 GHz on a microstrip Printed Circuit Board (PCB) with an effective dielectric constant $\varepsilon_{\text{eff}} \approx 4.4$, the guided wavelength is approximately 71.6 mm. Therefore, a half-wavelength trace would be around 35.8 mm in length (Lee, 2004).

This length can be exploited to match complex structures or build resonant devices with predictable impedance profiles and standing wave patterns. However, due to physical size and loss at higher frequencies, care must be taken to minimize

attenuation and control trace geometry (Steer, 2019).

2.5 Impedance Control and Matching in PCB Transmission Lines

The concept of impedance control in printed circuit board (PCB) transmission lines is fundamental in the design of high-frequency and high-speed digital circuits. As signal frequencies increase, typically entering the GHz range, the interconnects on Printed Circuit Boards (PCBs) no longer behave as simple wires but act as distributed transmission lines. In this regime, any discontinuity in characteristic impedance causes reflections that degrade signal quality, timing accuracy, and power transfer efficiency (Pozar, 2012).

In a transmission line, the **characteristic impedance** Z_0 is not just a property of the materials used but also of the geometry of the trace. It is determined by the width of the conductor, the thickness of the dielectric, the height from the ground plane, and the relative permittivity of the dielectric substrate. Printed Circuit Board (PCB) design often involves controlling Z_0 to a specific target, typically 50 Ω for single-ended or 100 Ω for differential pairs, in order to match with driver and receiver impedance and avoid reflections.

2.5.1 Microstripline and Stripline Impedance Control

A **microstripline** is a planar transmission line where the trace lies on the top layer of the Printed Circuit Board (PCB) and has a ground plane underneath it. The fields around the conductor are partially in air and partially in the dielectric substrate. Because of this, the effective dielectric constant ε_{eff} is less than the actual dielectric constant ε_r of the substrate, making microstripline impedance frequency-dependent. The impedance equation is governed by empirical relations involving trace width W, substrate height H, and dielectric constant ε_r (Wadell, 1991).

On the other hand, a **stripline** is an embedded transmission line placed between two ground planes, ensuring symmetric field confinement within the dielectric. This provides better shielding from external noise and improved signal integrity, especially in dense multilayer Printed Circuit Boards (PCBs). However, stripline introduces

more dielectric loss because the electromagnetic fields are fully contained in the substrate, making it less ideal at very high frequencies unless low-loss laminates like Rogers are used (Johnson & Graham, 2003).

2.5.2 Differential Microstripline and Differential Stripline Impedance Control

When two traces carry equal and opposite signals with respect to a reference (rather than ground), they form a **differential pair**. The impedance control here involves ensuring not only that the individual traces have consistent characteristic impedance, but also that the **differential impedance** Z_{diff} between the pair is tightly controlled. Z_{diff} is affected by the spacing between the traces and the mutual coupling of their electromagnetic fields. Differential microstriplines have fields that interact with the air and ground plane below, while differential striplines are shielded and more symmetric.

The equation for differential impedance is generally expressed as:

$$Z_{diff} = 2Z_0(1 - c) \tag{2.19}$$

where Z_0 is the characteristic impedance of each trace and c is the coupling factor. In tightly coupled pairs, c is significant, reducing Z_{diff} and increasing the risk of skew and common-mode noise if not well-matched (Bogatin, 2009).

2.5.3 Reflection and The Need For Impedance Matching

A signal traveling along a transmission line will encounter a reflection if there is a mismatch between the characteristic impedance Z_0 of the line and the load impedance Z_L. The degree of reflection is governed by the **reflection coefficient** Γ, defined as:

$$\Gamma = \frac{Z_L - Z_0}{Z_L + Z_0} \tag{2.20}$$

If $\Gamma = 0$, the impedance is perfectly matched and no reflection occurs. If $\Gamma = 1$ or -1, there is a complete reflection, indicating an open or short circuit respectively.

Reflections can result in waveform distortion, overshoot, and undershoot, especially at high frequencies where rise and fall times are very short. This can disrupt timing margins and cause false triggering of logic circuits (Smith, 1997).

2.5.4 VSWR as a Measure Of Matching Quality

The **Voltage Standing Wave Ratio (VSWR)** is another parameter that quantifies how well a load is matched to a transmission line. It is derived from the magnitude of the reflection coefficient:

$$VSWR = \frac{1 + |\Gamma|}{1 - |\Gamma|} \tag{2.21}$$

A Voltage Standing Wave Ratio (VSWR) of 1 indicates a perfect match, while higher values indicate progressively worse mismatch. Voltage Standing Wave Ratio (VSWR) is easily measurable with a Vector Network Analyser (VNA) and often used as a real-time metric during Radio Frequency (RF) tuning and debugging.

2.5.5 The Smith Chart For Impedance Matching

The **Smith Chart** is a graphical tool that maps complex impedances and reflection coefficients onto a normalized polar plane. It is invaluable in visualizing impedance matching networks and tuning stubs. In a Smith Chart (shown in figure 2.6), the center point represents a perfect match ($\Gamma = 0$), the outer edge represents total reflection ($|\Gamma| = 1$), and all passive loads lie within the circle.

As the signal propagates down a transmission line, its impedance changes depending on the length and frequency, and this is seen as a rotation around the Smith Chart. By adding capacitive or inductive elements (stubs or matching networks), the impedance can be moved to the center of the chart, achieving a match (Pozar, 2012).

Stub Matching for Impedance Control in PCB Transmission Lines

Stub matching is a well-established technique in RF and high-speed PCB design for achieving impedance matching between a transmission line and a load. This method relies on introducing one or more reactive stubs, open-circuited or short-circuited

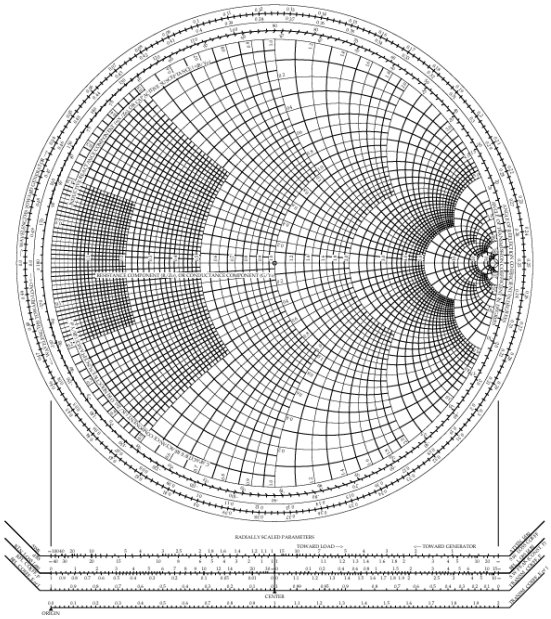

Figure 2.6: The Smith Chart

transmission line segments, at specific locations along the main signal path. These stubs alter the input impedance seen at the junction, enabling transformation to the line's characteristic impedance, e.g 50 Ω (pozar 2012). The Smith Chart serves as a powerful tool for visualizing and designing such matching configurations due to its ability to represent impedance and admittance transformations graphically across a complex plane (pozar 2012).

In the context of PCB transmission lines, stubs can be fabricated using microstrip or stripline geometries, depending on the layer stackup and the type of transmission line in use. These stubs are designed to act as reactive elements whose behavior is dictated by their electrical length, termination, and physical placement. When integrated correctly, they help mitigate reflections, improve signal integrity, and ensure maximum power transfer across interconnects and interfaces (Johnson 2003).

A single stub can be used to match a specific load impedance by providing the exact amount of susceptance required to cancel the reactive component of the load at a certain distance from the source. This configuration is effective in narrowband applications and is often implemented as a printed open-circuited stub in microstrip PCBs (Wadell 1991). The matching process involves transforming the complex impedance of the load to the center of the Smith Chart through the effect of the stub's reactive admittance (pozar 2012).

However, due to the frequency dependence and physical placement limitations of single stubs, double-stub configurations are often preferred in practical PCB systems where tunability and flexibility are desired. A double-stub tuner consists of two stubs placed at fixed distances along the line, which together provide two degrees of freedom, allowing a wider range of load impedances to be matched without adjusting the position of the stubs. This makes them suitable for automated impedance tuning or adaptable RF circuits in multilayer PCBs (wadell 1991).

Triple-stub matching extends this concept by introducing a third stub, allowing complete control over both magnitude and phase of the reflection coefficient. This is particularly useful in applications involving complex or highly mismatched loads where high matching precision is required. On a Smith Chart, the combined effect of these stubs appears as successive moves along constant VSWR circles, ultimately leading to the center of the chart, representing a perfectly matched condition (pozar 2012).

On PCBs, these stubs are not merely theoretical, they are implemented as precisely designed trace geometries. For example, in microstrip configurations, open-circuited stubs are left unterminated at the edge of the board, while short-circuited ones are grounded using **via fences**. In differential pairs, stub matching can be achieved using coupled-line segments designed to maintain symmetry and minimize mode conversion (Johnson 2003).

Overall, the Smith Chart provides a visual framework to understand how stub lengths and positions impact impedance. By overlaying the effect of stubs directly on the chart, designers can iteratively converge on a matching solution without extensive numerical computations. This method remains a cornerstone in RF PCB layout and high-speed signal design, especially in the sub-2 GHz range where distributed effects are dominant and stub implementation is practical in terms of board real estate (pozar 2012).

2.6 S-Parameter Characterization

S-parameters, or scattering parameters, describe the electrical behavior of high-frequency networks by relating incident and reflected waves at each port. They

are complex numbers representing both the magnitude and phase of signals and are used to analyze characteristics like reflection, transmission, input impedance, and frequency response. S-parameters are measured using a vector network analyzer (VNA) and are crucial for designing and optimizing Radio Frequency (RF) and high-speed electronic system. For a 2-port network (such as a Printed Circuit Board (PCB) transmission line):

- S_{11} represents the reflection coefficient at port 1 (input)
- S_{21} represents the forward transmission from port 1 to port 2
- S_{12} represents reverse transmission
- S_{22} represents the reflection at port 2 (output)

From these, other quantities can be extracted. For example, **Return Loss (RL)** is derived from S_{11} as:

$$RL = -20 \log_{10} |S_{11}| \tag{2.22}$$

and **Insertion Loss (IL)** is derived from S_{21}:

$$IL = -20 \log_{10} |S_{21}| \tag{2.23}$$

These measurements are essential to validate whether a Printed Circuit Board (PCB) trace or interconnect has the expected performance. Unknown impedances, such as those of connectors, VIAs, or discontinuities in the PCB, can be back-calculated from measured S_{11} using the relation:

$$Z_L = Z_0 \cdot \frac{1 + S_{11}}{1 - S_{11}} \tag{2.24}$$

Such impedance extraction is critical in debugging signal integrity issues after fabrication (Bogatin, 2009).

2.7 Bounce Diagrams And Transient Reflection Analysis

Bounce diagrams are time-domain tools used to analyze voltage reflections in a transmission line with impedance mismatches. They are particularly useful when working with digital signals where the concern is how transients settle over time. A bounce diagram is constructed by plotting signal reflection events over time as they bounce between mismatched interfaces.

Each step in the diagram shows a reflected or transmitted voltage component as it travels back and forth between the source and the load. These are derived using the step response of the line and the reflection coefficients at both ends. The cumulative voltage at each reflection point helps visualize how long it takes for the signal to stabilize. This is especially critical in long traces or differential pairs where skew and propagation delay can affect performance.

Bounce diagrams also help identify phenomena such as:

- Ringing due to underdamped reflections
- Standing waves in long mismatched lines
- Interaction between multiple reflection points in complex routing

This method is often paired with **TDR (Time Domain Reflectometry)** functionality on a VNA or oscilloscope to validate simulated models (Johnson & Graham, 2003).

Impedance control and matching in PCB transmission lines are indispensable for ensuring signal integrity, especially in high-speed digital and RF designs. By understanding the role of physical geometry, materials, and interconnect layout in microstrip and stripline configurations, including their differential variants, engineers can tailor transmission line performance to application requirements. Analytical tools like the Smith Chart and VSWR provide insight into matching quality, while experimental tools like the VNA offer precise S-parameter measurement for reflection, insertion loss, and impedance extraction. Finally, time-domain techniques

such as bounce diagrams provide intuitive understanding of transient behavior in real-world PCB environments, bridging the gap between theory and practice.

2.8 Review of Related Works

S. Bulja & D. Mirshekar-Syahkal (2010) proposed a novel wideband vertical transition for connecting the coplanar waveguide (CPW) to the microstrip line. This transition can be very useful for millimeter-wave packaging and vertical interconnects. It is multilayered, partly tapered, and consists of only one via interconnect. Two different transitions are designed. The first transition allows connectivity of a CPW with $Z_0 = 50\,\Omega$ to a microstrip line with $Z_0 = 16\,\Omega$ with a bandwidth of 10 GHz to 60 GHz. The second transition has the same characteristic impedance, $Z_0 = 50\,\Omega$, at the two ports. In this case, the operating frequency is from 40 MHz to 60 GHz. The return losses of both transitions are generally lower than -10 dB over their indicated frequency ranges, while the maximum measured insertion losses are 1.8 dB and 2.4 dB for the first and second transition, respectively. To extract the S-parameters of the transitions, a new thru-line technique, based on the standard thru-reflect-line two-tier calibration is introduced. Simulation and experimental results, showing good agreement, are presented and discussed.

Lai (2020) proposed a dynamic control algorithm for three-stub tuners that enables continuous, automatic, real-time impedance matching under varying load conditions. The method divides the Smith Chart into operating regions and sequentially adjusts stub lengths to minimize reflection peaks during dynamic tuning transitions. Both simulation and experimental results demonstrated stable matching performance and minimized reflection coefficients across broadband variations. This adaptive impedance-matching approach provides an intelligent framework for implementing multi-stub matching in PCB-based RF systems, directly applicable to microstrip and stripline triple-stub networks designed on FR4 substrates.

Tu (2022) examined the influence of dielectric loss on the RF performance of microstrip multi-resonant circuits. Using U-shaped microstrip resonators fabricated

on various substrates, including FR4, textile, and low-loss dielectric materials. The study quantified how dielectric loss affects key parameters such as insertion loss, notch depth, and Q-factor. It was observed that FR4 substrates exhibited higher losses and reduced resonance sharpness due to their higher loss tangent. The research provides valuable guidance for substrate selection and design optimization in microstrip resonant and stub-based filter circuits.

Hussein, Mezaal, and Alameri (2023) designed and analyzed a miniaturized microstrip diplexer on FR4 substrate for dual-band wireless communication applications. The proposed design employed meandered microstrip lines and step-impedance resonators to achieve compactness and effective channel separation. Simulation and measurement results showed low insertion loss and good port isolation across both frequency bands. Although the work focuses on diplexer design, the underlying principles of impedance transformation and microstrip coupling are relevant to broadband transmission line design and impedance-matching networks on FR4 substrates.

Sim et al. (2016) explored the fabrication and performance of planar transmission lines printed using silver nanoparticle ink on FR4 and polyimide substrates. The study measured insertion and return losses between 300 kHz and 1 GHz using SOLT calibration, providing quantitative insights into how substrate type and printed conductor quality influence RF behavior. Results showed that FR4-based lines exhibited slightly higher attenuation ($\sim$0.12 dB/cm at 1 GHz) due to its higher dielectric loss tangent compared to polyimide. The findings are valuable for understanding conductor and substrate losses in low-GHz transmission line applications and educational PCB prototypes.

Xu et al. (2014) carried out an in-depth study on microstrip-to-stripline transitions in multilayer RF circuits, focusing on how to minimize signal reflection and mode conversion. Their work explored different ground via fence arrangements and transition geometries to achieve smooth impedance continuity between layers. Using electromagnetic simulations and experimental validation, they showed that a

well-optimized transition can significantly improve broadband signal performance. This research is highly relevant to the current project, which also involves both microstrip and stripline structures on a six-layer FR4 PCB, where maintaining consistent impedance and low reflection across layers is essential for reliable high-frequency transmission.

E. Y. Terán-Bahena et al. (2018) presented a full characterization of transmission lines fabricated on printed circuit boards. For this purpose, the frequency at which the attenuation curves associated with the conductor and dielectric losses cross over is first determined to exactly separate the corresponding contribution to the total attenuation. Afterward, permittivity, loss tangent, effective geometry, and rms roughness are obtained from the propagation constant and characteristic impedance data for allowing the transmission line representation up to 20 GHz. Using the extracted parameters, the excellent model experiment correlation for the S-parameters of the lines is observed. In fact, the curves of complex-impedance versus frequency are also corrected from undesired resonances typically occurring in experimental data. Finally, it is demonstrated that the extracted parameters allow performing causal time domain simulations.

Santavicca and Prober (2008) designed a compact, impedance matched stripline low-pass filter aimed at reducing high-frequency noise and improving signal integrity in broadband cryogenic applications. Their method incorporated a dissipative dielectric material within the stripline geometry to achieve deep attenuation while maintaining low reflection across a wide frequency range. The filter achieved over 100 dB of attenuation in the stopband and return loss greater than 10 dB up to 40 GHz. By employing an optimized stripline configuration and lossy dielectric loading, the design successfully balanced insertion loss with suppression of undesired harmonics and reflections. This approach proved especially effective for maintaining impedance continuity, making it suitable for high-frequency transmission lines in noise-sensitive systems. The study contributed to the field by demonstrating how passive transmission line components can be engineered to offer broadband attenuation while maintaining impedance matching.

Vasjanov and Barzdenas (2021) investigated the effects of asymmetric dielectric stack-ups on microstrip impedance compensation using reference-plane cutouts. Their study evaluated multiple multilayer PCB configurations that replicate real world manufacturing scenarios, from high end dielectric laminates to cost-optimized FR4 hybrid stacks, aiming to maintain impedance control without major performance degradation. Through S-parameter measurements and validation with time-domain reflectometry (TDR), the authors demonstrated that asymmetric dielectric distributions and localized cutouts significantly influence impedance discontinuities and reflection coefficients. The results provide quantitative guidance for compensating impedance mismatches in multilayer PCB designs, offering practical insight into balancing performance and cost in high-frequency applications. This directly supports the optimization of FR4-based microstrip structures in this project, where layer asymmetry and dielectric transitions are critical for impedance integrity.

Zhang et al. (2010) proposed an effective approach to characterize frequency-dispersive sheet materials over a wide RF and microwave frequency range based on planar transmission line geometries and a genetic algorithm. S-parameters of a planar transmission line structure with a sheet material under test as a substrate of this line are measured using a vector network analyzer (VNA). The measured S-parameters are then converted to ABCD matrix parameters. With the assumption of TEM/quasi-TEM wave propagation on the measured line, as well as reciprocity and symmetry of the network, the complex propagation constant can be found, and the corresponding phase constant and attenuation constant can be retrieved. Attenuation constant includes both dielectric loss and conductor loss terms. At the same time, phase term, dielectric loss, and conductor loss can be calculated for a known transmission line geometry using corresponding closed-form analytical or empirical formulas. These formulas are used to construct the objective functions for approximating phase constants, conductor loss, and dielectric loss in an optimization procedure based on a genetic algorithm (GA). The frequency-dependent dielectric properties of the substrate material under test are represented as one or a few terms following the Debye dispersion law. The parameters of the Debye dispersion law are

extracted using the GA by minimizing the discrepancies between the measured and the corresponding approximated loss and phase terms. The extracted data is verified by substituting these data in full-wave numerical modeling of structures containing these materials and comparing the simulated results with experimental.

Arar (2023) offered an accessible yet technically detailed explanation of stub-based impedance matching using the Smith Chart, covering single and double stub configurations applied to RF transmission lines. The article explains how placing a shunt or series stub at appropriate distances from the load enables impedance cancellation and perfect matching at target frequencies. It illustrates how one uses the Smith Chart to graphically locate normalized load points and determine stub lengths and positions for optimal VSWR and return loss. The work emphasizes stubs' reactive behavior as either inductive or capacitive depending on electrical length and termination. This resource serves as a clear, practical guide for designing matching networks on microstrip and stripline structures, especially relevant for low-cost FR4 PCB implementations.

Smith (1969) provided one of the most comprehensive early treatments of the Smith Chart, extending its application far beyond basic impedance matching into the realms of waveguide analysis, microwave circuit modeling, and component characterization. The book systematically integrates theoretical concepts with practical graphical methods for visualizing reflection coefficients, normalized impedance, and admittance transformations. Through detailed discussions of stub tuning, quarter-wave transformers, and impedance transformation networks, Smith demonstrated the chart's versatility in solving complex transmission line problems. Although originally tailored for coaxial and waveguide systems, the foundational principles of normalization and conjugate matching outlined in this work remain directly applicable to modern microstrip and stripline RF PCB design on substrates such as FR4.

Babic and Akyel (2021) introduced an analytical method for triple-stub matching configurations, where series-connected stubs are positioned at optimal distances from the load to achieve maximum power transfer between the source and mis-

matched load. The method provides explicit formulas for stub lengths and spacing, as well as conditions under which a unique matching solution exists. Verified using standing wave ratio (SWR) metrics, their approach offers increased bandwidth and design flexibility over single-stub or double stub systems. This theoretical framework could directly inform the design of single, double, and triple stub networks on PCB substrates like FR4.

Liu et al. (2024) introduced a low-reflection tuning strategy for triple-stub waveguide networks, designed for real-time impedance matching in dynamic load conditions. They developed an improved input-impedance calculation method by adding correction factors to account for stub depth and loading effects. A novel tuning algorithm then sequences stub adjustments to suppress large reflections during tuning, validated using Smith Chart region segmentation. Results demonstrated stabilized S_{11} below $-15\,\text{dB}$ despite load mutations, illustrating a robust multi-stub matching methodology with minimal iterative tuning and enhanced bandwidth. This approach is directly applicable to microstrip stub networks and multi-stub matching strategies on PCB structures using FR4, and suggests how Smith Chart guidance can minimize high reflection events during tuning.

Papapolymerou et al. (2003) proposed a reconfigurable double-stub tuning network based on RF Micro-Electro Mechanical System (MEMS) switches to enable real-time impedance matching in adaptive RF front-end modules. The tuner employs two shunt stubs with MEMS-controlled susceptance values, permitting optimization over a wide impedance range for bands including DCS1800, UMTS, and WLAN. Fabricated prototypes demonstrated low insertion loss ($< 0.2\,\text{dB}$), high isolation ($> 30\,\text{dB}$), and a VSWR of $\leq 1.48:1$ across $1.8\,\text{GHz}$ to $5.9\,\text{GHz}$. This design integrates MEMS switches to dynamically configure stub admittances, enabling intelligent signal matching and harmonic tuning. This study contributes a deployable, high-performance solution for reconfigurable matching networks, with direct relevance to the multi-stub design approach on FR4 PCBs.

Grieg and Engelmann (1952) introduced microstrip transmission lines as a novel

technique for high-frequency signal propagation in the kilomegacycle (MHz) range. Their pioneering work established the fundamental structure of microstrip, a conducting strip over a dielectric substrate with a ground plane beneath, and analyzed its quasi-TEM mode behavior, field distribution, and loss characteristics. This publication marked a shift from bulky waveguide systems to planar, compact, and low-cost transmission lines, laying the groundwork for modern RF PCBs and integrated circuits. The principles established in this early work directly underpin the microstrip structures used in design and simulation of high-frequency lines on FR4 substrates.

Jarry and Beneat (2009) explored the design, modeling, and fabrication of miniaturized microwave and RF filters using fractal geometries and resonator miniaturization techniques. Their work is particularly relevant to space-constrained RF systems, where compact filter topologies must balance performance with size limitations. The book presents detailed case studies of planar filters employing folded stubs, meandered lines, and fractal layouts, offering insight into how geometric transformations can shift resonant frequencies and improve filter selectivity without increasing board area. These principles are closely related to the stub-based filtering and impedance control strategies employed particularly on FR4 substrates where real estate and fabrication precision are limited.

Pozar (2012) provides a comprehensive theoretical foundation for microwave transmission line analysis, including microstrip and stripline geometries, impedance matching, and scattering parameters. In his work *Microwave Engineering*, Pozar introduces the wave-based analysis framework using S-parameters, which is particularly useful for characterizing high-frequency circuits where traditional voltage-current analysis becomes impractical. His treatment of impedance matching techniques, such as quarter-wave transformers and stub tuners, is highly applicable to planar PCB-based RF designs. The book also provides practical insights into reflection coefficients, power transfer, and Smith Chart usage, all of which are essential to simulation and matching network design.

Ponchak and Katehi (1997) systematically analyzed open- and short-circuit terminated series stubs in finite-width coplanar waveguide (CPW) structures on silicon substrates. Their work combined full-wave electromagnetic modeling and experimental validation to characterize how stub termination and substrate properties (e.g., silicon conductivity, CPW dimensions) influence the reflection coefficient (S_{11}) and input impedance. Results demonstrated frequency-dependent behavior up to several gigahertz, with analytical models accurately predicting reactive stub input behavior across both open and short terminations. This study provides a foundational understanding of stub discontinuities and reactive tuning in planar CPW structures critical for the analysis and design of stub matching in FR4 PCB environments and high-speed interconnect layouts.

Cebik & W4RNL presented a comprehensive tutorial on single-stub matching techniques for transmission lines. The work systematically derives the underlying equations, illustrates the use of the Smith Chart to determine optimal stub lengths and positions, and provides worked examples for practical understanding. The tutorial emphasizes the pedagogical aspects of stub tuning, making it highly suitable for educational experiments and low-cost lab implementations. Its clear exposition and practical guidance are particularly relevant for designing and testing single-stub impedance matching networks on microstrip and stripline PCBs, including FR4-based substrates.

Zhang et al. (2012) investigated a hybrid stack-up approach for printed circuit boards (PCBs) targeting high-speed networking systems. The study addresses signal integrity challenges in high-frequency PCBs by selectively integrating low-loss dielectric materials near critical high-speed traces while retaining conventional FR4 for other layers. This approach minimizes signal attenuation, reduces crosstalk, and controls electromagnetic interference, all without incurring the cost of a full low-loss PCB. Their results, validated through both time- and frequency-domain simulations, show improved transmission characteristics, making the design particularly relevant for differential microstrip and stripline layouts in high-speed, sub-2 GHz to multi-GHz PCB applications.

Bharathi Bhat and Shiban K. Koul (1989) presented a foundational treatment of stripline and stripline-like transmission lines in their book *Stripline-like Transmission Lines for Microwave Integrated Circuits*. Their work provides detailed theoretical and practical guidance for designing embedded transmission lines with high field confinement, low radiation loss, and controlled impedance, making it particularly suitable for high-frequency multilayer PCBs. The authors analyzed both symmetrical and asymmetrical geometries, offering analytical expressions and design charts for determining key parameters such as characteristic impedance, effective dielectric constant, and attenuation. Their treatment of quasi-stripline configurations also addresses fabrication tolerances and integration issues common in microwave integrated circuits. This work remains highly relevant for modern PCB-based stripline and differential stripline designs, particularly in applications requiring compact routing and minimal electromagnetic interference, such as the FR4-based stripline structures explored in this project.

Rahman, Nielsen, and Samuel (2025) explored key design principles and challenges in achieving electromagnetic compatibility (EMC) in PCB layouts, particularly for high-speed and high-frequency circuits. Their work emphasizes trace spacing, grounding techniques, and differential pair routing, all of which directly impact signal integrity and mode suppression in differential microstrip and stripline structures. The study highlights best practices for mitigating unintended radiation, ensuring impedance continuity, and reducing common-mode interference, all crucial for reliable performance in RF environments.

Famoriji and Shongwe (2022) developed a comprehensive analytical model for characterizing and predicting transmission line behavior in printed circuit boards, focusing on microstrip channels fabricated on FR4 substrates. Their model examined the effects of via stub discontinuities, conductor loss, and dielectric dispersion on signal integrity. Using analytical formulations and full-wave electromagnetic simulations, the study compared stub-discontinuous and stub-free configurations, demonstrating excellent agreement between the model and experimental results.

The proposed model effectively predicts attenuation and impedance characteristics, providing valuable insights for high-frequency transmission line design, modeling, and optimization on FR4 PCBs.

Ali et al. (2024) presented an advanced dielectric characterization of FR4 substrates using a free-space measurement technique validated through vector network analyzer (VNA) data. By employing the Nicholson-Ross-Weir algorithm within the 8.5 GHz to 11.5 GHz frequency range, they accurately extracted the relative permittivity and loss tangent of FR4. The measured data closely matched simulation results, confirming the material's suitability for mid-GHz applications. This work provides a reliable experimental framework for verifying dielectric parameters used in electromagnetic simulations of FR4-based microstrip and stripline transmission lines.

Duan et al. (2009) investigated the electromagnetic (EM) emissions produced by differential signals traversing between connected PCBs in the gigahertz band. Their experimental setup examined differential pair routing across board interconnects and measured far-field emissions to assess how inter-board connections contribute to radiation. The study showed that discontinuities at board edges, gaps between boards, and connector-induced mode conversion significantly influence emission levels, even when differential currents are presumed balanced. The authors discussed mitigation strategies such as tight coupling, return path continuity, and shielding between boards. Their findings are relevant for your project's differential microstrip and stripline designs on a multilayer FR4 board, especially when considering connector interfaces, transitions, and common-mode leakage across board boundaries.

Archambeault et al. (2008) presented a systematic design methodology for synthesizing power distribution networks (PDNs) on multilayer printed circuit boards (PCBs), emphasizing practical approaches for noise control and signal integrity enhancement. The study addressed key challenges such as determining the optimal number and placement of decoupling capacitors, minimizing loop inductance, and managing resonant behavior between power and ground planes. Through analytical

modeling and experimental validation, the authors demonstrated how proper PDN synthesis can ensure stable reference planes and reduce electromagnetic interference (EMI) in high-speed digital and RF circuits. The proposed design flow improves voltage stability and mitigates coupling between PDN and signal layers. This work is directly relevant to high-frequency transmission line design, such as microstrip and stripline structures on FR4 substrates, where PDN stability significantly influences impedance control and noise performance.

Mondal et al. (2007) conducted an electrical analysis of multi-board PCB systems employing differential signaling, accounting explicitly for non-ideal common ground connections. Their work showed how imperfections in the ground paths, such as finite impedance, ground loops, or conductor resistance can cause differential-to-common mode conversion, degrade signal integrity, and generate EMI across board interfaces. Through both modeling and measurement across interconnected boards, they demonstrated that the integrity of the common ground is as critical as differential trace symmetry for reliable high-speed operation. Their findings provide direct caution for multi-board or stacked PCB systems in your project, where you may have differential microstrip or stripline lines crossing board boundaries or sharing ground reference planes.

Gao & Zhang (2017) proposed an innovative method to suppress crosstalk between differential microstrip lines by exploiting mode mismatch between conventional transmission lines and spoof surface plasmon polaritons (SPPs). By introducing periodic structures that support SPPs, the authors demonstrated significant attenuation of unwanted coupling, enhancing signal integrity in high-speed circuits. This approach is particularly relevant for our project, where minimizing crosstalk between closely spaced differential traces is critical for maintaining signal quality.

Wu et al. (2014) explored the design of differential microstrip lines incorporating surface plasmon polaritons (SPPs) to achieve enhanced common-mode rejection. The study demonstrated that by carefully designing the periodic structures on the microstrip lines, it is possible to control the propagation characteristics of the SPPs,

leading to improved isolation between differential signals. This work provides valuable insights into advanced techniques for reducing common-mode noise in high-speed differential signaling.

Yu & Kam (2022) explored how ground-mesh asymmetry affects signal integrity in differential pairs routed over meshed grounds in flexible printed circuit boards (FPCBs). Recognizing that conventional meshes introduce asymmetric return paths and degrade performance, they proposed an offset mesh design that deliberately staggers the mesh pattern between top and bottom ground layers. Through both time- and frequency-domain simulations using HFSS, CST, and ADS tools, they showed that the offset mesh reduces mode conversion, intra-pair and inter-pair skew, and characteristic impedance variation. The offset mesh achieved more uniform insertion loss, reduced impedance variation (only $\sim 3\,\Omega$ vs $\sim 14\,\Omega$ in conventional mesh), and improved eye-diagram performance, enabling higher density differential routing without additional guard traces. This work is especially relevant when designing differential microstrip or stripline pairs over meshed ground layers (or cutout ground layers) in multilayer FR4 systems, since it offers a practical method to mitigate mode conversion and maintain signal integrity.

Carlsson (1994) examined crosstalk phenomena between parallel conductors on printed circuit boards (PCBs) and multiconductor cables. The study employed a lumped-circuit equivalent model and derived per-unit-length parameters to analyze coupling effects between traces. Theoretical computations were validated through experimental measurements and exact multiconductor transmission line equations. Several PCB layouts were evaluated to demonstrate how design geometry and trace configuration influence crosstalk levels, providing practical insights into minimizing electromagnetic interference in multilayer PCB designs. This work is highly relevant to understanding coupling and signal integrity in differential and single-ended microstrip structures.

Caverly (2021) explored the use of low-cost Vector Network Analyzers (VNAs), such as nanoVNAs, in undergraduate RF and wireless circuit laboratories. The

study demonstrates how these affordable VNAs, capable of measuring S-parameters up to 3GHz, can be integrated into hands-on experiments to visualize impedance matching, reflection coefficients, and transmission line behavior. Results indicate that even budget VNAs provide effective learning experiences, enhancing student understanding of high-frequency signal propagation, Smith Chart interpretation, and practical RF concepts. This approach aligns with multi-layer PCB design studies, particularly for testing stub responses and transmission line mismatches in laboratory setups.

2.9 Research Gap

Although numerous studies have examined the design and analysis of transmission lines for RF and microwave applications, key limitations still persist in the existing body of work. Early studies such as Grieg and Engelmann (1952) and Smith (1969) established the theoretical foundations of microstrip lines and impedance matching, yet these works focused primarily on ideal or coaxial systems rather than printed circuit implementations on low-cost substrates. Later research, including Xu et al. (2014), Vasjanov and Barzdenas (2021), and Jarry and Beneat (2009), advanced the understanding of multilayer PCB transitions and compact filter topologies but often utilized specialized high-performance substrates (e.g., Rogers, LTCC) rather than conventional FR4 materials widely used in academic and industrial prototyping.

Similarly, while several studies such as Babic and Akyel (2021), Arar (2023), and Liu et al. (2024) have explored single, double, and triple-stub impedance matching networks, these were primarily modeled for waveguide or coaxial environments with limited consideration for planar PCB realizations. The lack of comprehensive simulation-based evaluation of multiple stub configurations, particularly on FR4 substrates below 2 GHz represents a notable gap in understanding matching behavior in practical PCB systems.

Hence, this project addresses these gaps by focusing on the simulation, analysis, and comparison of microstrip, stripline, and differential line structures, along with single, double, and triple-stub matching networks on a multilayer FR4 PCB substrate using HFSS. By combining impedance analysis, S-parameter evaluation, and

Smith Chart techniques, the study bridges theoretical and practical understanding of high-frequency transmission lines within the sub-2 GHz range on an educational and economically viable platform.

Chapter Three

Methodology

3.1 Introduction to Methodology

This chapter presents the systematic procedures adopted in the design, simulation, and analysis of the high-frequency transmission line experiment system. It outlines the methods used to translate the theoretical framework of transmission line principles into a practical PCB-based implementation. The approach integrates schematic design, layout development, and electromagnetic simulation to evaluate the performance of microstrip, stripline, and stub configurations. Emphasis is placed on achieving accurate impedance control, realistic modelling of high-frequency behaviour, and reliable validation through virtual measurement of S-parameters (Return Loss).

3.2 Research Design

3.2.1 Overview

This research adopted an experimental and simulation-based design approach. The methodology was structured to model, simulate, and analyze high-frequency transmission line structures on an FR4 PCB substrate. The study employed a quantitative approach, emphasizing measurable electrical characteristics such as impedance, reflection coefficient, and scattering parameters (S_{11}).

The research workflow consisted of three major phases: schematic design and PCB layout in Altium Designer, electromagnetic simulation in Ansys HFSS (serving as a virtual measurement environment), and analytical comparison with theoretical transmission line models. This design ensured a logical progression from conceptual

modeling to performance validation, enabling the accurate evaluation of microstrip, stripline, and stub-based configurations for RF and microwave educational experiments.

3.2.2 Design and Analysis Method

The design and analysis process utilized **Altium Designer** and **ANSYS Electronics Desktop.** Altium was employed for modeling and creating an impedance-controlled PCB layout, while ANSYS facilitated electromagnetic analysis to assess signal behavior and confirm the performance of the transmission structures developed.

Schematic-Level Modeling

The schematic-level modeling represents the initial phase of the system design, where all circuit components, electrical interconnections, and logical relationships were defined within Altium Designer. At this stage, the system was defined in terms of its electrical connectivity rather than its physical geometry. Each circuit element was logically represented and interconnected to establish a clear signal path and functional relationship before translating the design into the PCB layout stage.

Each transmission line configuration microstrip, stripline, differential microstrip, and differential stripline was classified into distinct net classes according to its experimental category and intended propagation mode. This classification ensured that related transmission structures were logically organized within the schematic, allowing for consistent rule assignment and enhancing the efficiency of signal integrity analysis during the PCB layout and simulation phases.

To enable simulation and future electromagnetic validation, schematic components such as SMA ports, the Balun IC for differential pairs, and transmission line models were mapped to their corresponding PCB footprints and simulation models. The schematic connections were carefully reviewed to ensure that all nets were properly defined and that each circuit element maintained a valid signal and ground reference.

This schematic-level modeling provided a hierarchical and error-free logical foundation for subsequent PCB layout design and EM-based performance analysis, en-

suring that each subsystem of the transmission experiment board was accurately represented for high-frequency operation.

PCB Layout Design

The Printed Circuit Board (PCB) layout design represents the physical realization of the schematic model and serves as the foundation for electromagnetic (EM) simulation. This stage involved defining the physical stack-up, assigning signal layers, and implementing controlled-impedance routing for various transmission line configurations. The layout process was carried out using Altium Designer, leveraging its integrated design environment to maintain synchronization between schematic connectivity and physical implementation.

Achieving true high-frequency transmission on a printed circuit board (PCB) requires that the electrical length of the transmission line be comparable to the operating signal wavelength. At low frequencies, the physical length of interconnections is much smaller than the wavelength ($l \ll \lambda$), and signals can be analyzed using lumped circuit models, where voltage and current are assumed uniform along the line. However, as the frequency increases and the line length becomes a significant fraction of the wavelength ($l \geq \lambda/10$), distributed effects such as signal delay, phase variation, reflection, and standing waves become dominant.

In this project, the printed circuit board (PCB) was designed to operate within the sub-2 GHz frequency range, where the guided wavelength on an Flame Retardant grade 4 (FR-4) substrate becomes comparable to the physical trace length. At these frequencies, transmission-line phenomena such as reflection, phase delay, and the formation of standing waves become significant, and the circuit can no longer be modelled as a lumped network.

As the electromagnetic wave propagates within the dielectric medium of the substrate rather than in free space, the signal velocity is governed by the effective dielectric constant of the structure. For Flame Retardant grade 4(FR-4) material, the relative permittivity (ε_{r}) is approximately 4.3. The propagation velocity and the guided wavelength were therefore determined using the relations:

$$\lambda_g = \frac{v_p}{f} \tag{3.1}$$

and the propagation velocity in the medium is

$$v_p = \frac{c}{\sqrt{\varepsilon_{\mathrm{r}}}} \tag{3.2}$$

where c is the speed of light in free space and f is the operating frequency.

The transmission line lengths were then selected to be a measurable fraction of λ_g, typically between $\lambda_g/4$ and $\lambda_g/2$ to allow the observation of resonance, reflection, and standing wave phenomena within the simulation environment.

This design approach ensured that each structure microstrip, stripline, and stub configurations demonstrated the fundamental behaviour of high-frequency propagation. By making the transmission lines electrically long, rather than electrically short, the Printed Circuit Board (PCB) was able to replicate the real-world conditions of Radio Frequency (RF) and microwave circuits. This allowed the experiment system to serve as an effective educational platform for understanding transmission line effects, impedance matching, and wave propagation in high-frequency applications.

Our propagating velocity will be

$$V_p = \frac{3 \times 10^8}{\sqrt{4.3}}$$

$$V_p = 1.45 \times 10^8$$

The length of the transmission was designed at 1GHz and 2GHz frequency

Where

For 1GHz we have

$$\lambda_{1g} = \frac{1.45 \times 10^8}{1 \times 10^9}$$

$$\lambda_{1g} = 0.145m = 145mm$$

For 2GHz we have

$$\lambda_{2g} = \frac{1.45 \times 10^8}{2 \times 10^9}$$

$$\lambda_{2g} = 0.0725m = 72.5mm$$

The following outlines the experiments conducted on the transmission line:

1. **Microstrip Line**

   The microstrip line was designed on the FR-4 substrate in Altium Designer, where the line width corresponding to the target impedance was obtained using the built-in impedance calculator. The structure consists of a conducting trace on the top layer separated from the ground plane by a dielectric substrate.

2. **Stripline**

   The stripline section was also modelled in Altium Designer, with the conductor embedded between two parallel ground planes within the dielectric layer. The trace width was automatically computed by the software for the desired impedance, as manual calculation is complex due to field confinement within the substrate.

3. **Differential Microstrip Line**

   A differential microstrip pair was implemented on the PCB surface to support balanced-mode signal propagation. The spacing and width of the traces were determined using Altium's impedance control tool to achieve the required differential impedance, ensuring proper coupling and minimal crosstalk. This structure is particularly suitable for demonstrating high-frequency differential signalling on open-surface lines.

4. **Differential Stripline**

   The differential stripline pair was realised within the inner layers of the PCB, with both conductors symmetrically placed between two ground planes. The required impedance and spacing values were computed using Altium's field solver. This configuration provides excellent electromagnetic isolation.

5. **Transmission Line as an inductor:**

   Short circuit (S.C)

   The condition for an Inductor as a short circuit is $0 < L_{sc} < \lambda/4$

Let's take $L_{sc} = \lambda/10$

$L_{sc} = 7.25mm$ at 2GHz

$L_{sc} = 14.5mm$ at 1GHz

Open Circuit (O.C)

The condition for an Inductor as an open circuit is

$\lambda/2 < L_{oc} < \lambda/4$

Let's take $L_{oc} = 3\lambda/8$

$L_{oc} = 27.2mm$ at 2GHz

$L_{oc} = 54.4mm$ at 1GHz

6. **Transmission as a Capacitor:**

   Short circuit (S.C)

   The condition for Capacitor as short circuit is

   $\lambda/2 < L_{sc} < \lambda/4$

   $L_{sc} = 27.2mm$ at 2GHz

   $L_{sc} = 54.4mm$ at 1GHz

   Open Circuit (O.C)

   The condition for Capacitor as an open circuit is

   $0 < L_{oc} < \lambda/4$

   $L_{oc} = 7.25mm$ at 2GHz

   $L_{oc} = 14.5mm$ at 1GHz

7. **Transmission as parallel resonance circuit:**

   Use Open Circuit Transmission line at $L = \lambda/2$

   $L = 72.5/2 = 36.25mm$ at 2GHz

   $L = 145/2 = 72.5mm$ at 1GHz

8. **Transmission line as series resonant circuit:**

   Use Open Circuit Transmission line at $L = \lambda/4$

$L = 72.5/4 = 18.125mm$ at 2GHz

$L = 145/4 = 36.25mm$ at 1GHz

9. **Single Short Circuit Parallel/Shunt Stub Matching**

   $Z_L = (90 - 25j)ohms$ $Z_o = 50$ohms

   At 2GHz

   $L_s = 0.152 \times \lambda = 0.152 \times 72.5 = 11.02mm$

   $L_1 = 0.123 \times \lambda = 0.123 \times 72.5 = 8.9175mm$

   At 1GHz

   $L_s = 0.152 \times \lambda = 0.152 \times 145 = 22.04mm$

   $L_1 = 0.123 \times \lambda = 0.123 \times 145 = 17.835mm$

10. **Single Short Circuit Series Stub Matching**

    $Z_L = (0.5 + 1.5j)ohms$ $Z_o = 50$ ohms

    At 2GHz

    $L_s = 0.183 \times \lambda = 0.183 \times 72.5 = 13.2675mm$

    $L_1 = 0.146 \times \lambda = 0.146 \times 72.5 = 10.585mm$

    $Z_L = (50 + 30j)ohms$

    At 1GHz

    $L_s = 0.164 \times \lambda = 0.164 \times 145 = 21.17mm$

    $L_1 = 0 \times \lambda = 0$

11. **Single Open Circuit Shunt Stub Matching**

    $Z_L = (100 - 80j)ohms$ $Z_o = 75$ohms

    At 2GHz

    $L_s = 0.125 \times \lambda = 0.125 \times 72.5 = 9.0625mm$

    $L_1 = 0.272 \times \lambda = 0.272 \times 72.5 = 19.72mm$

12. **Single Open Circuit Series Stub Matching**

    $Z_L = (75 - 20j)ohms$ $Z_o = 75$ohms

At 1GHz

$L_s = 0.292 \times \lambda = 0.292 \times 145 = 42.34mm$

$L_1 = 0 \times \lambda = 0mm$

13. **Double Stub Short Circuit Series Matching**

$Z_L = (0.8 - 0.6j)ohms\ Z_o = 50\text{ohms}$

At 2GHz

$L_1 = 0$

$L_{s1} = 0.084 \times \lambda = 0.084 \times 72.5 = 6.09mm$

$L_2 = 0.375 \times \lambda = 0.375 \times 72.5 = 27.1875mm$

$L_{s2} = 0.038 \times \lambda = 0.038 \times 72.5 = 2.755mm$

14. **Double Stub Short Circuit Stub Matching**

$Z_L = (60 - 80j)ohms\ Z_o = 50\text{ohms}$

At 2GHz

$L_1 = 0.07 \times \lambda = 0.07 \times 72.5 = 5.075mm$

$L_{s1} = 0.133 \times \lambda = 0.133 \times 72.5 = 9.6425mm$

$L_2 = 0.125 \times \lambda = 0.125 \times 72.5 = 9.0635mm$

$L_{s2} = 0.164 \times \lambda = 0.164 \times 72.5 = 11.89mm$

At 1GHz

$L_1 = 0.07 \times \lambda = 0.07 \times 145 = 10.15mm$

$L_{s1} = 0.133 \times \lambda = 0.133 \times 145 = 19.285mm$

$L_2 = 0.125 \times \lambda = 0.125 \times 145 = 18.125mm$

$L_{s2} = 0.164 \times \lambda = 0.164 \times 145 = 23.78mm$

15. **Double Stub Short Circuit and Open Circuit Shunt**

$Z_L = (60 - 80j)ohms\ Z_o = 50\text{ohms}$

Short Circuit at 2GHz

$L_1 = 0.07 \times \lambda = 0.07 \times 72.5 = 5.075mm$

$L_{s1} = 0.133 \times \lambda = 0.133 \times 72.5 = 13.195mm$

Open Circuit at 2GHz

$L_2 = 0.25 \times \lambda = 0.25 \times 72.5 = 18.125mm$

$L_{s2} = 0.164 \times \lambda = 0.164 \times 145 = 8.14mm$

16. **Double Stub Open Circuit Shunt Stub**

$Z_L(\text{normalized}) = (0.5 - 0.625j)Z_o = 50\text{ohms}$

At 2GHz

$L_1 = 0.125 \times \lambda = 0.125 \times 72.5 = 9.025mm$

$L_{s1} = 0.425 \times \lambda = 0.425 \times 72.5 = 3.2625mm$

$L_2 = 0.375 \times \lambda = 0.375 \times 72.5 = 27.1875mm$

$L_{s2} = 0.134 \times \lambda = 0.134 \times 72.5 = 9.715mm$

At 1GHz

$L_1 = 0.125 \times \lambda = 0.125 \times 145 = 18.125mm$

$L_{s1} = 0.425 \times \lambda = 0.425 \times 145 = 6.525mm$

$L_2 = 0.375 \times \lambda = 0.375 \times 145 = 54.375mm$

$L_{s2} = 0.134 \times \lambda = 0.134 \times 145 = 19.43mm$

17. **Triple Stub Short Circuit and Open Circuit Shunt**

$Y_L(\text{normalized}) = (0.15 + 1.0j)Z_o = 50\text{ohms}$

Short circuit at 2GHz

$L_1 = 0.25 \times \lambda = 0.25 \times 72.5 = 18.125mm$

$L_{s1} = 0.17 \times \lambda = 0.17 \times 72.5 = 12.325mm$

$L_2 = 0.375 \times \lambda = 0.375 \times 72.5 = 27.1875mm$

$L_{s2} = 0.039 \times \lambda = 0.039 \times 72.5 = 2.8275mm$

Open Circuit at 2GHz

$L_3 = 0.25 \times \lambda = 0.25 \times 72.5 = 18.125mm$

$L_{s3} = 0 \times \lambda = 0 \times 72.5 = 0mm$

18. **Triple Short Circuit and Open Circuit Series Stub**

    $Z_L = (80 + 40j) ohms$ $Z_o = 50$ohms

    Short circuit at 1GHz

    $L_1 = 0.2 \times \lambda = 0.2 \times 145 = 29mm$

    $L_{s1} = 0.188 \times \lambda = 0.188 \times 145 = 27.26mm$

    $L_2 = 0.125 \times \lambda = 0.125 \times 145 = 18.125mm$

    $L_{s2} = 0.191 \times \lambda = 0.191 \times 145 = 27.695mm$

    Open Circuit at 1GHz

    $L_3 = 0.375 \times \lambda = 0.375 \times 145 = 54.375mm$

    $L_{s3} = 0.25 \times \lambda = 0.25 \times 145 = 36.25mm$

19. **Triple Short Circuit Shunt Stub**

    $Z_L = (60 - 80j) ohms$ $Z_o = 50$ohms

    At 2GHz

    $L_1 = 0.154 \times \lambda = 0.154 \times 72.5 = 11.165mm$

    $L_{s1} = 0.25 \times \lambda = 0.25 \times 72.5 = 18.125mm$

    $L_2 = 0.375 \times \lambda = 0.375 \times 72.5 = 27.1875mm$

    $L_{s2} = 0.062 \times \lambda = 0.062 \times 72.5 = 4.7125mm$

    $L_3 = 0.375 \times \lambda = 0.375 \times 72.5 = 27.1875mm$

    $L_{s3} = 0.048 \times \lambda = 0.048 \times 72.5 = 3.48mm$

20. **Triple Short Circuit Series Stub**

    Z_L(normalized) $= 3 - j$ $Z_o = 50$ohms

    At 1GHz

    $L_1 = 0 \times \lambda = 0mm$

    $L_{s1} = 0.25 \times \lambda = 0.25 \times 145 = 36.25mm$

    $L_2 = 0.375 \times \lambda = 0.375 \times 145 = 54.375mm$

    $L_{s2} = 0.053 \times \lambda = 0.053 \times 145 = 7.685mm$

$L_3 = 0.375 \times \lambda = 0.375 \times 145 = 54.375mm$

$L_{s3} = 0.066 \times \lambda = 0.066 \times 145 = 9.57mm$

21. **Impedance Mismatching**

In this design, transmission lines with characteristic impedances of 50 Ω and 75 Ω were utilized to illustrate the impact of impedance mismatch in high-frequency circuits. When two lines or components with different impedances are connected, a portion of the signal is reflected back toward the source, leading to power loss and signal distortion. This mismatch was deliberately incorporated into the board layout to enable the observation of reflection phenomena and standing wave patterns during experimental measurements.

22. **Impedance Matching**

In this design, transmission lines with characteristic impedances of 50 Ω and 75 Ω were utilized to illustrate the impact of impedance matching. This was approached using a quarter-wave transformer for line matching.

The quarter wave transformer uses a transmission line section with a specific characteristic impedance and Length to match two impedances which in this case it's between the 50ohms and 75ohms. The transformers impedance Z_t is given by:

$$Z_t = \sqrt{Z_1 Z_2} \tag{3.3}$$

Where $Z_1 = 50$ohms and $Z_2 = 75$ohms

$$Z_t = \sqrt{50 \times 75} = 61.24$$

The length of the transmission line has to be equal to a quarter of the wavelength ($\lambda/4$) at the the operating frequency.

i.e Length of transmission line $L_{TX} = \lambda/4$

With the operating frequency at 2GHz, $\lambda = 72.5mm$

Therefore $L_{TX} = 72.5/4 = 18.125mm$

To maintain high-frequency integrity, the design focused on proper ground referencing and minimizing discontinuities along the transmission paths. SMA connectors were accurately placed at the edges of the board to function as excitation and measurement ports, allowing direct access for simulation and potential hardware evaluation. Techniques such as copper pour and via stitching were utilized around signal traces to diminish parasitic effects and ensure uniform return paths for high-speed signals.

The final layout was validated through rule-driven checks to verify clearance, net connectivity, and stack-up adherence. This ensured that the PCB design faithfully represented the intended transmission structures and was prepared for electromagnetic analysis to extract its frequency-dependent characteristics.

3.3 Design Methodology

3.3.1 Flowchart of Methodology

The overall design and simulation procedure adopted in this work is illustrated in the flowchart shown in figure 3.1:

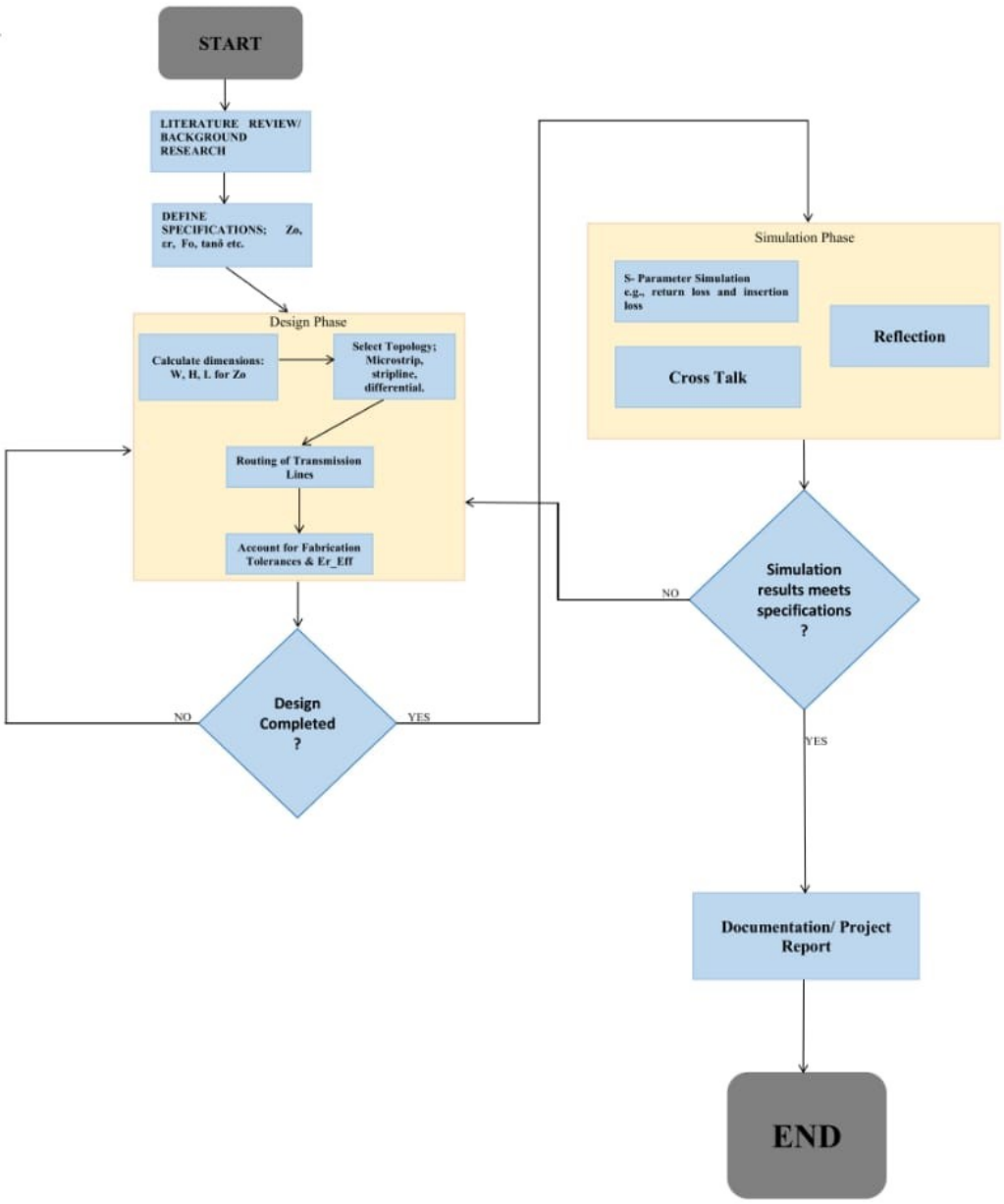

Figure 3.1: Flow Chart of Methodology

3.3.2 Printed Circuit Board Shape Redefinition and Rule Optimization

This stage defines the board's high-level architecture setup and design rules on Altium Designer.

1. **Project Setup**

(a) Open **Altium Designer Professional**

(b) In the menu bar, navigate to **File** → **New** → **Project** to define the workspace.

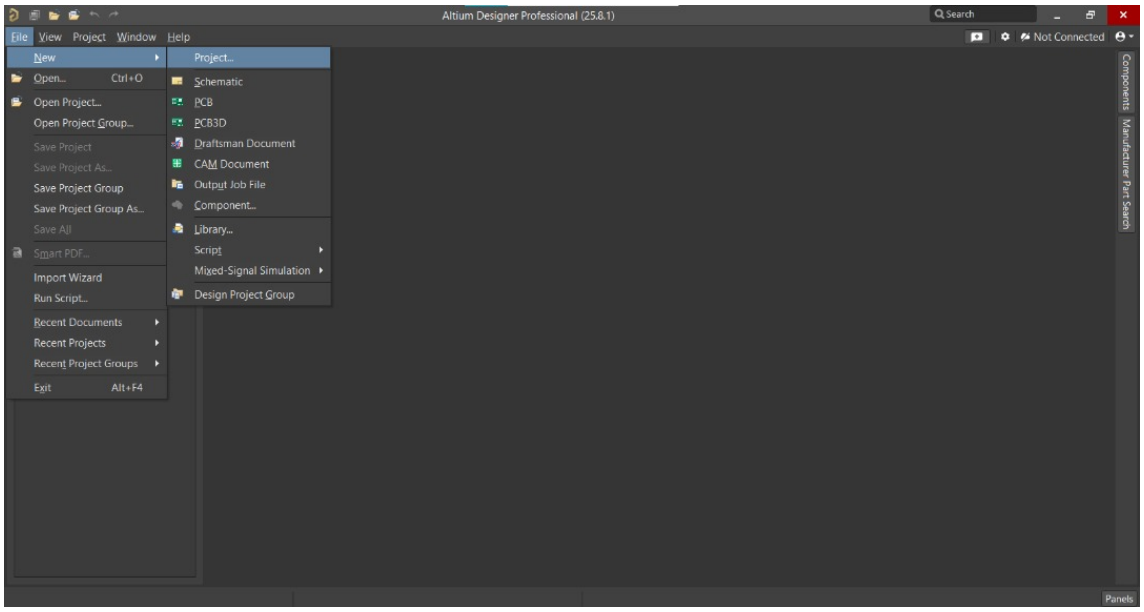

Figure 3.2: Setting up the workspace

(c) Input the project name and click **create** to create the project document.

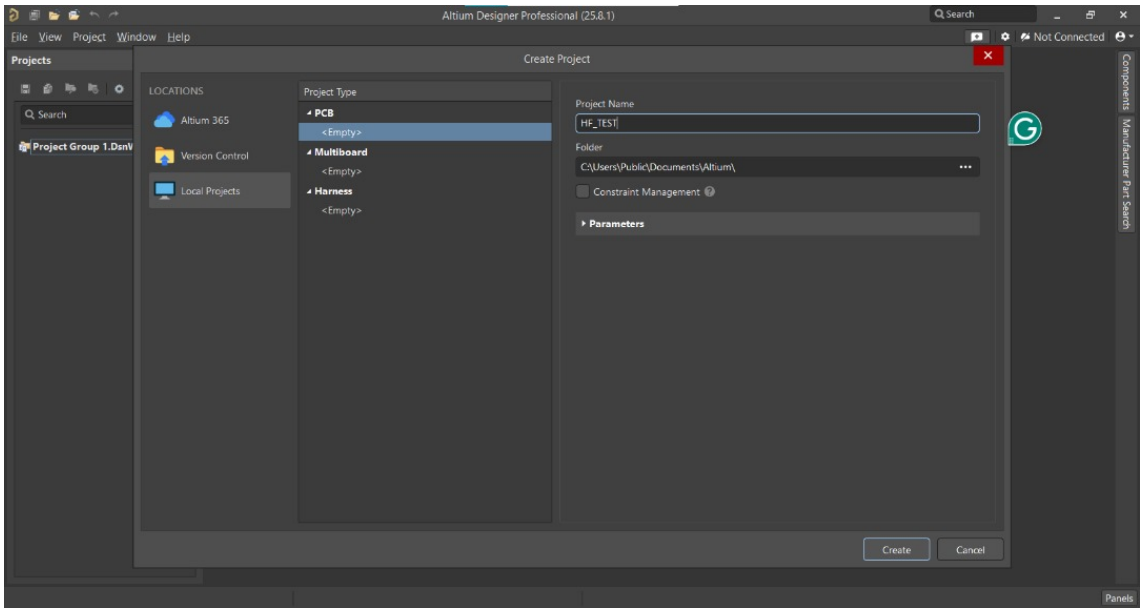

Figure 3.3: Input the project name

(d) Next, create a new schematic document and a new pcb document using the previous step.

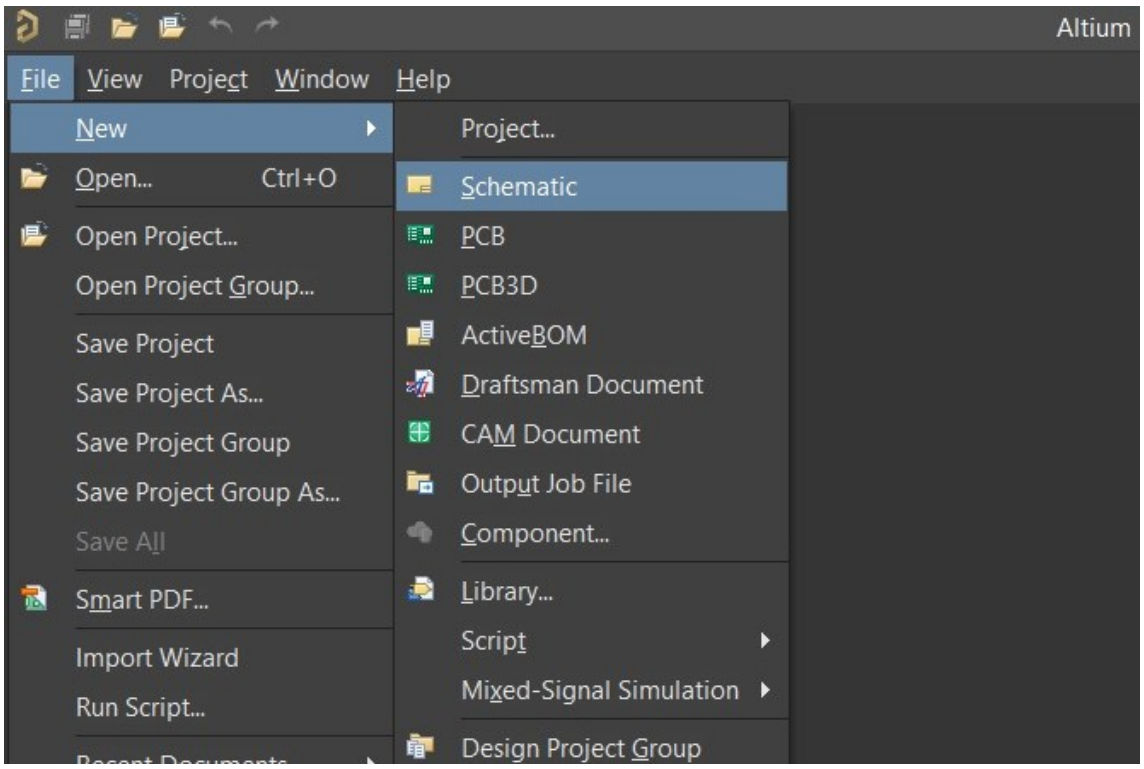

Figure 3.4: Create new schematic document

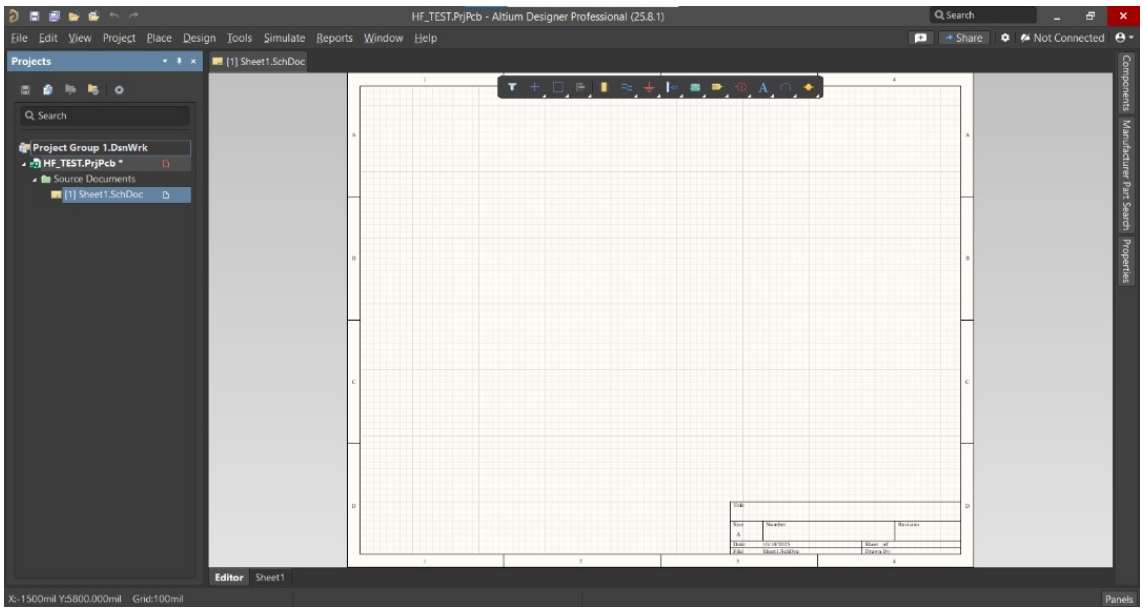

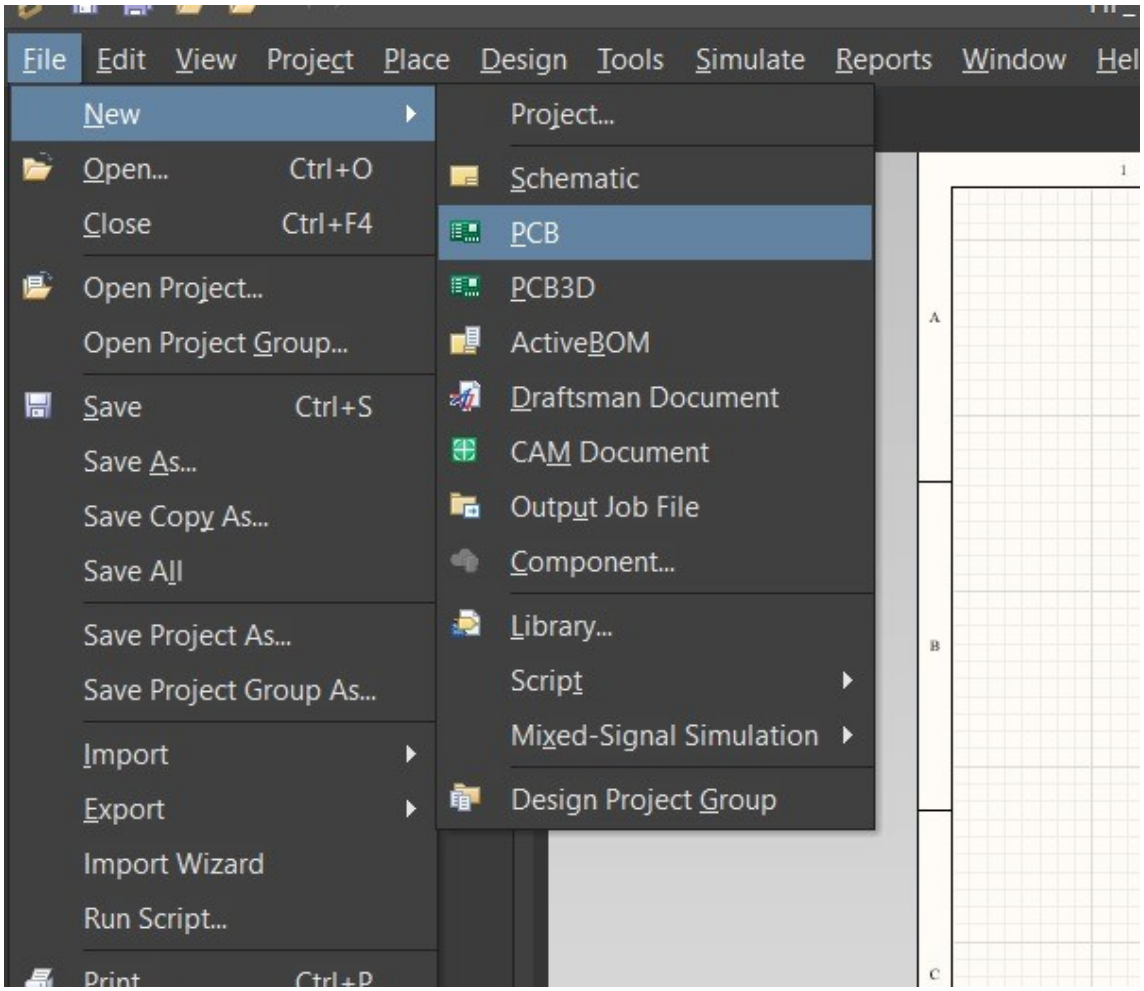

Figure 3.5: Create new PCB document

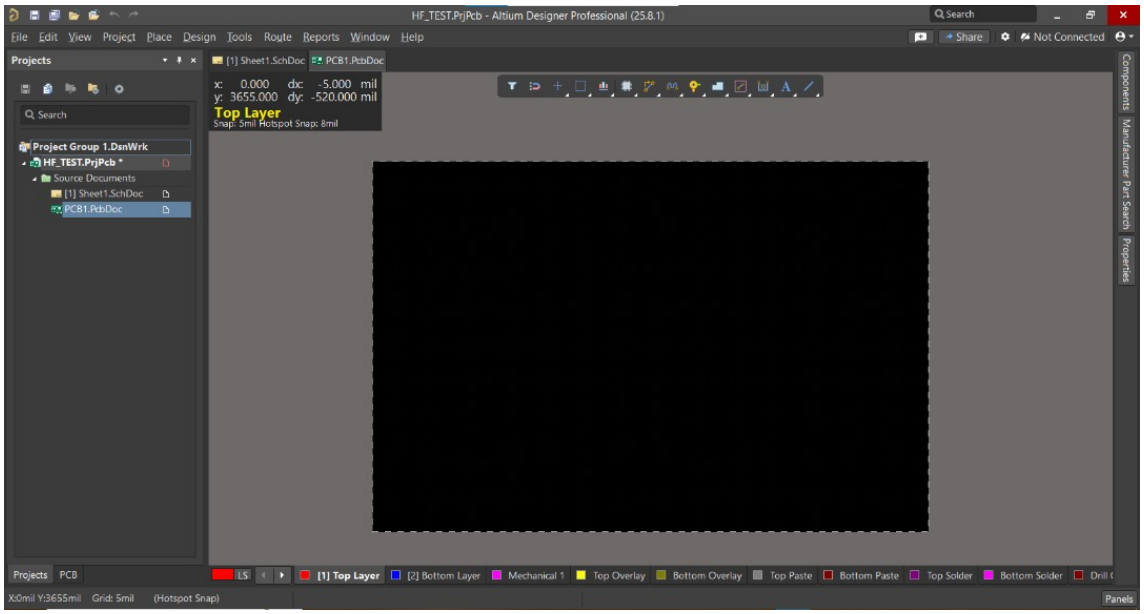

(e) Save the two documents using the name of the project to ensure and orderliness.

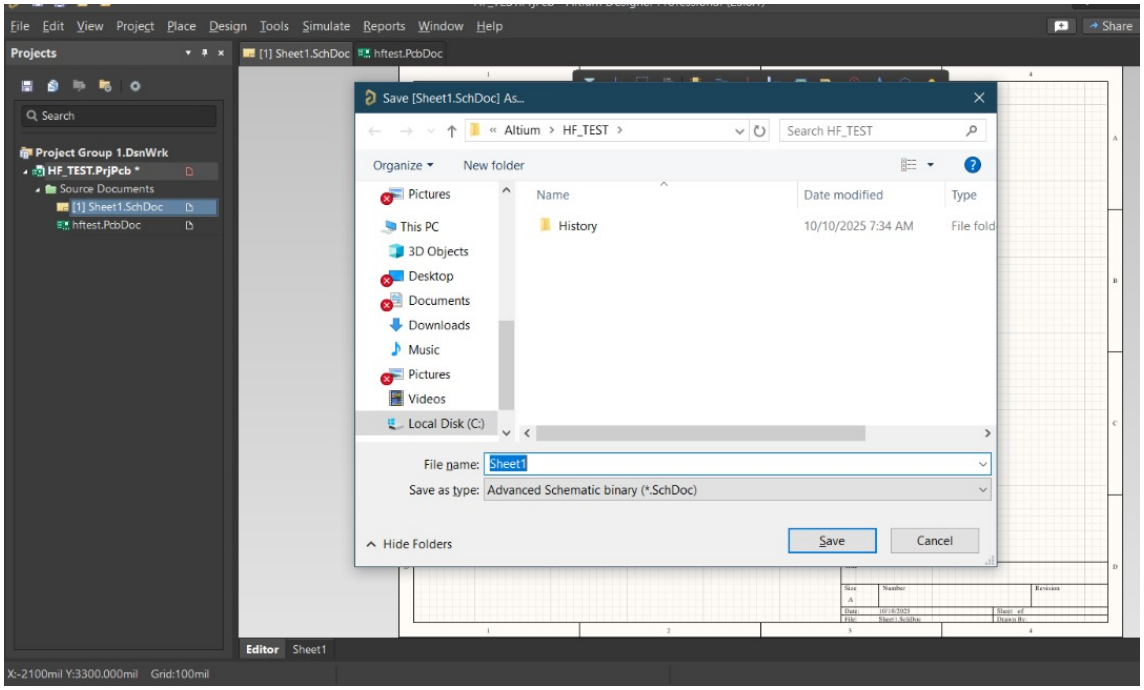

Figure 3.6: Save the two documents (i.e the schematic and PCB document)

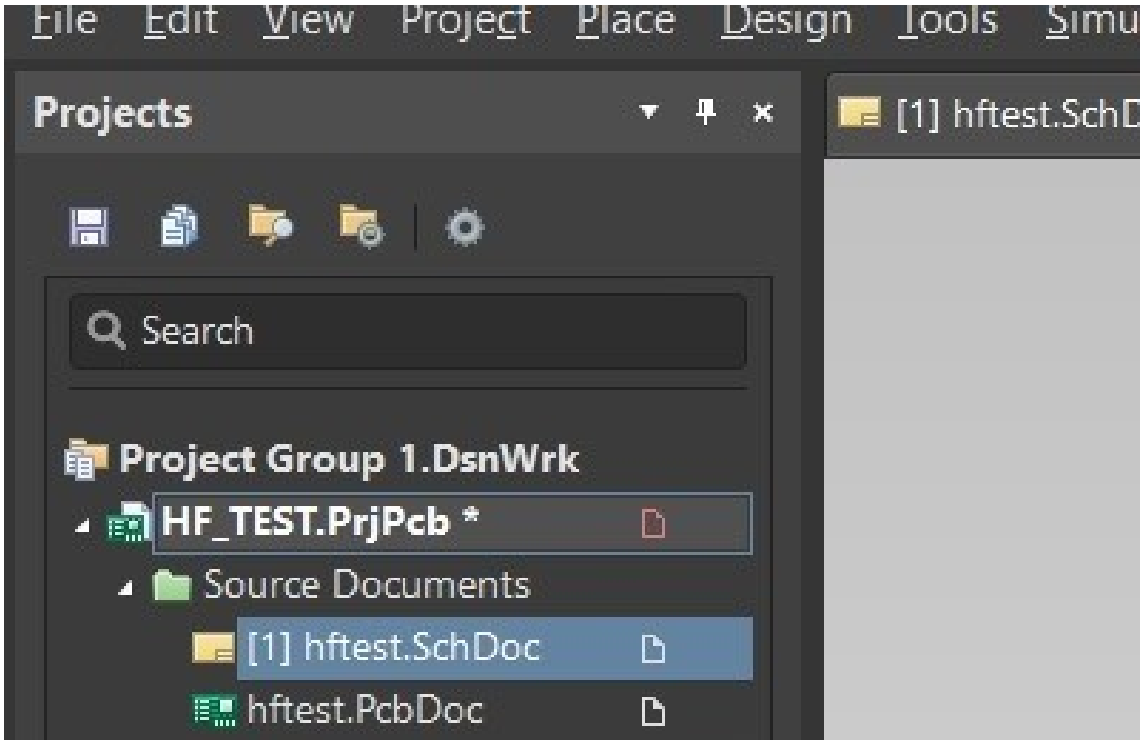

2. **Redefining the board shape**

(a) Change the dimension to **mm** using "spacebar + Q" and set your grid size to any grid of your choice in **mm** using "spacebar + G".

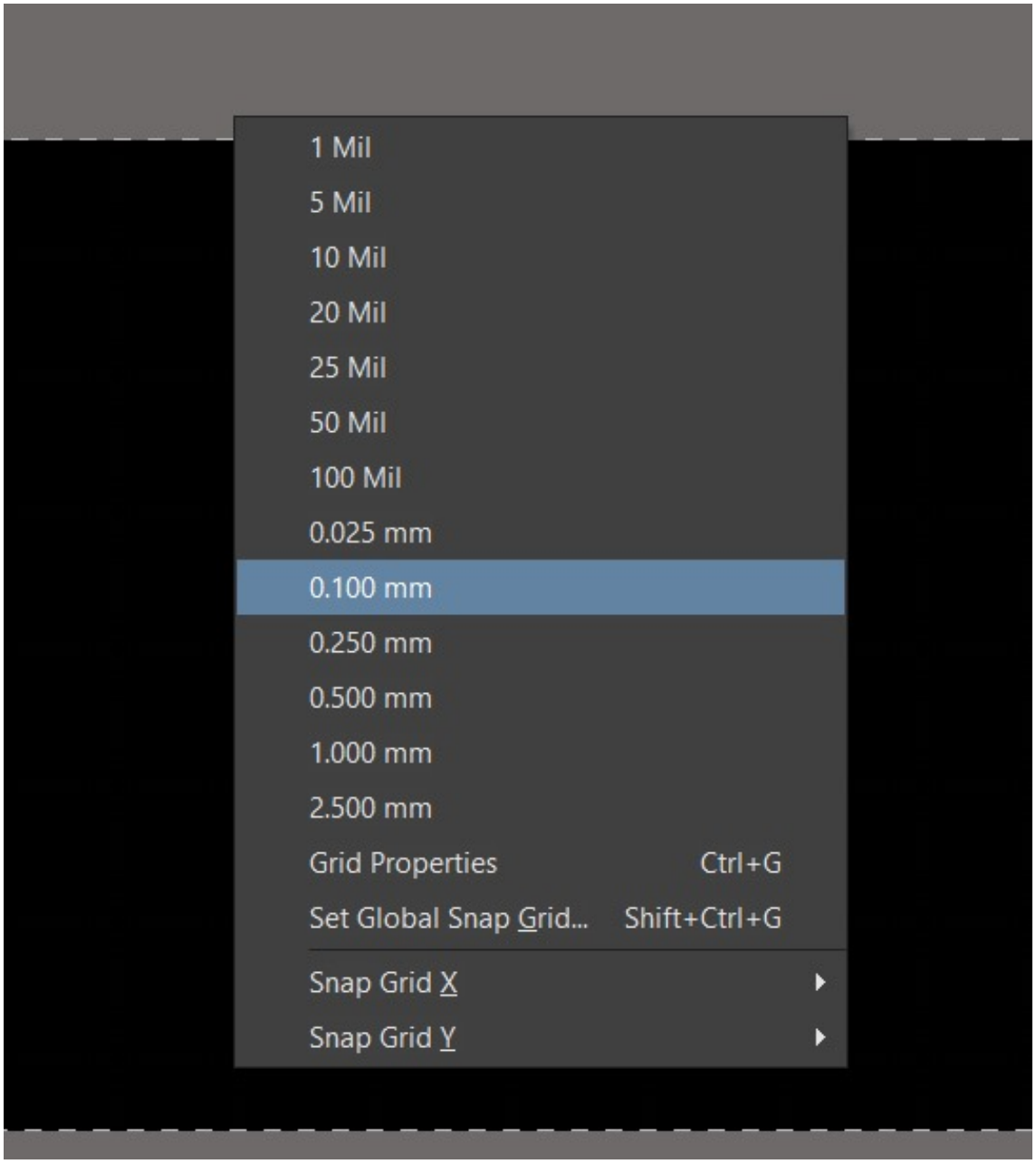

Figure 3.7: Change dimension and set grid size

(b) Set the origin of your pcb in order to redefine your board shape.

(c) In the menu bar, navigate to **Edit** → **Origin** → **Set** to define the origin of the board in 2D mode.

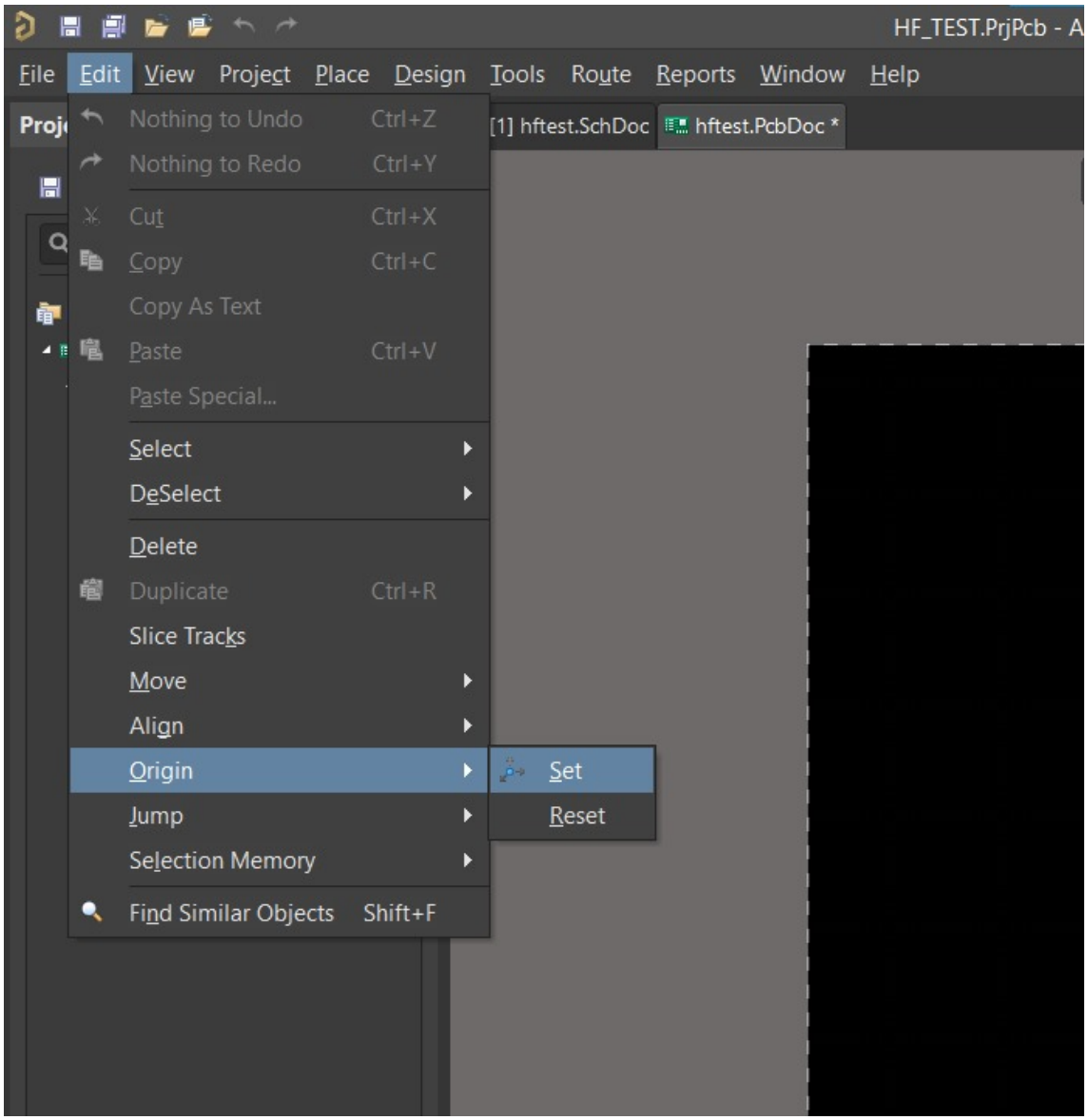

Figure 3.8: Set the Origin

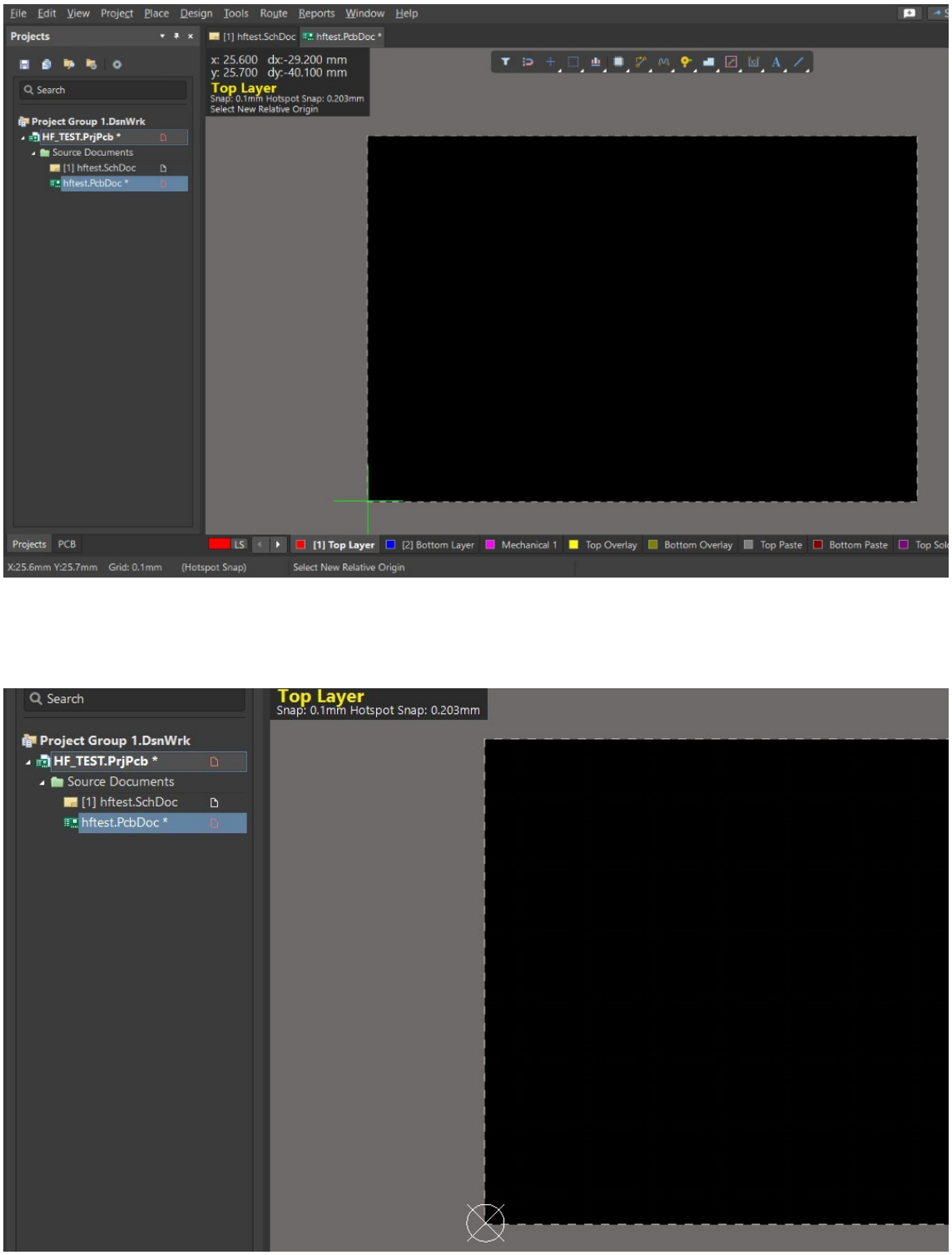

Figure 3.9: The new origin

(d) Enter the board planning mode using the shortcut by "pressing 1" or in the menu bar, navigate to **View → Board Planning Mode.**

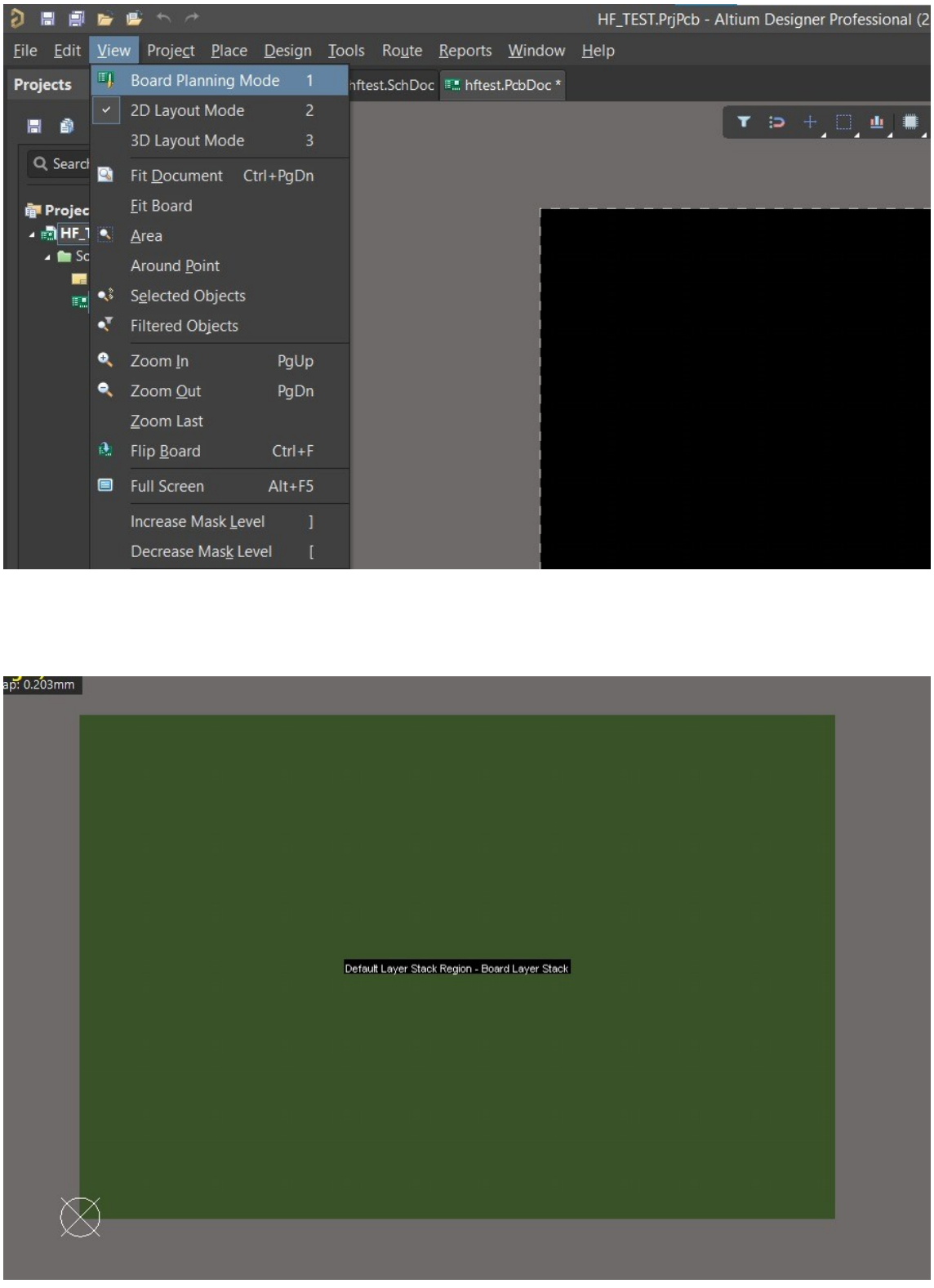

Figure 3.10: Board Planning Mode

(e) In the menu bar, navigate to **Design** → **Redefine Board Shape** to define the board size.

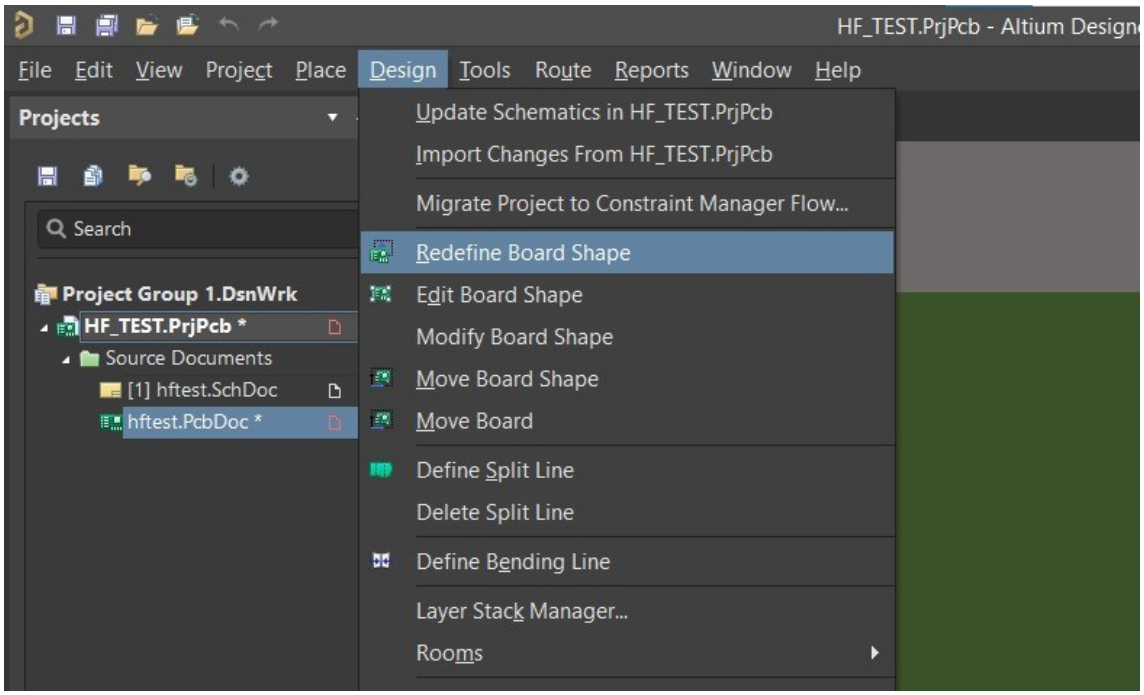

Figure 3.11: Redefining board shape and size

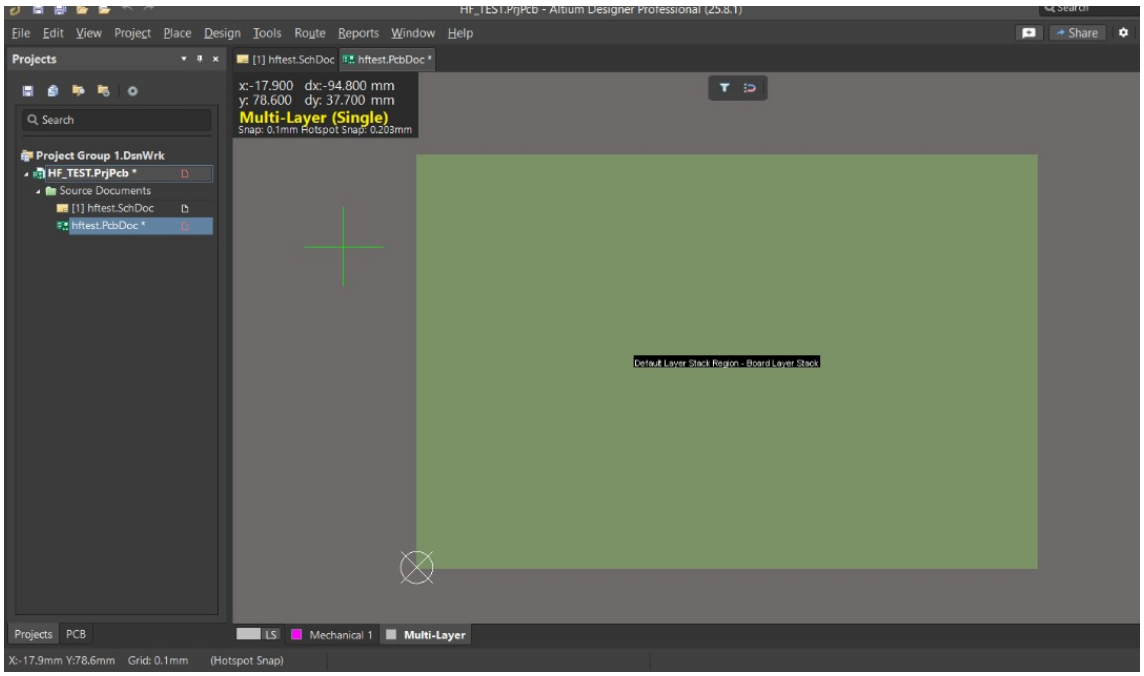

(f) Using "spacebar + J and spacebar + L", set the board dimensions.

(g) Press enter twice to define the first point at "x = 0mm and y = 0mm", which is set at the origin.

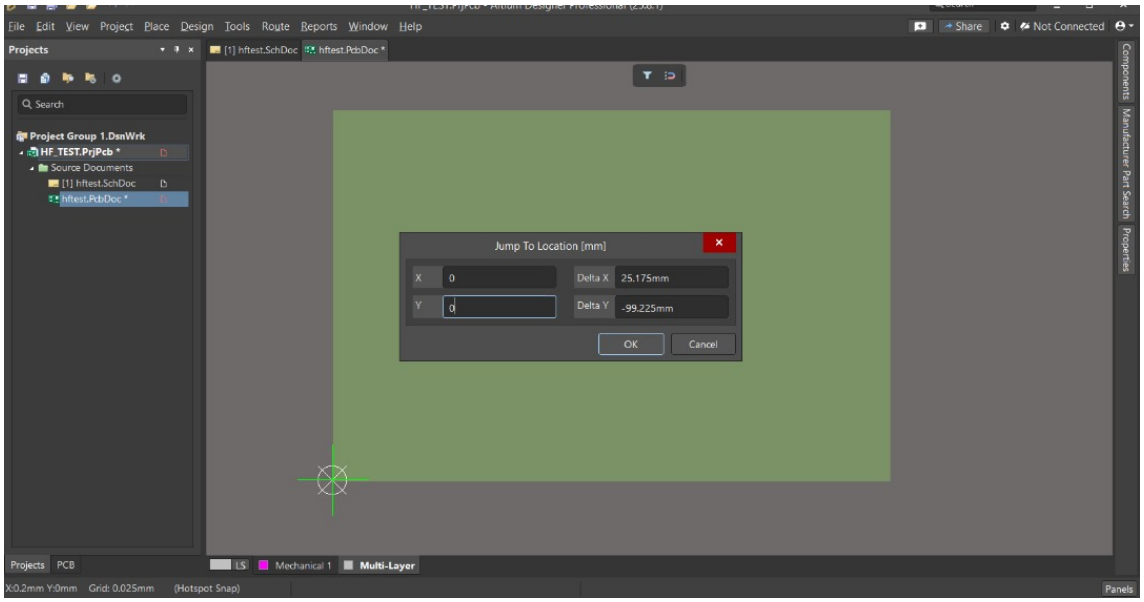

Figure 3.12: Set the board dimensions at first point

(h) Next, use "spacebar + J and spacebar + L" again to set the nest point.

(i) Press enter twice to define the second point at "x = 400mm and y = 0mm".

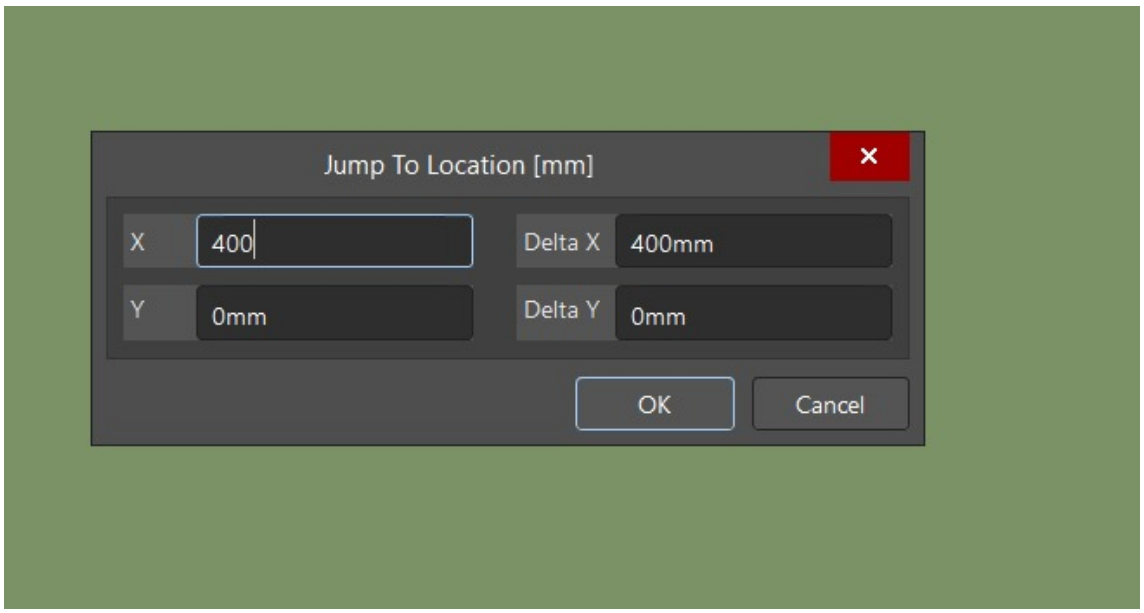

Figure 3.13: Set the board dimensions at second point

(j) Do the same for the third and fourth points at "x = 400mm and y =

400mm" and "x = 0mm and y = 400mm" respectively.

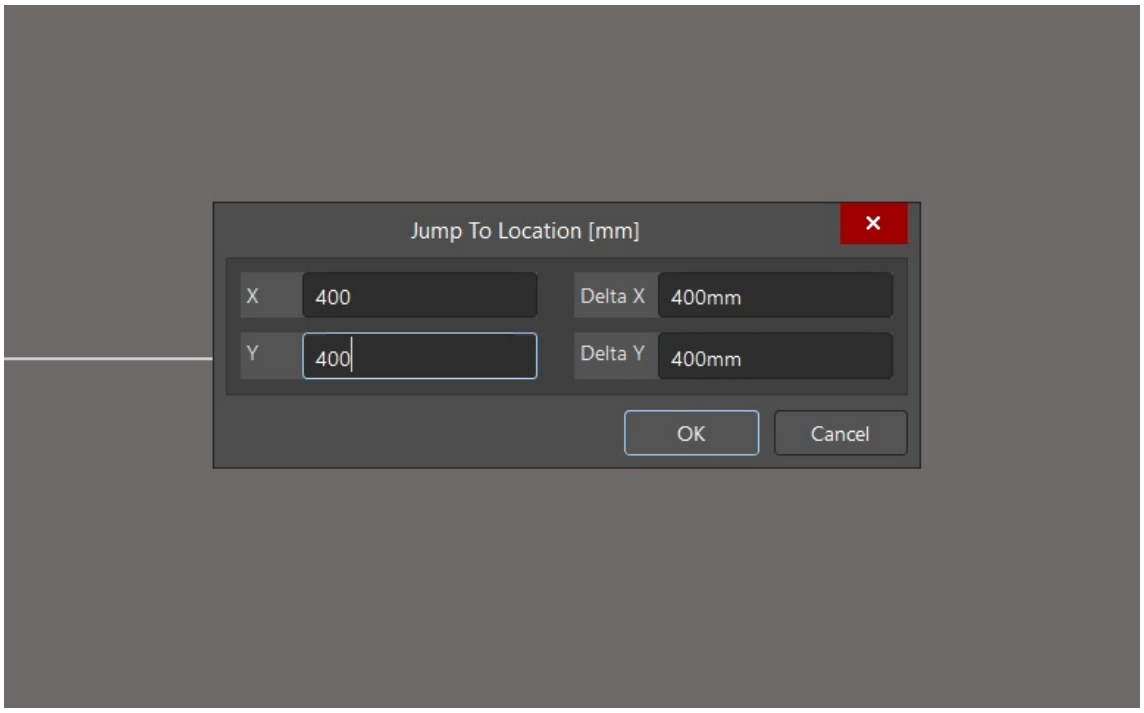

Figure 3.14: Set the board dimensions at third point

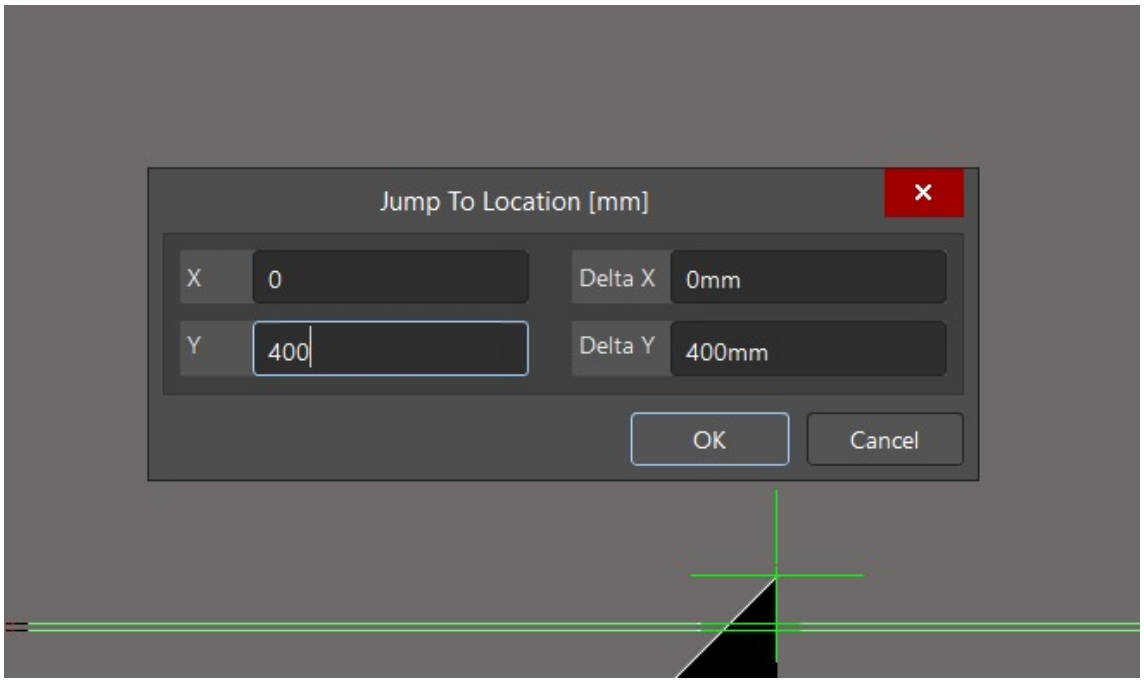

Figure 3.15: Set the board dimensions at fourth point

(k) Right click to remove the cursor to get the board shape (400mm x 400mm).

Figure 3.16: 400mm x 400mm Printed Circuit Board

(l) Next, Press 2 to go back to your PCB editor in 2D mode.

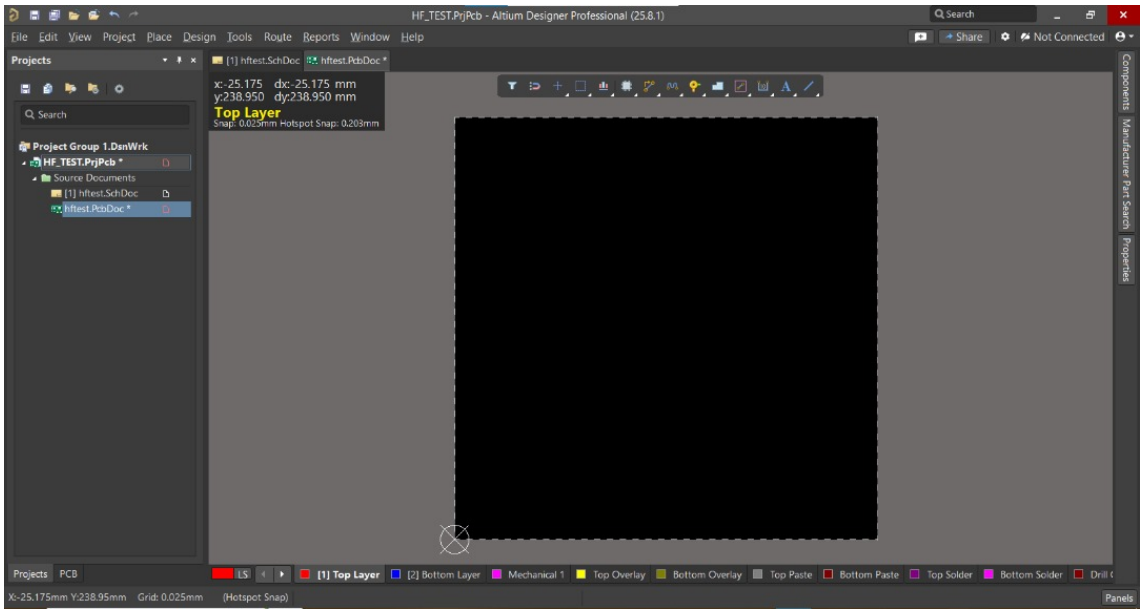

Figure 3.17: Printed Circuit Board (2D mode)

3. **Redefining the PCB Layer stackup**

   (a) In the menu bar, navigate to **Design** → **Layer stack manager** to enter the layer stack editor.

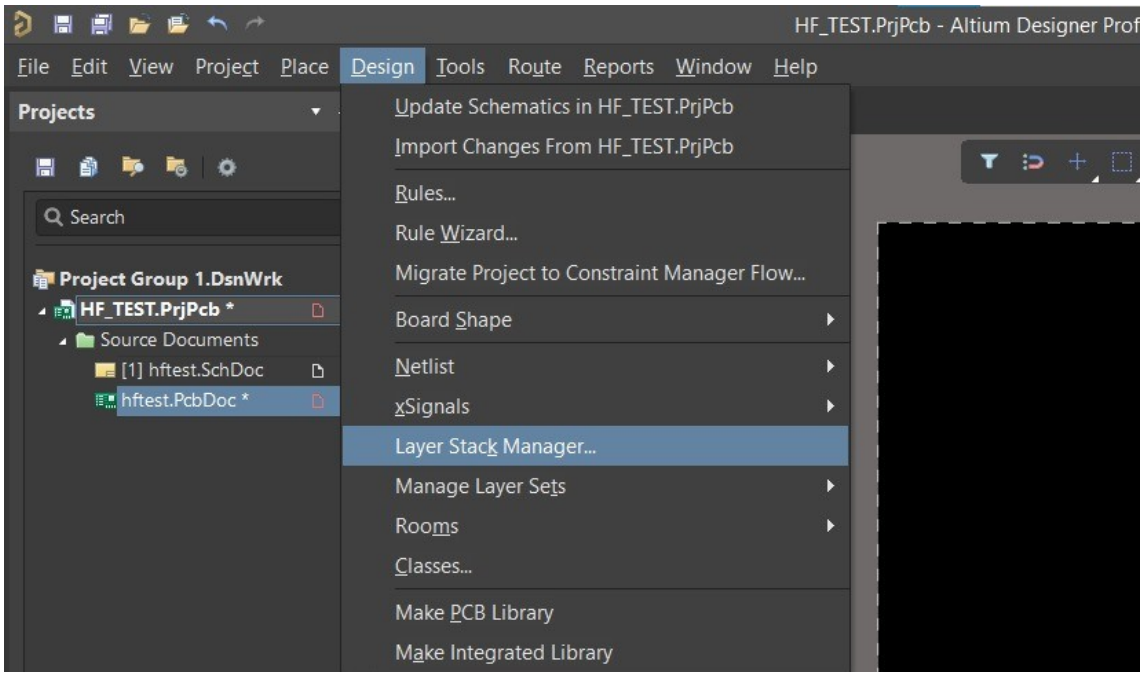

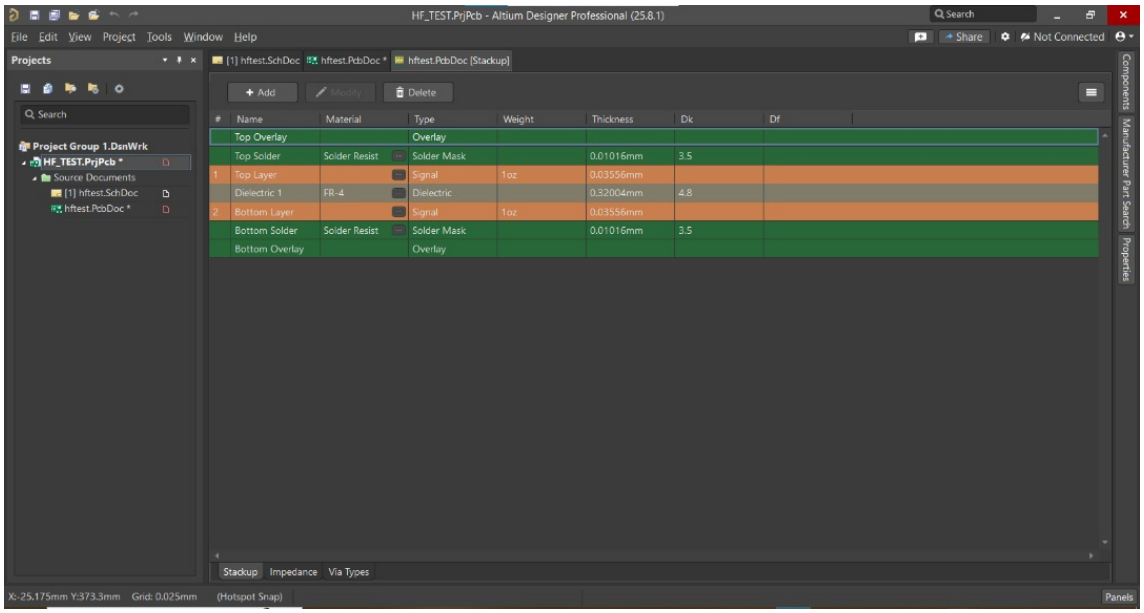

Figure 3.18: The Layer Stack Editor

(b) Use the **Add** button to add layers to your stack.

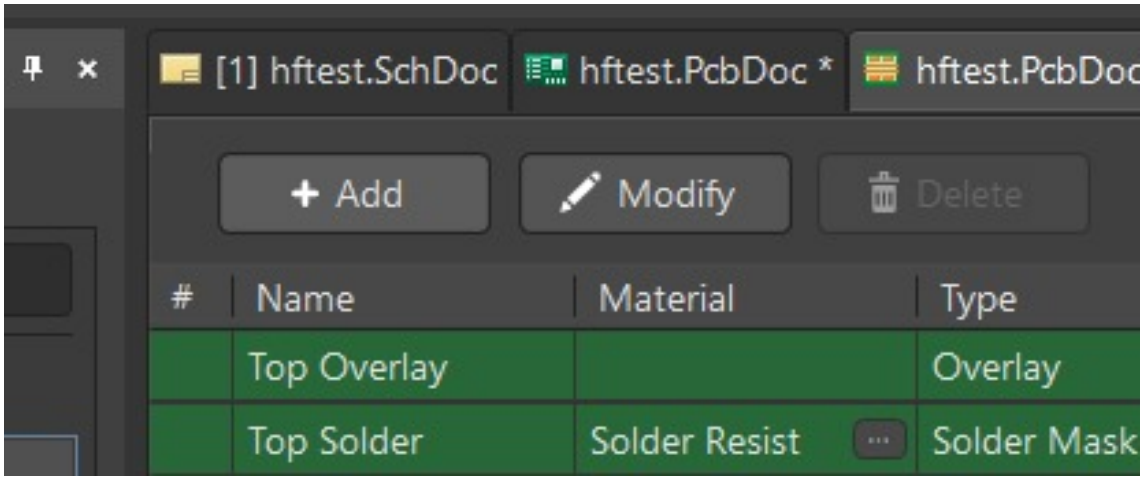

N.B: You can only add layers when you are in the stackup mode. This is at the bottom left corner of your screen.

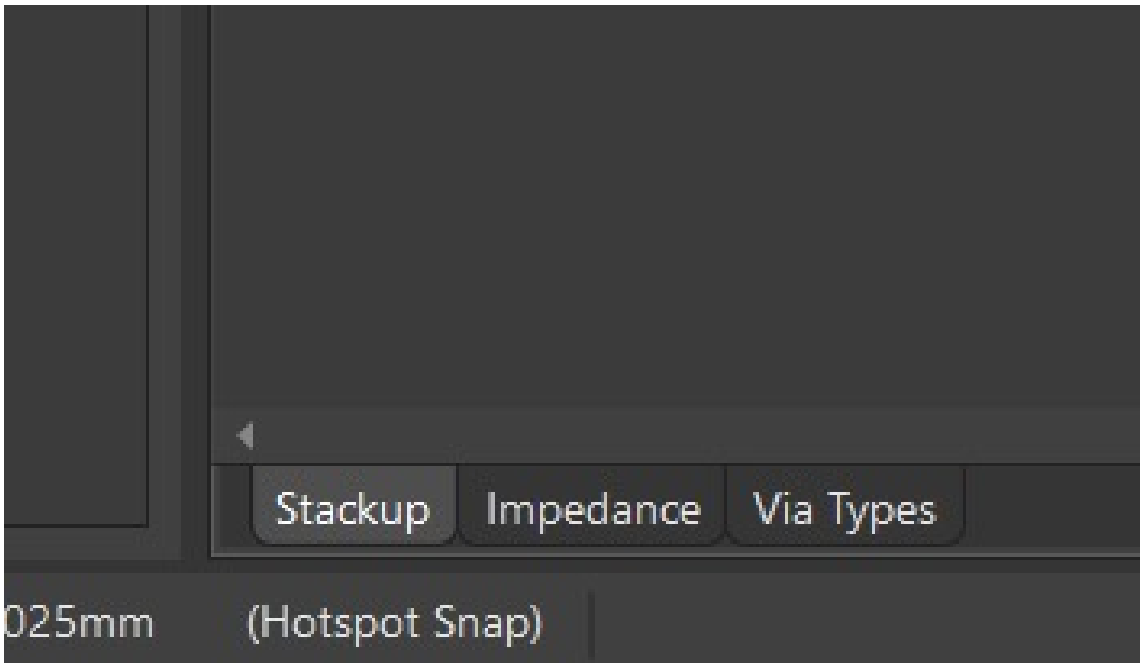

(c) After adding the layers, you can modify it based on your specifications (i.e. you can configure the name, material, type, weight, thickness, Dk and Df).

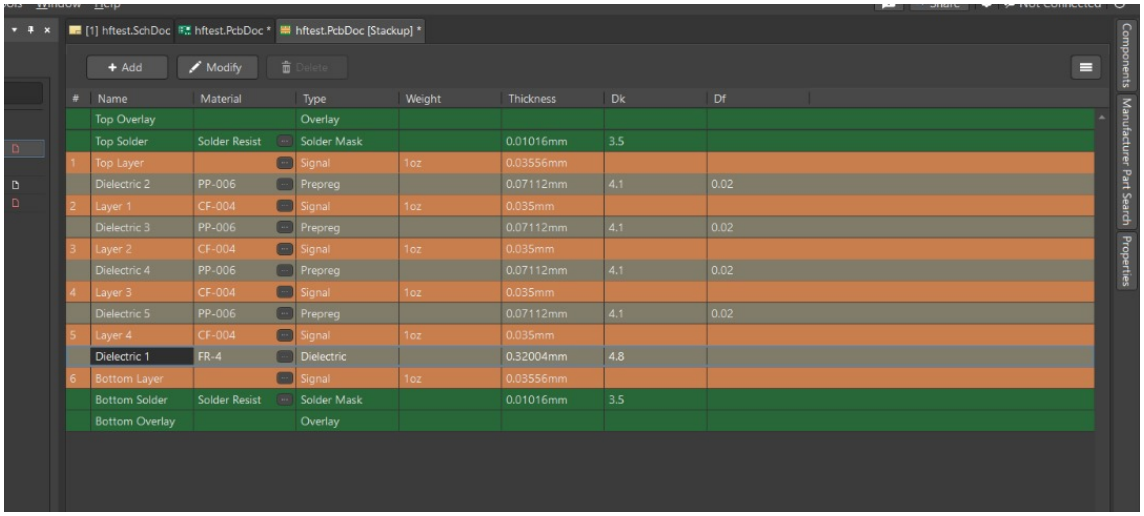

Figure 3.19: The Modified Layer Stack

4. **Setting up the Impedance Profile**

   (a) Click on impedance at the bottom left corner of the screen to add impedance profile.

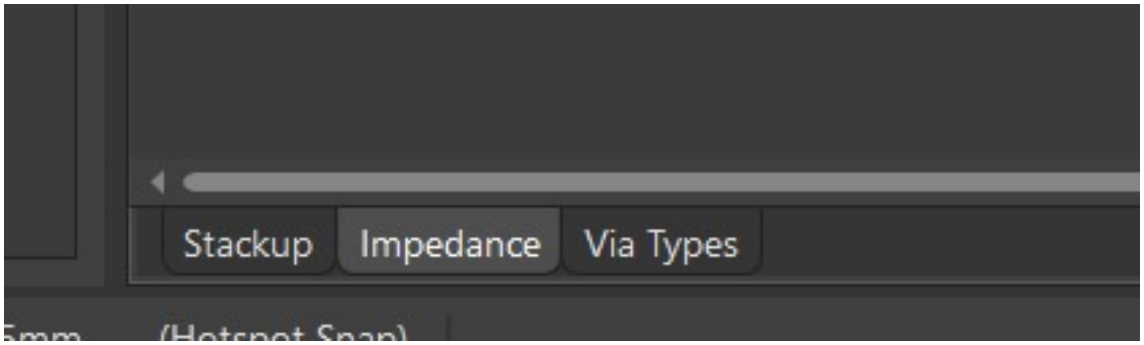

Figure 3.20: Impedance profile option

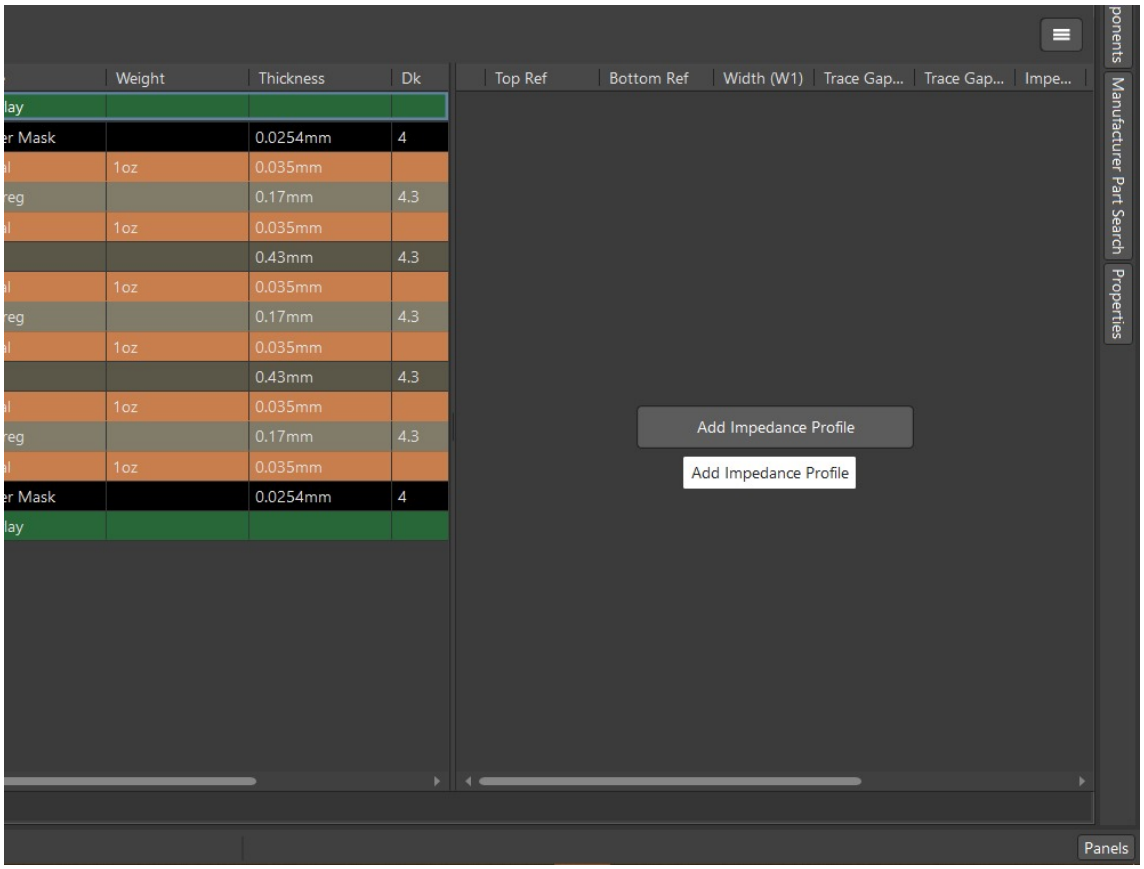

N.B: Impedance profile for different transmission lines are defined (i.e. 50 Ω microstrip, 50 Ω stripline, 100 Ω differential microstrip, 100 Ω differential stripline, 75 Ω microstrip and 25 Ω microstrip impedance profile).

(b) Uncheck all the boxes by the side and leave only the first box for microstrip and differential microstrip impedance profiles.

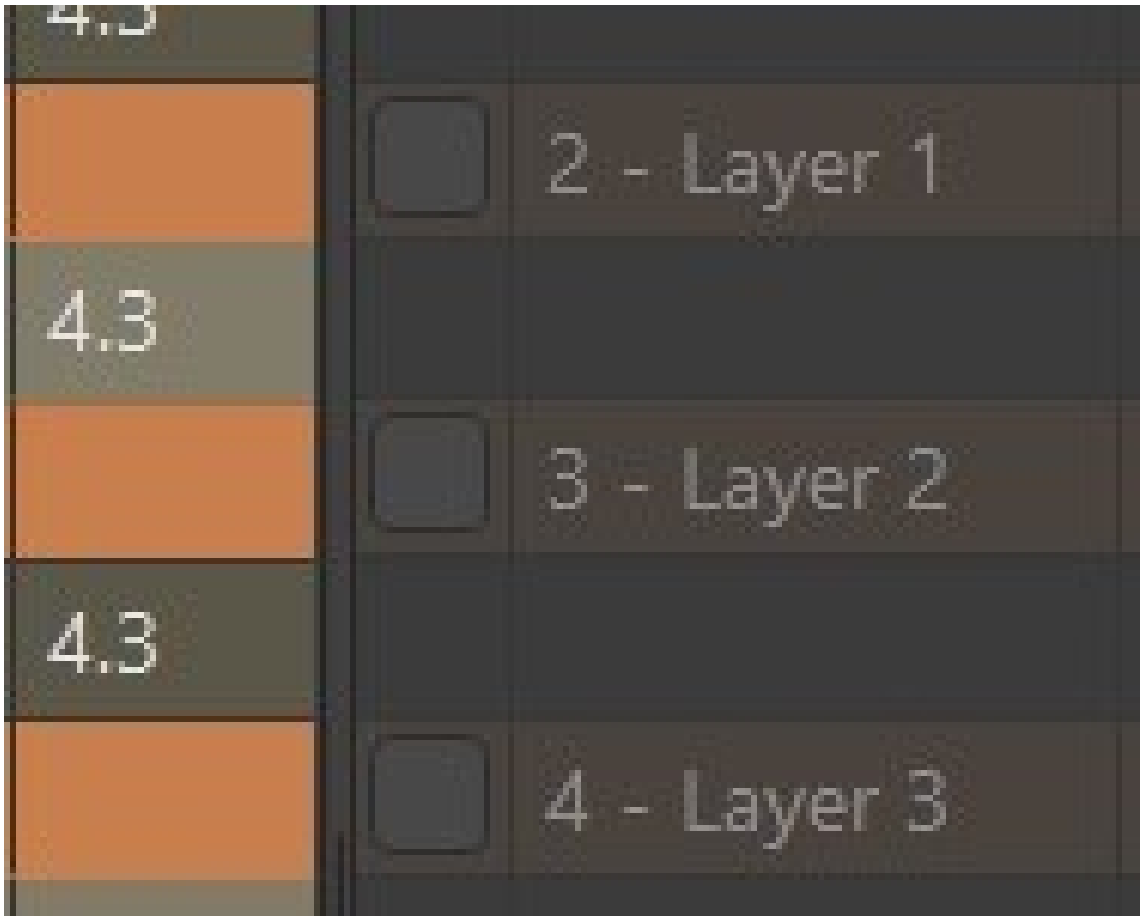

Figure 3.21: Unchecked boxes

(c) Define the $50\,\Omega$ single ended microstrip. Also, click on f_x.

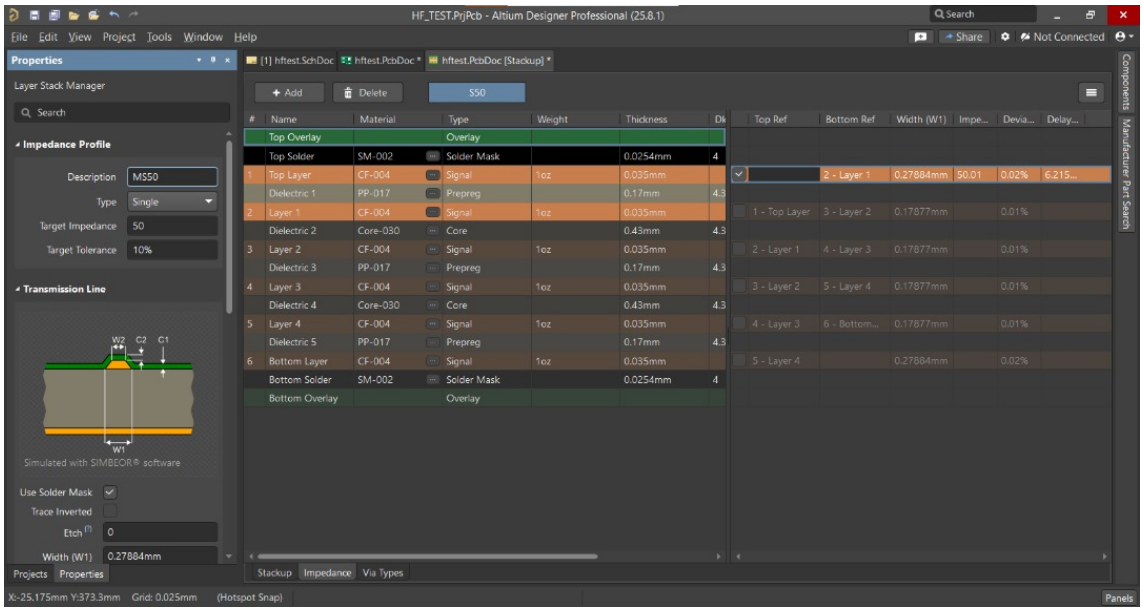

Figure 3.22: Microstrip impedance profile configuration

N.B: f_x helps calculate the width of the transmission line automatically, by clicking it.

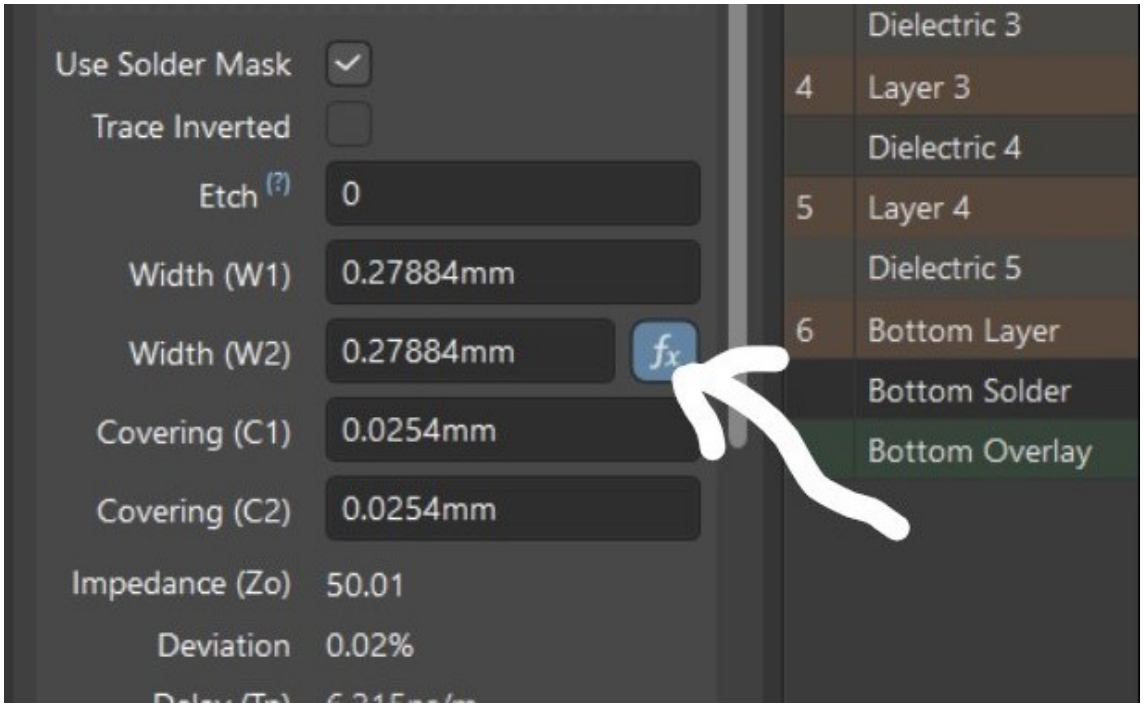

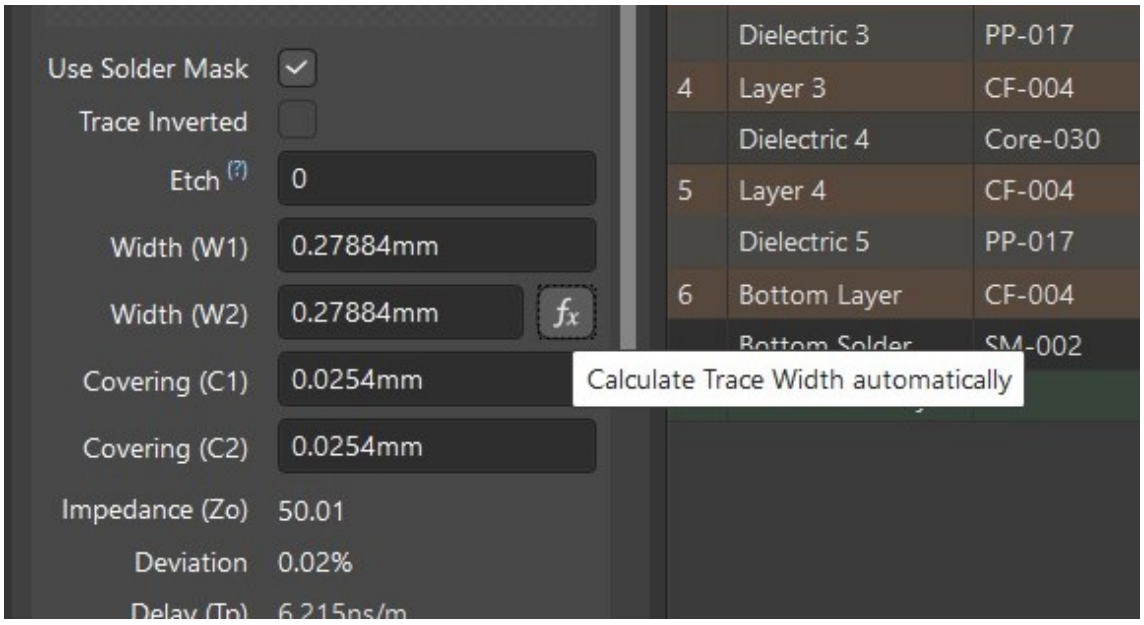

(d) After defining the first impedance profile, use the add button to add another impedance profile since you are on the impedance mode/option.

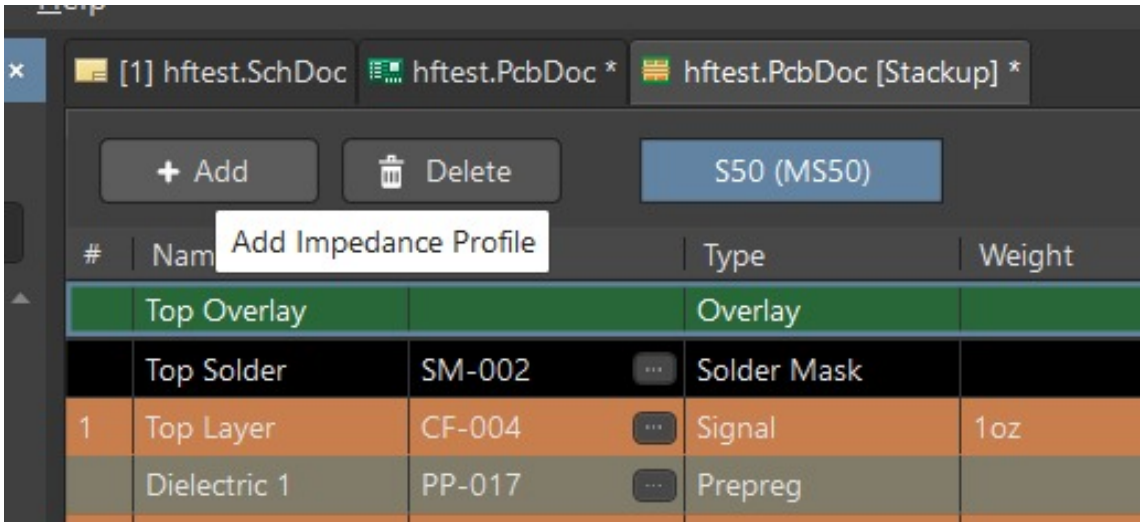

Figure 3.23: Add Impedance Profile

(e) Next, uncheck all the boxes by the side and leave only the second box when defining for stripline and differential stripline impedance profiles.

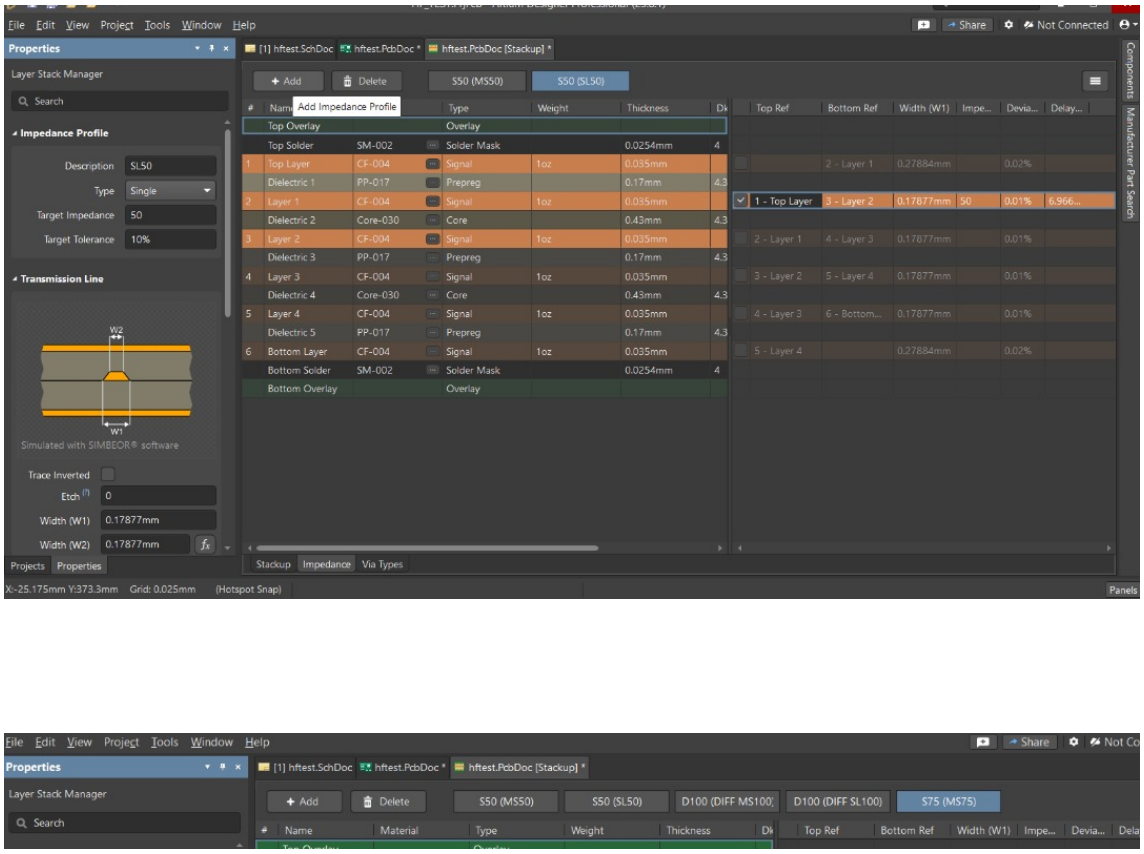

Figure 3.24: The impedance Profiles

5. **Setting up the Via Types**

   (a) Next, click on the via types option at the bottom of your screen to create the different via types.

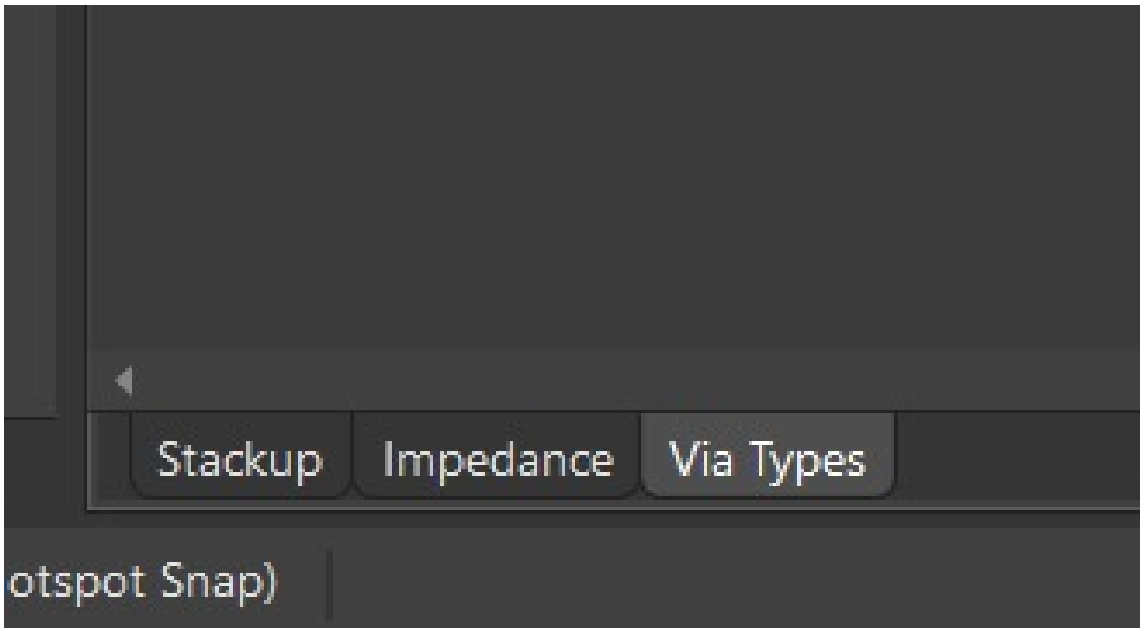

(b) Use add button to add via types since you are on the via types mode/option.

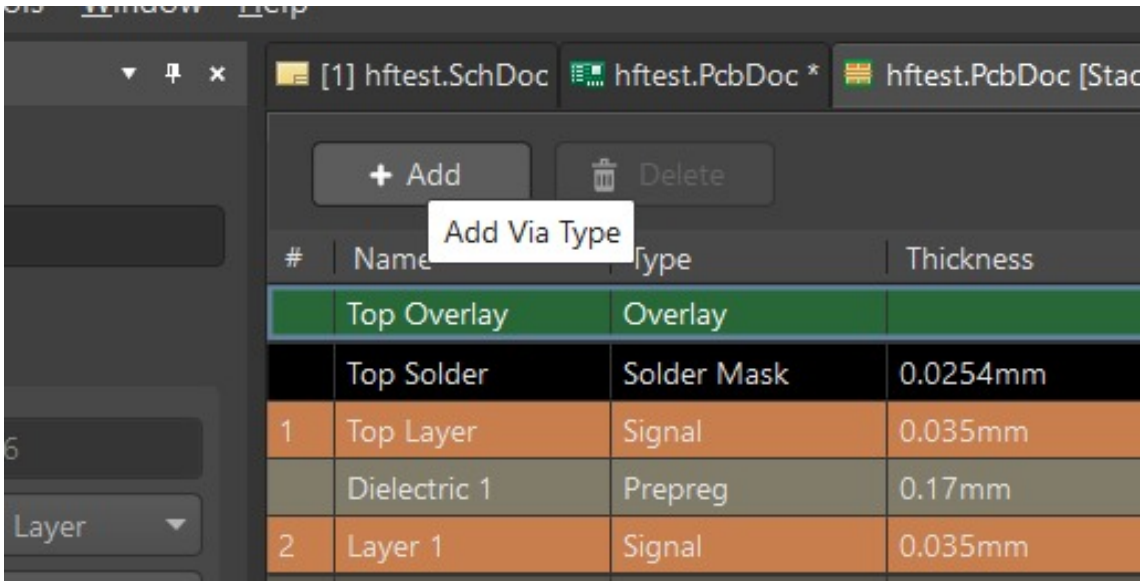

(c) Use the properties panel to modify your vias (i.e. you can change the start and termination layers of your vias).

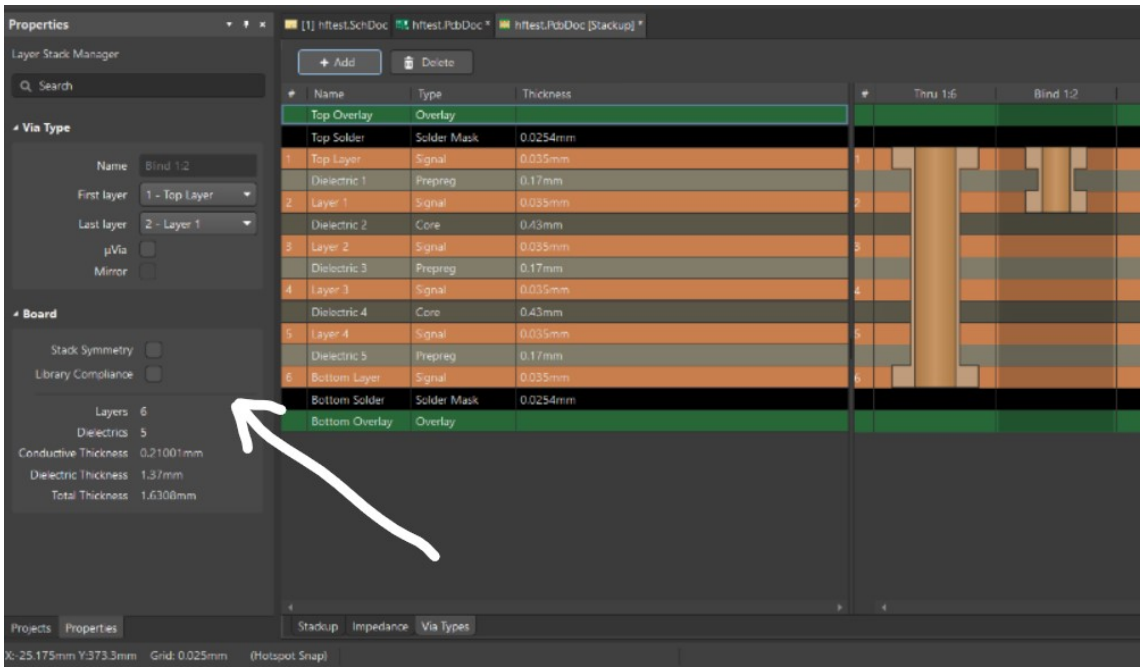

Figure 3.25: Modifying vias

(d) After defining all the via types required, save the layer stack modification by using **ctrl s**.

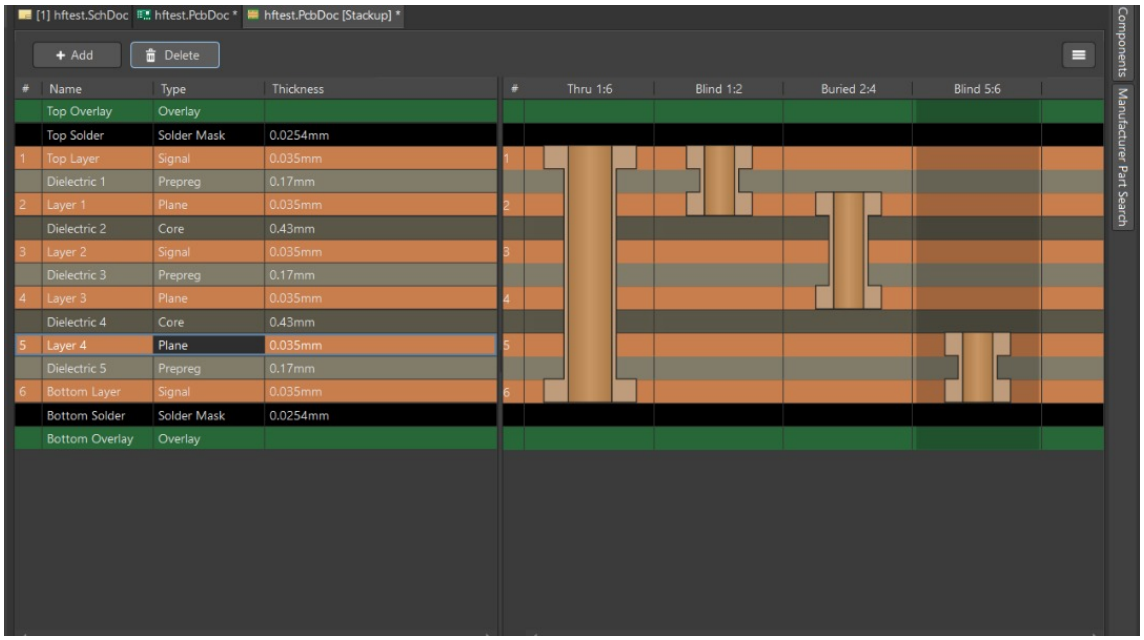

Figure 3.26: The via types

6. **Defining the design rules**

(a) In the menu bar, navigate to **Design** → **Rules** to open the PCB rules and constraint editor.

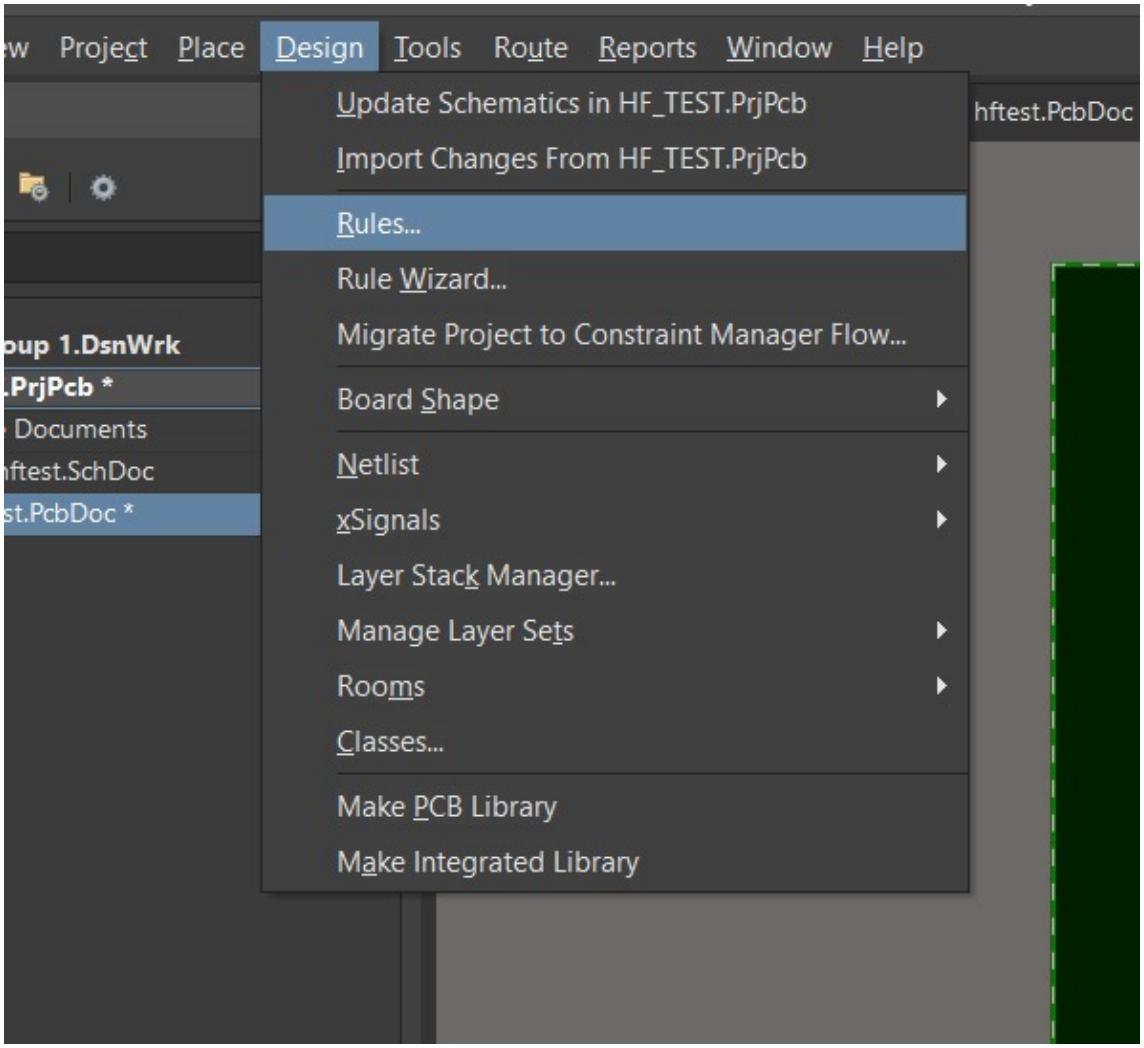

Figure 3.27: Define the rules

(b) Set all the necessary rules required for the project. Right click to add new rule and apply to save the new rules.

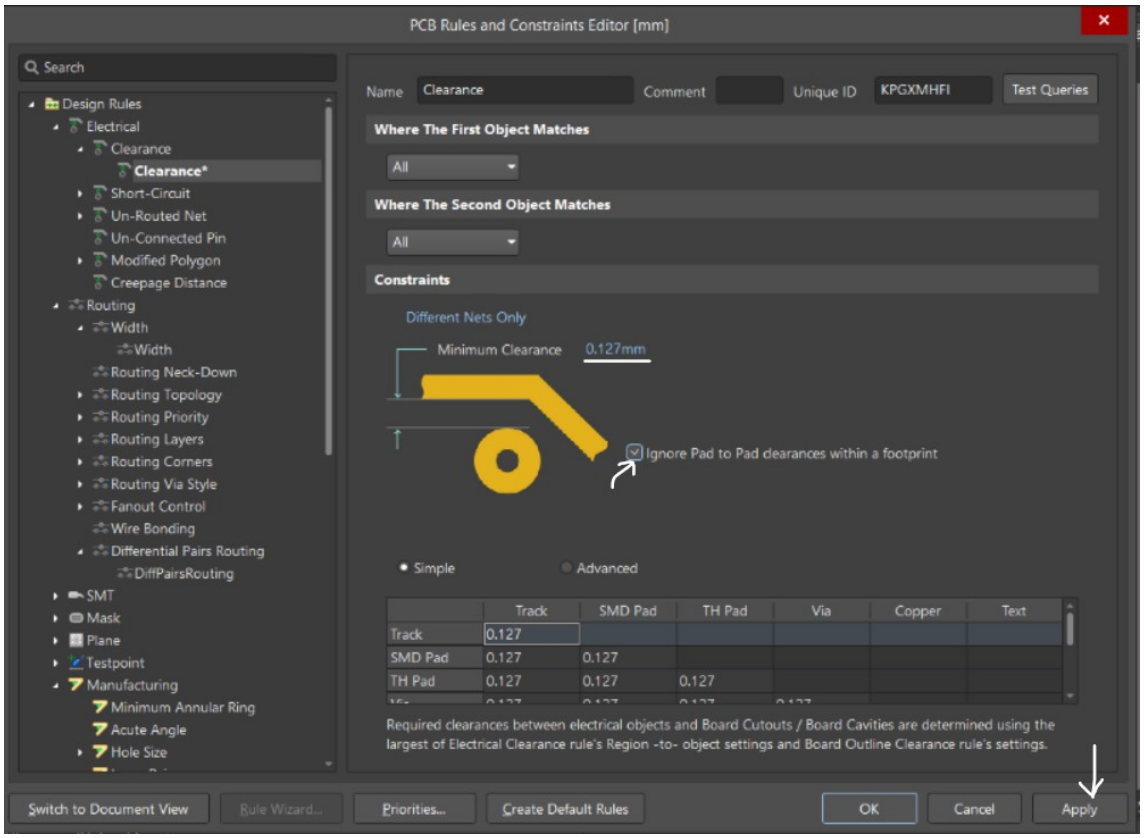

Figure 3.28: Defining minimum clearance Rule

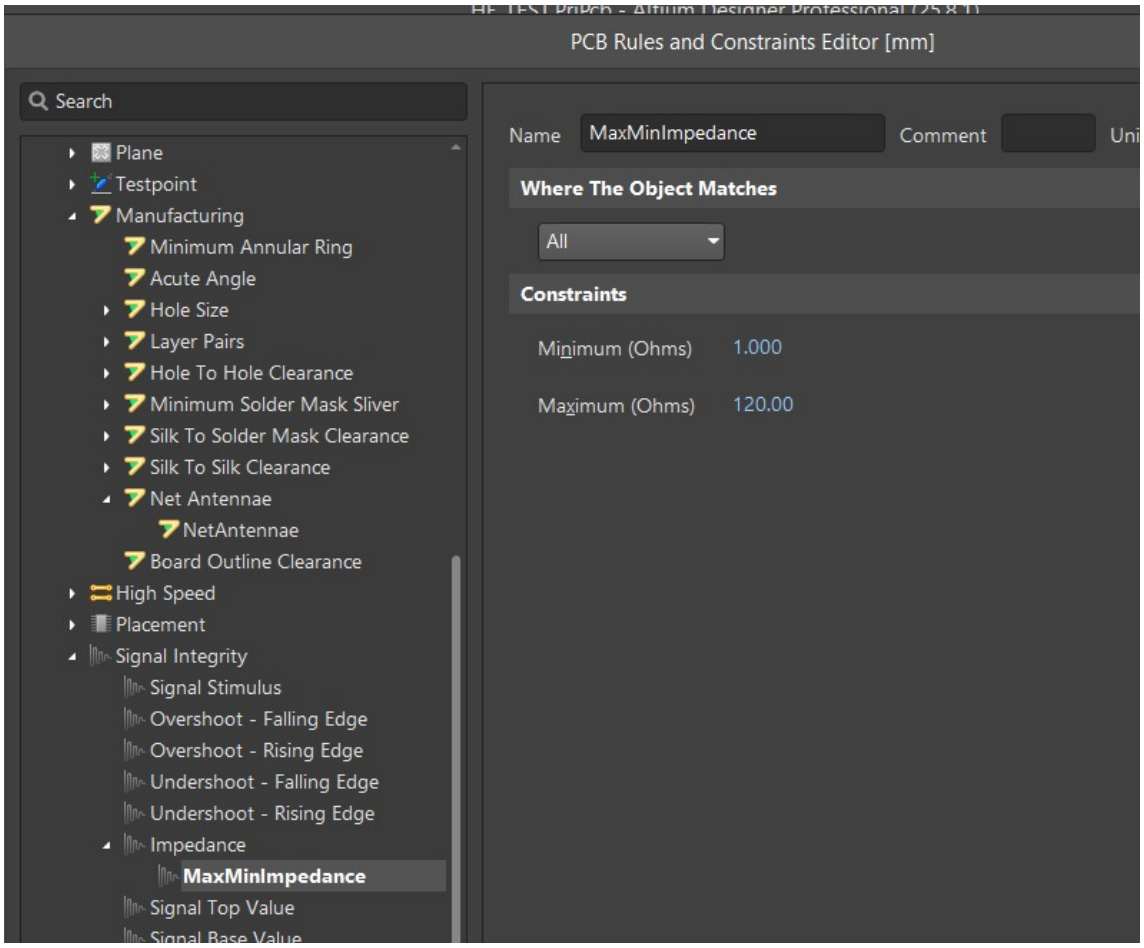

(c) Press OK after setting all the rules required for the project.

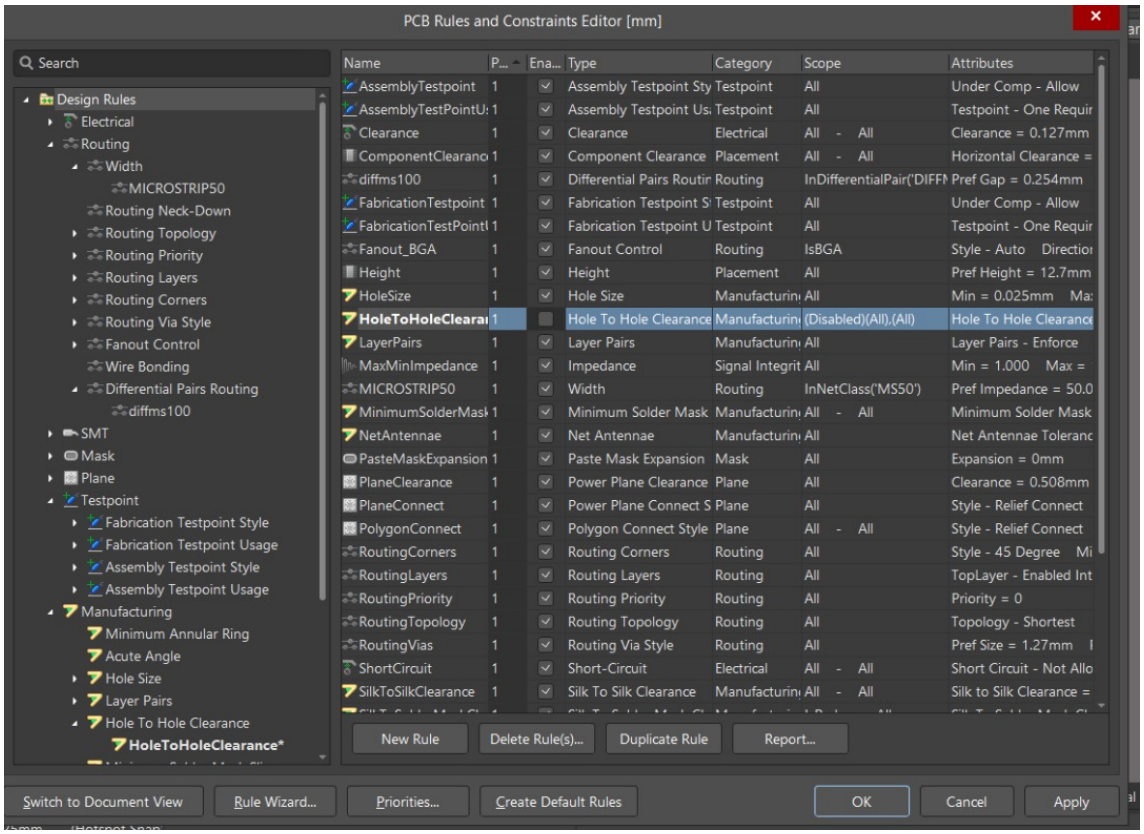

Figure 3.29: The Design Rules

3.3.3 Board Optimization: Adding components to the schematic and PCB in 2D mode

This stage characterizes different experiments designed and placed on the Printed Circuit Board.

1. **Adding Components to schematics**

   (a) On the schematics document already opened, add components to it.

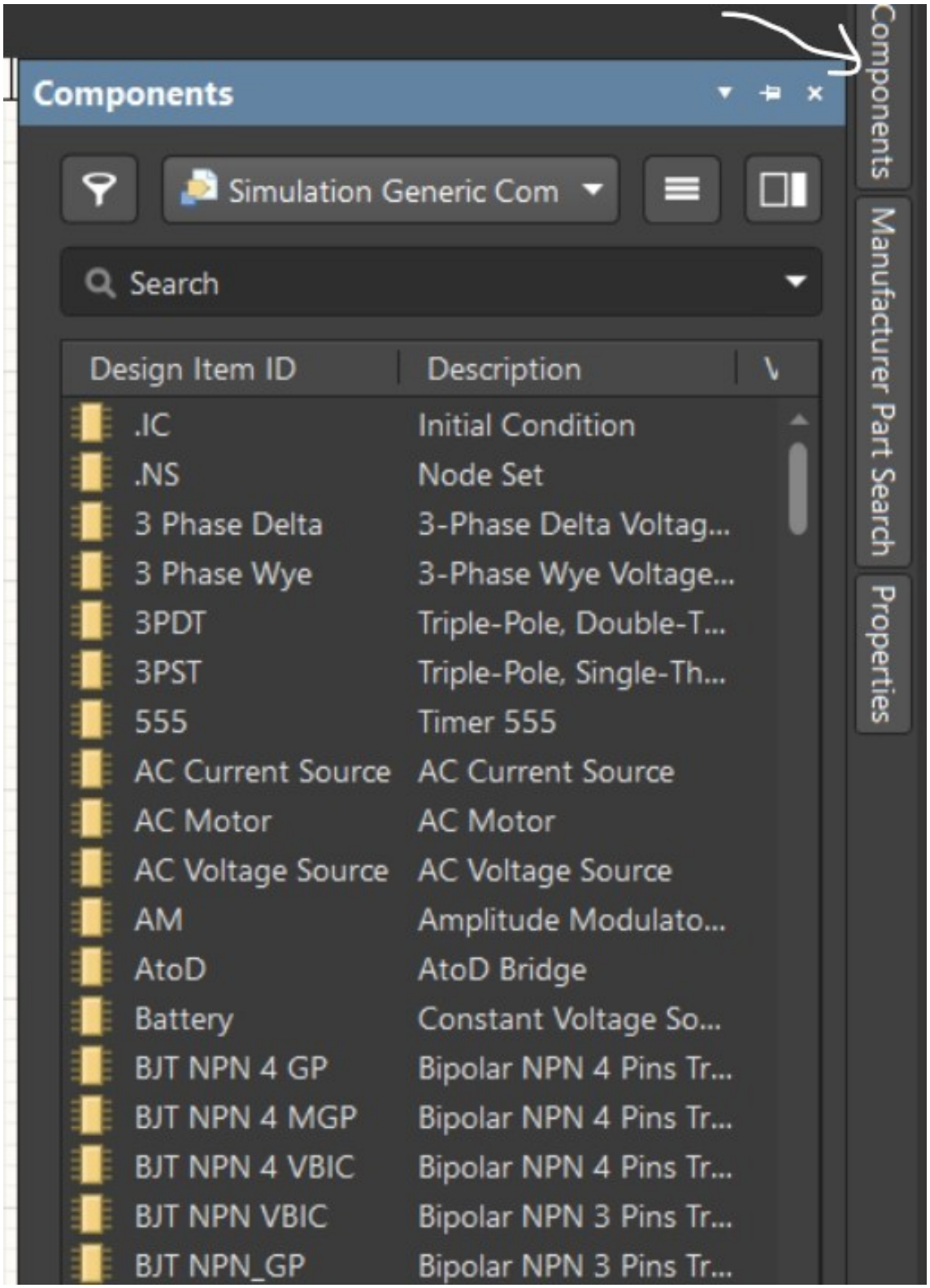

Figure 3.30: Adding components

N.B: You can install libraries of footprints and 2D models of components

that are not present in your altium to be able to use them.

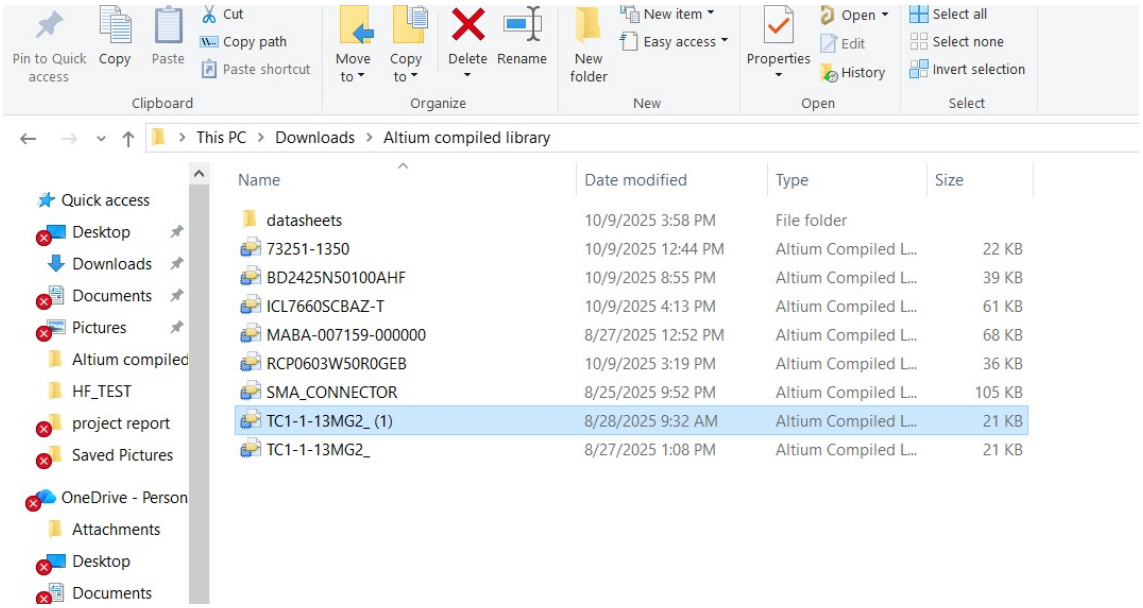

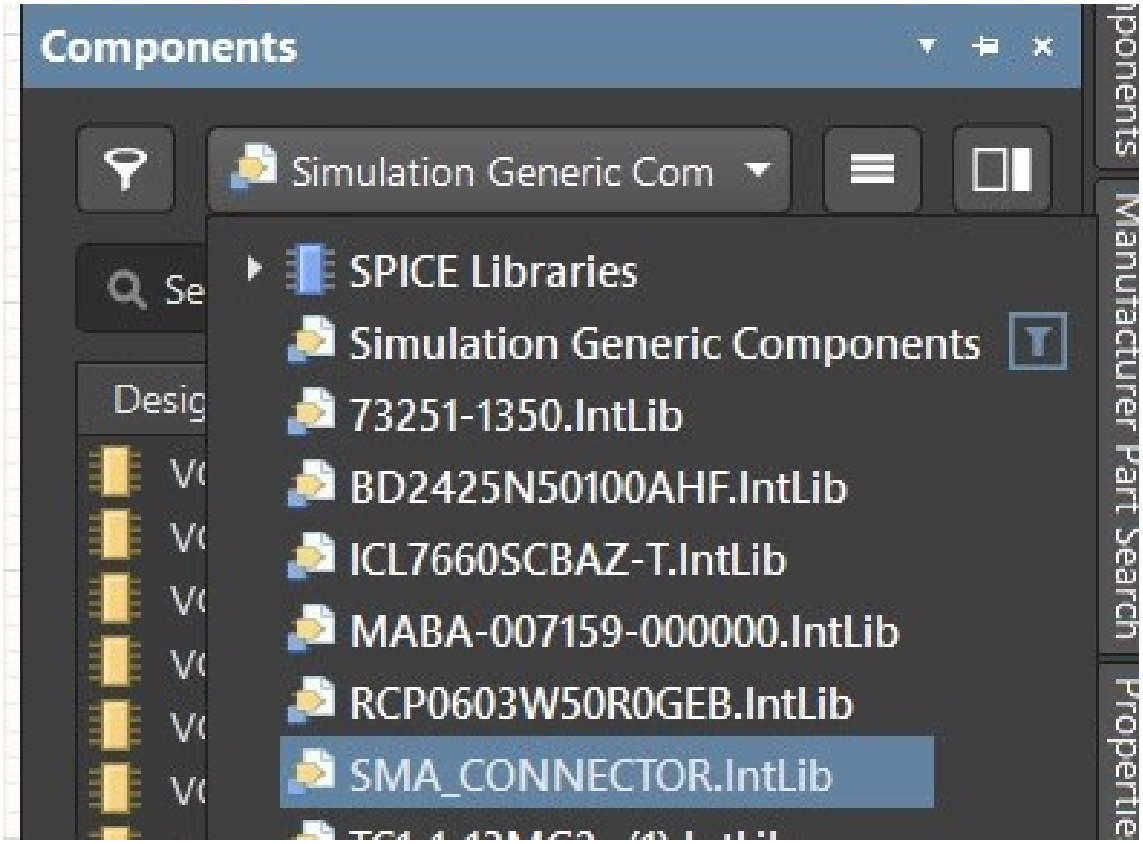

(b) Place two SMAs on the schematic and name it *sma*1 and *sma*2 respectively.

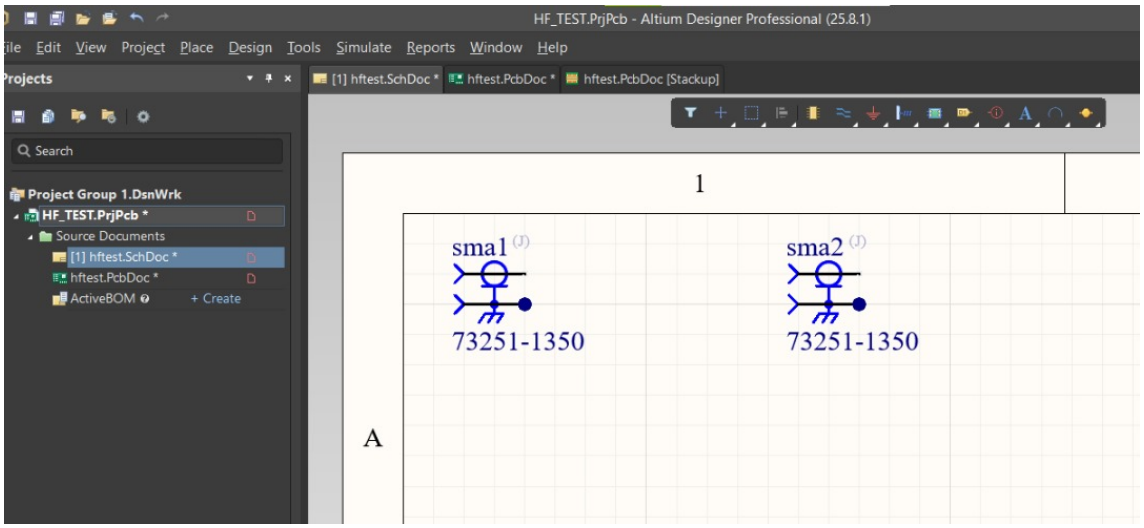

(c) Use the **place wire** option on the tool bar to connect the two SMAs to each other.

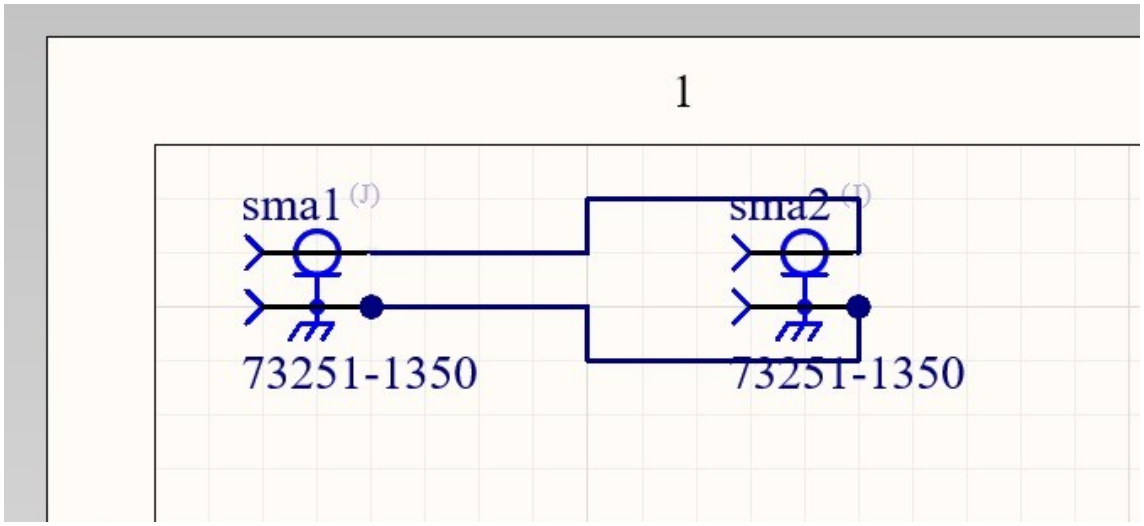

Figure 3.31: Microstrip connection on schematic editor

2. **Importing designs from schematics to PCB editor.**

(a) Go to the PCB editor. In the menu bar, navigate to **Design** → **Import changes** and the Engineering Change Order (ECO) field pops up.

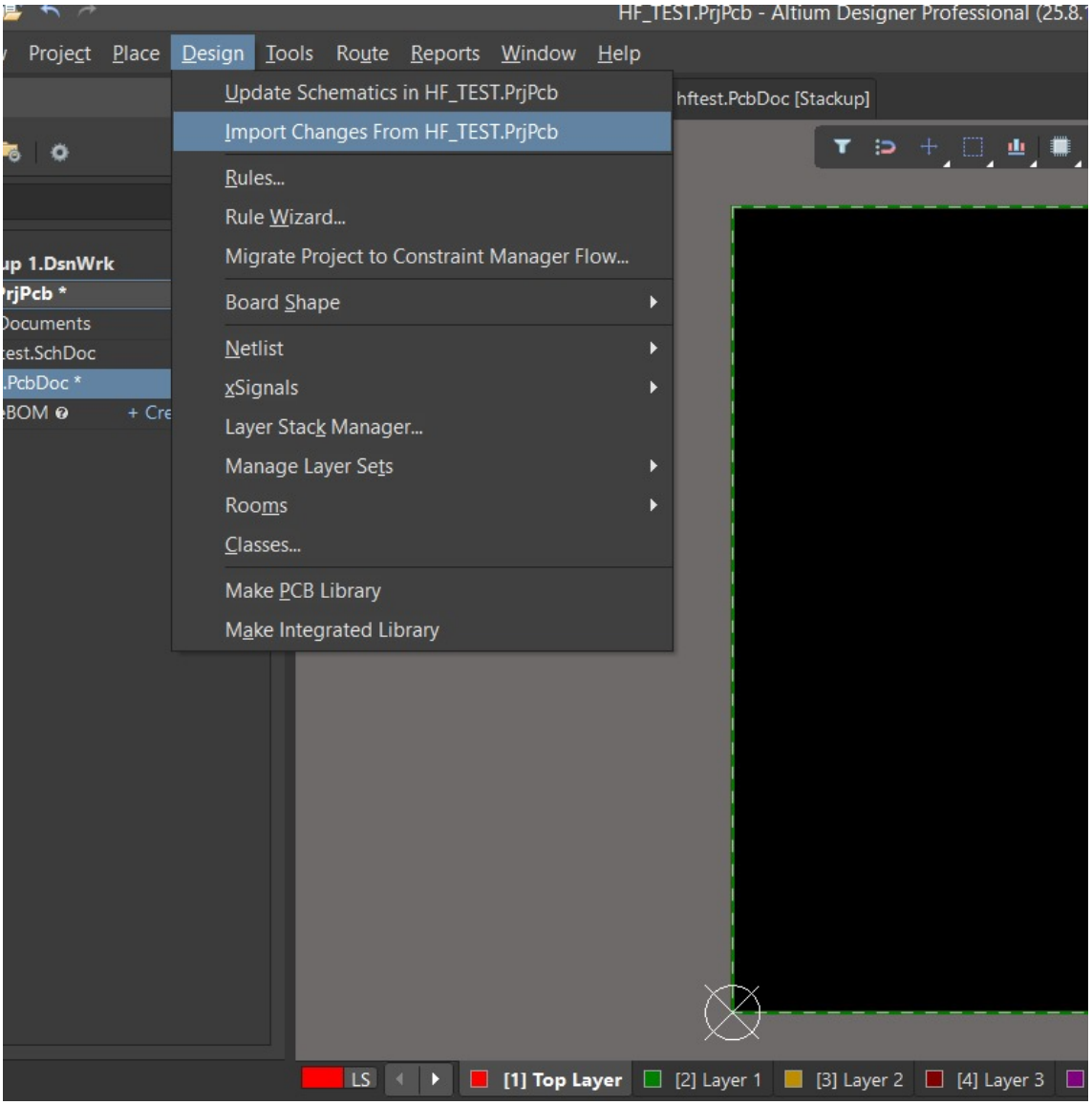

(b) **Validate and Execute changes** from the bottom left corner of the ECO field. This imports the 2D model of the component for routing (i.e. the SMAs) on your PCB.

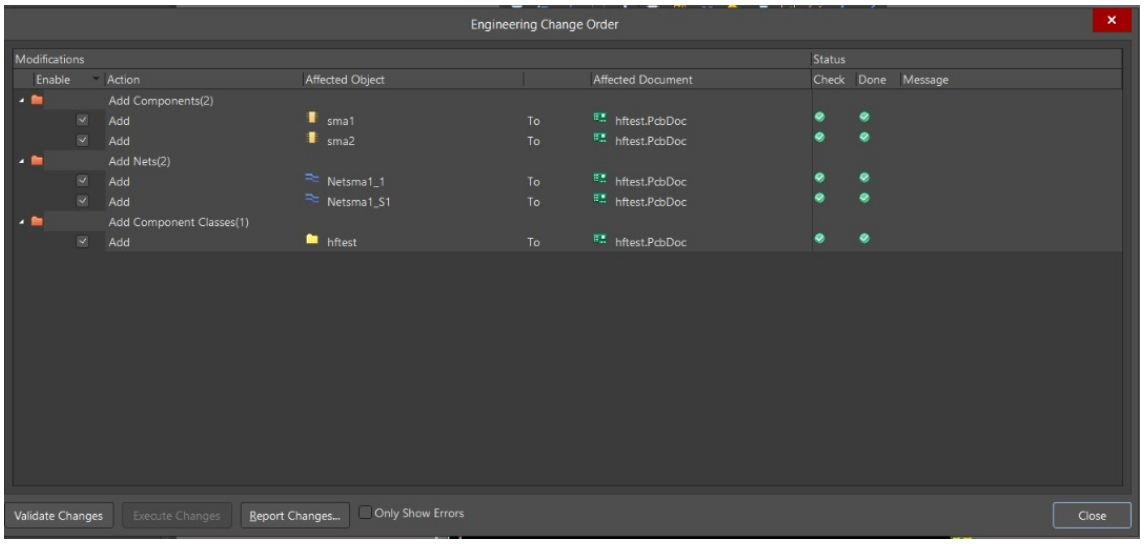

3. **Adding more Designs to the PCB.**

(a) On the Schematic editor, add more SMA components and name them such that no 2 SMA has the same value. You can change this by double-tapping on each SMA and changing the values in the properties panel.

(b) Also add the IC(i.e. the BALUN) for the differential pairs; For one set of SMA, add 2 BALUNs in between, connecting the wires as shown below.

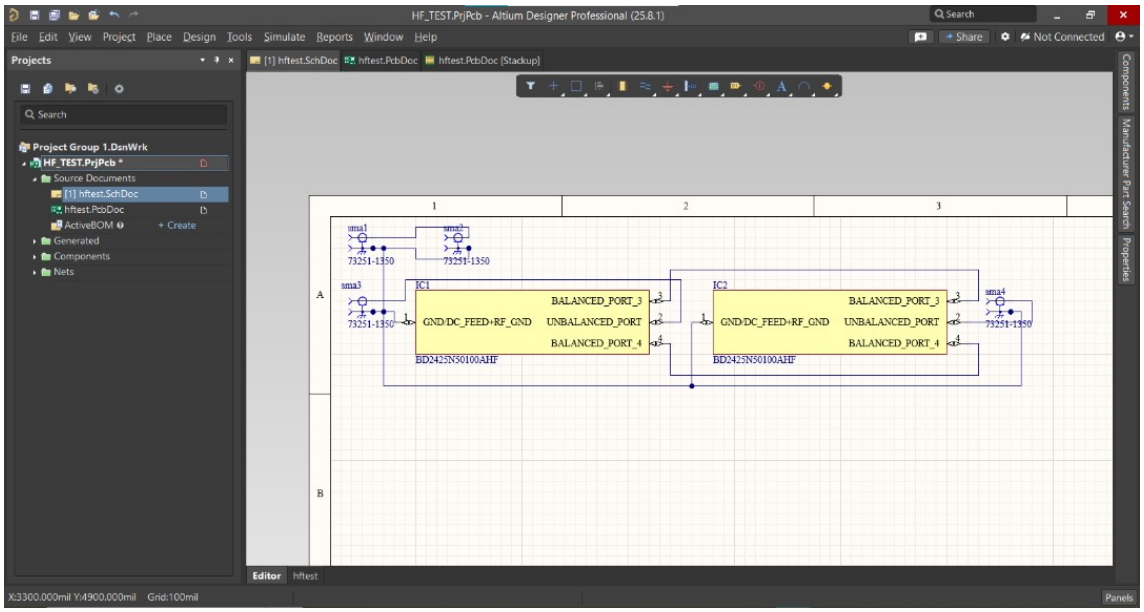

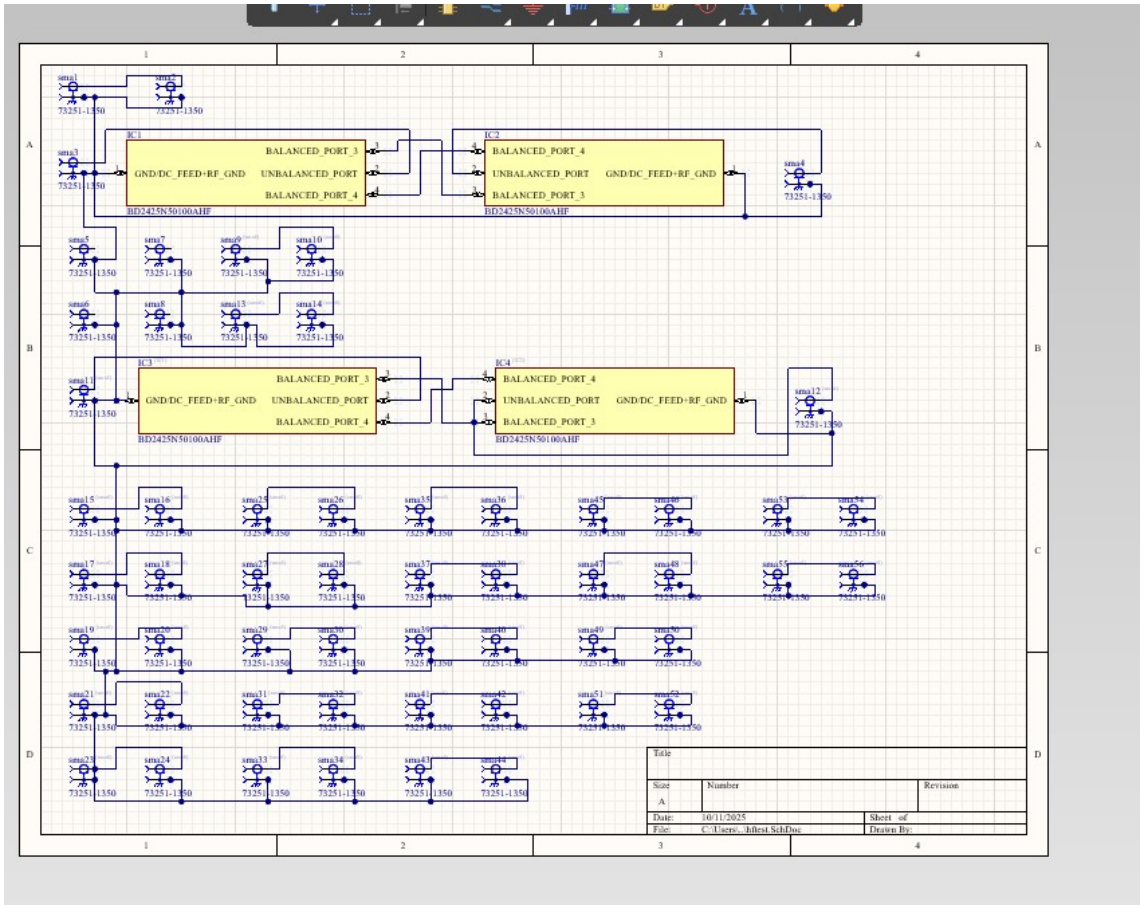

(c) Connect all the ground pins of the SMAs together as they are all to be connected to a Ground layer of the PCB.

4. **Importing Changes to the PCB editor**

(a) After making the designs on the schematics import the changes to your PCB as discussed earlier for a single pair of SMA.

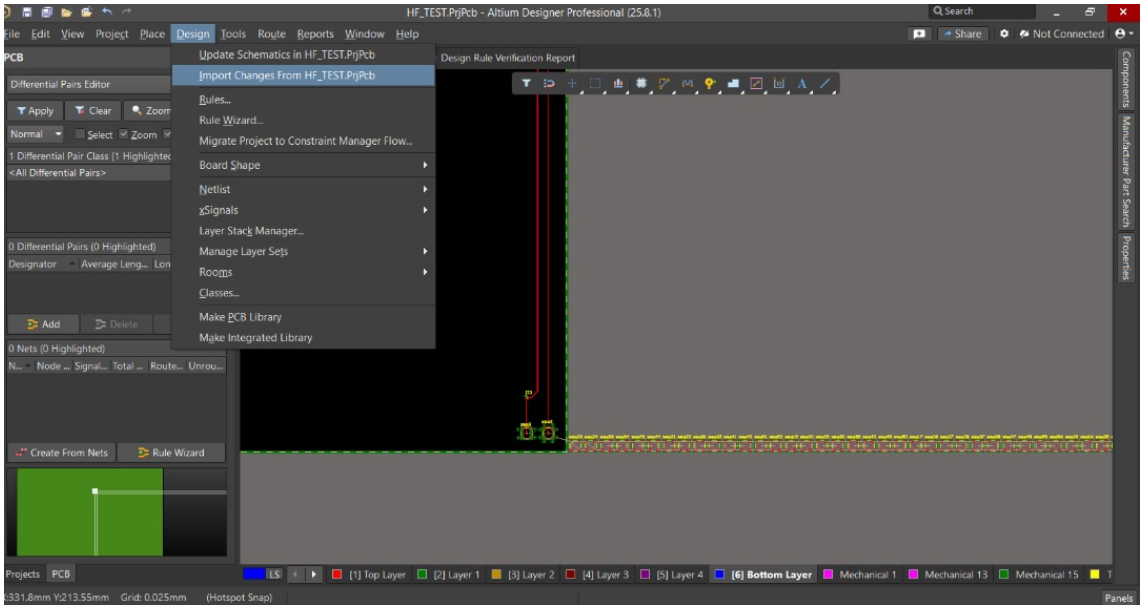

Figure 3.32: Making changes to PCB editor

(b) Due to all the connections made in the schematics, all the paired SMAs belong to different **Nets** but most of them belong to the same class. Hence group all nets using the same impedance profile to the same class and add a rule for the width of the line used for this class.

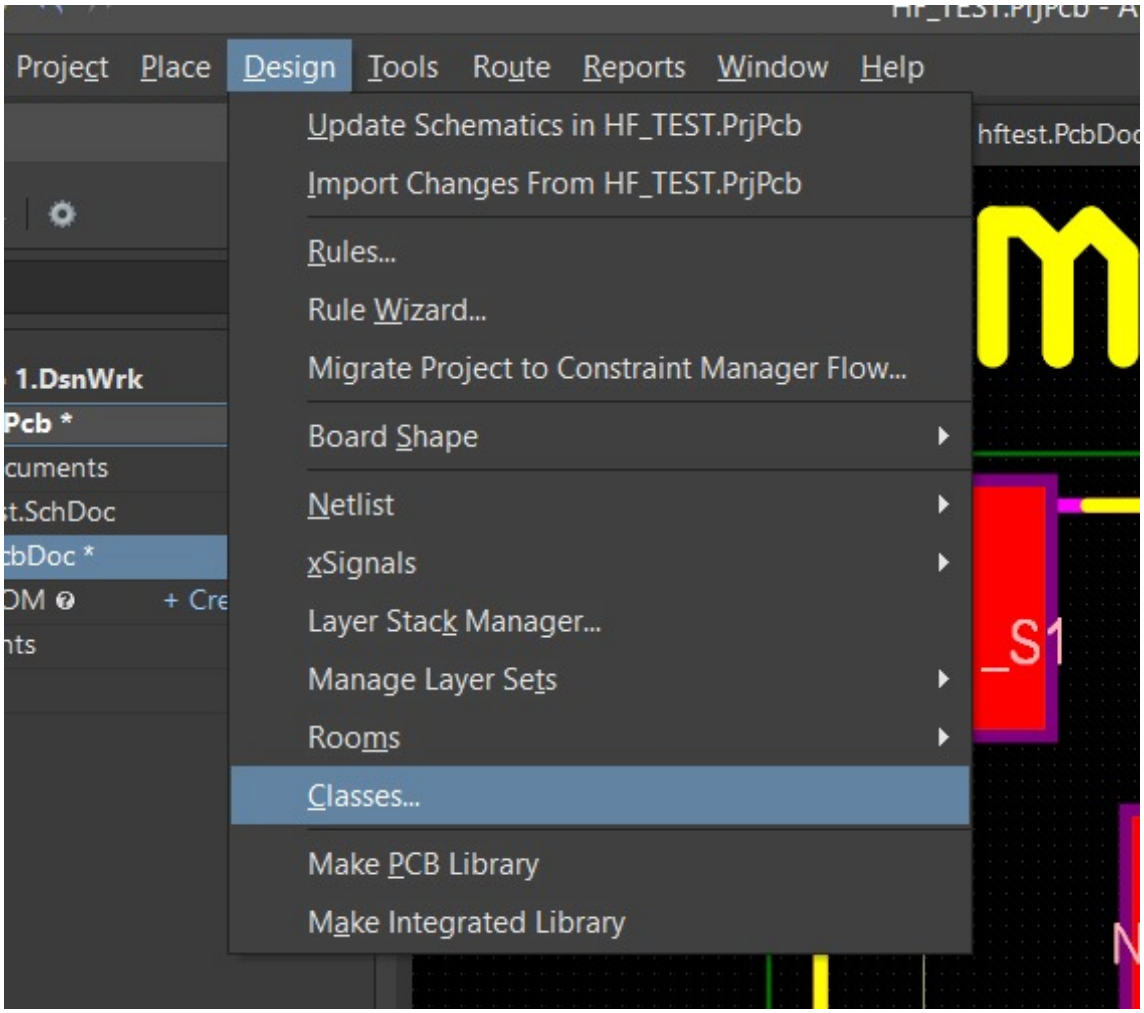

Figure 3.33: Creating Classes

(c) Add classes by right-clicking on the **all classes tab**.

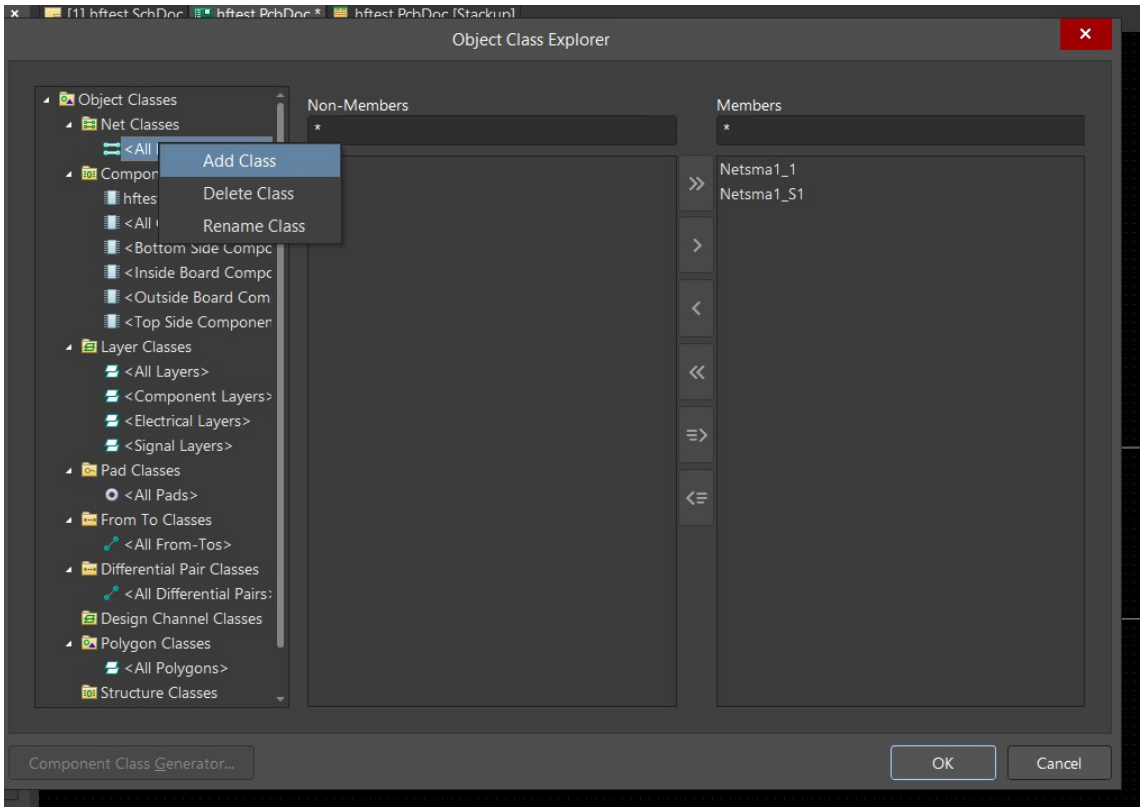

(d) Add all Nets using the 50 Ω microstrip impedance profile for your design to one class and the 50 Ω stripline impedance profile to another class.

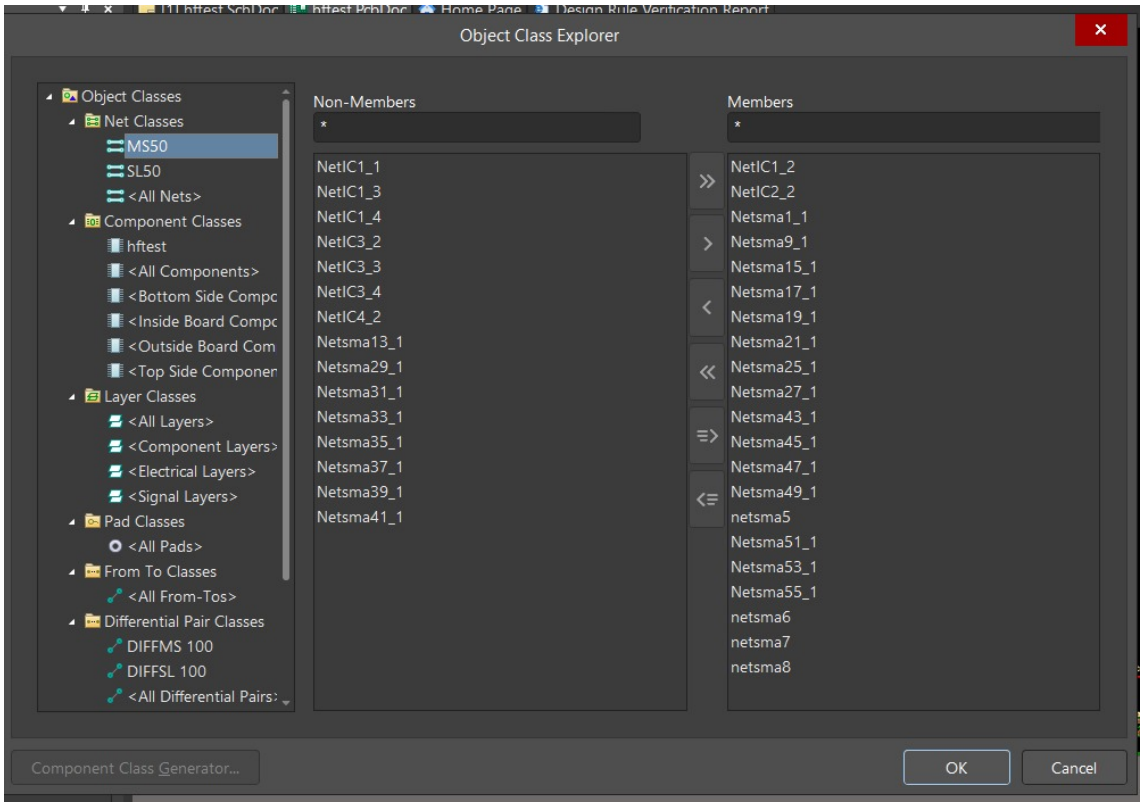

Figure 3.34: 50 Ω Microstripline Class

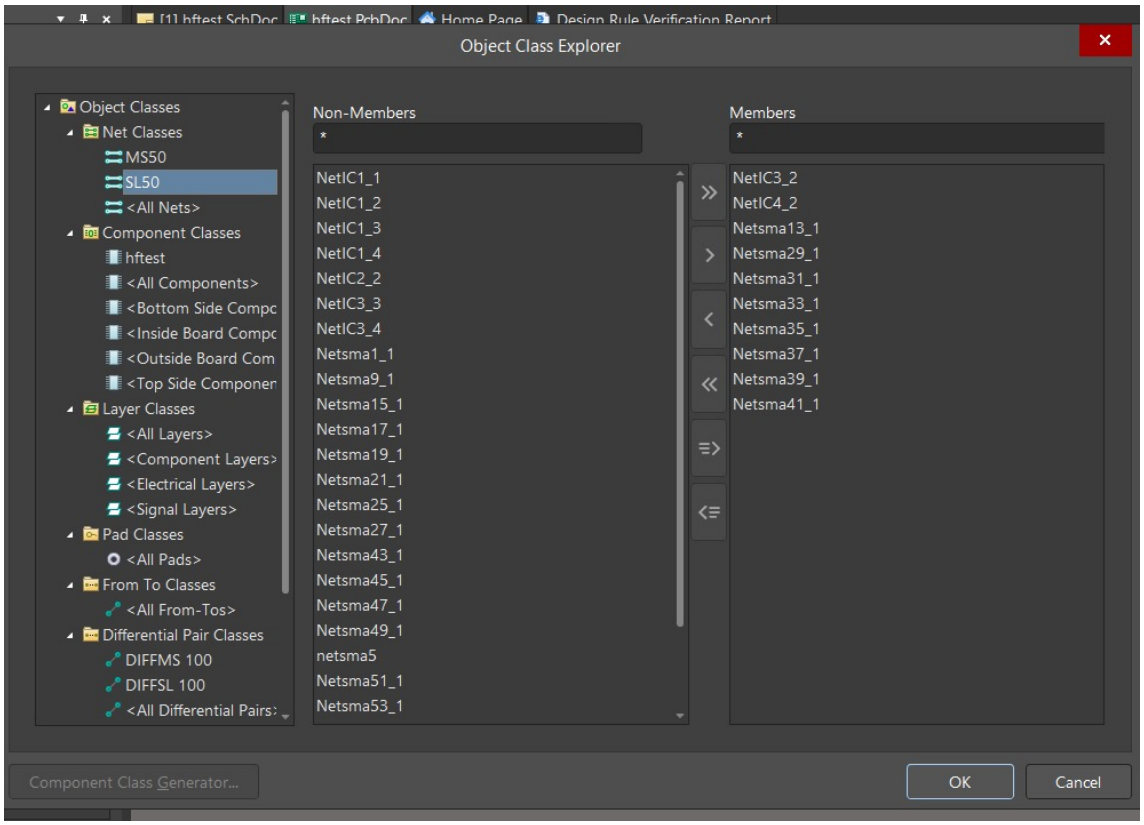

Figure 3.35: 50 Ω Stripline Class

5. **Creating the differential pair and adding more rules.**

   (a) Navigate to **panel** at the bottom right corner of your screen and click on PCB. A panel will pop up at the left side of the screen.

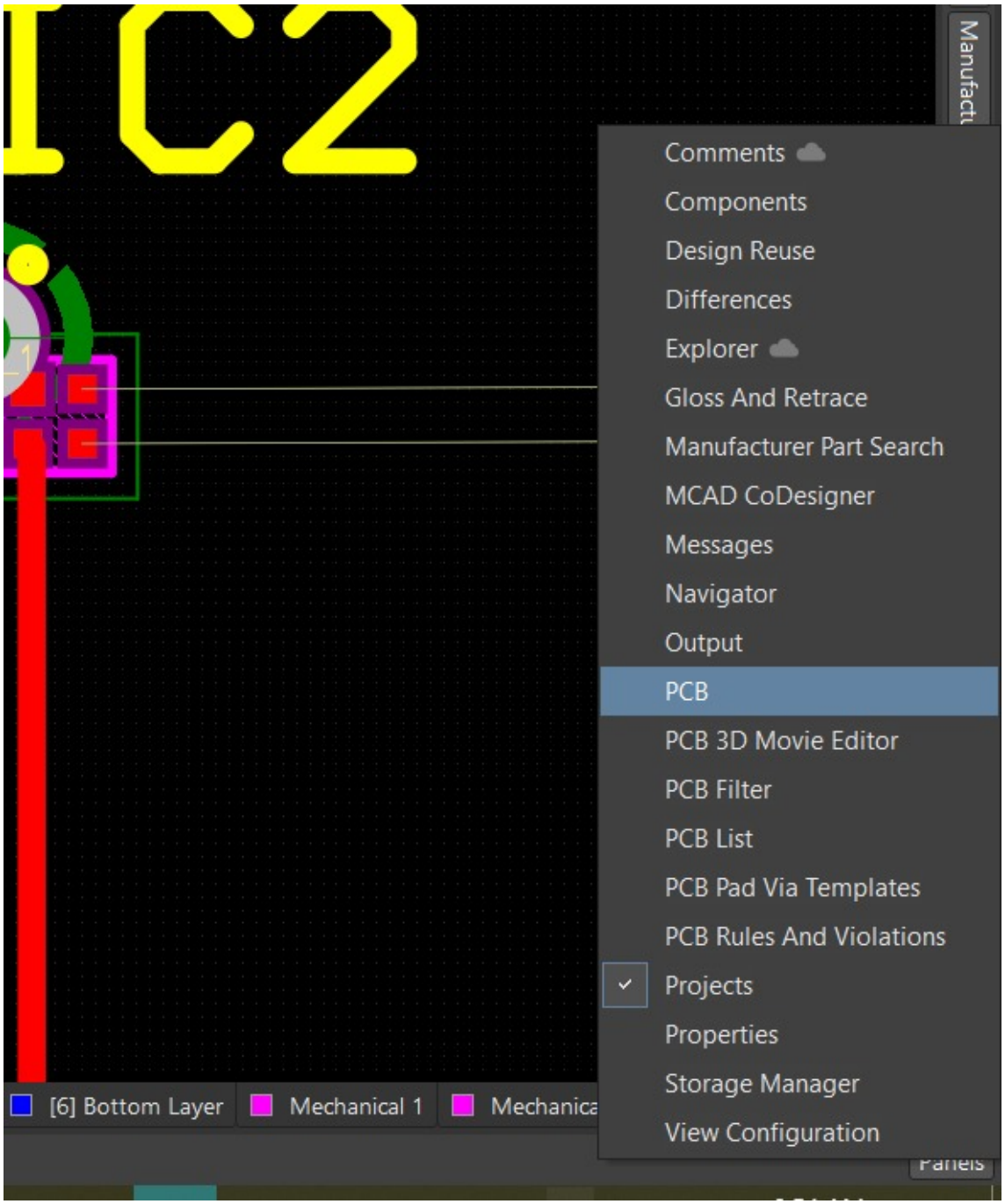
IC2
Manufacti
Comments
Components
Design Reuse
Differences
Explorer
Gloss And Retrace
Manufacturer Part Search
MCAD CoDesigner
Messages
Navigator
Output
PCB
PCB 3D Movie Editor
PCB Filter
PCB List
PCB Pad Via Templates
PCB Rules And Violations
Projects
Properties
Storage Manager
View Configuration
[6] Bottom Layer
Mechanical 1
Mechanica
Panels

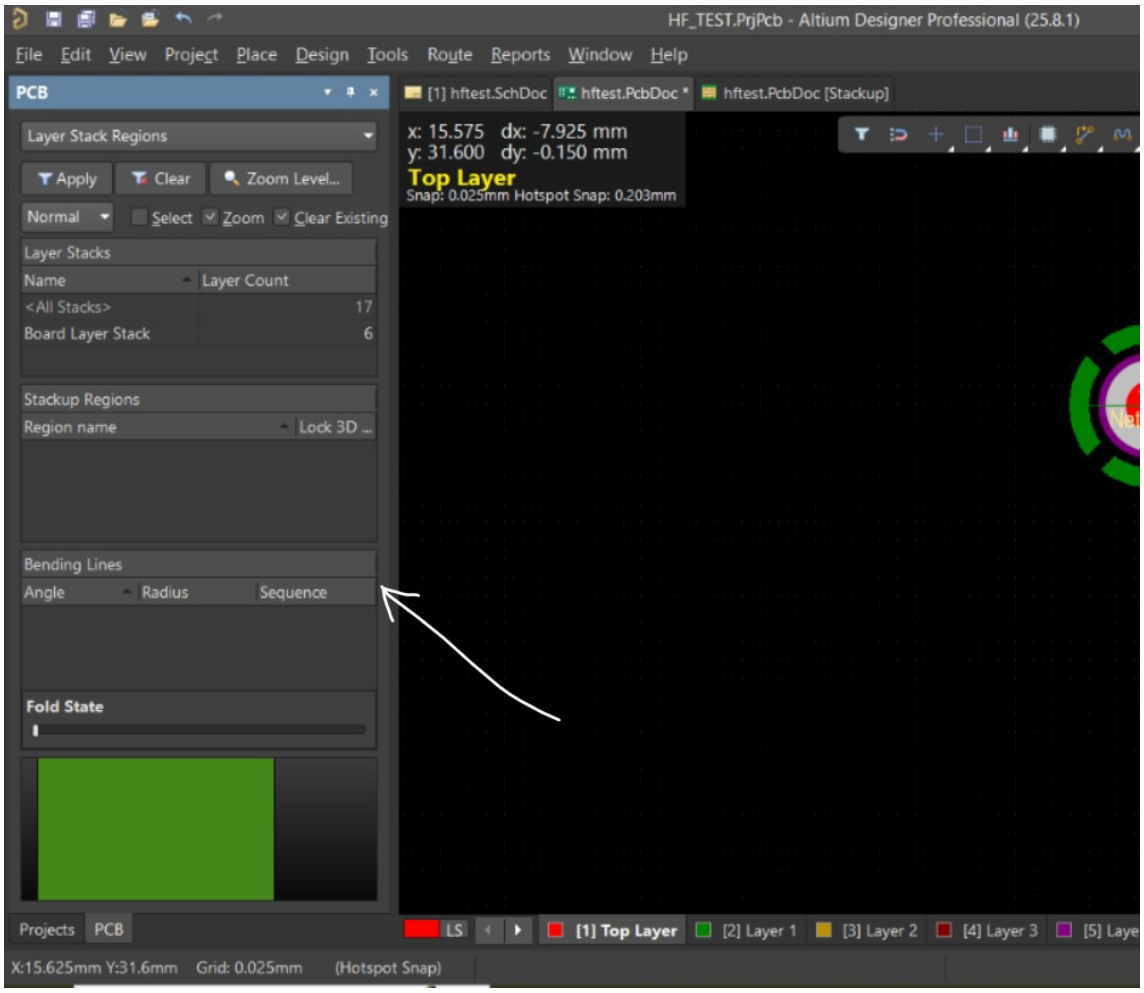

(b) Change the panel type to the differential pair editor using the drop down arrow.

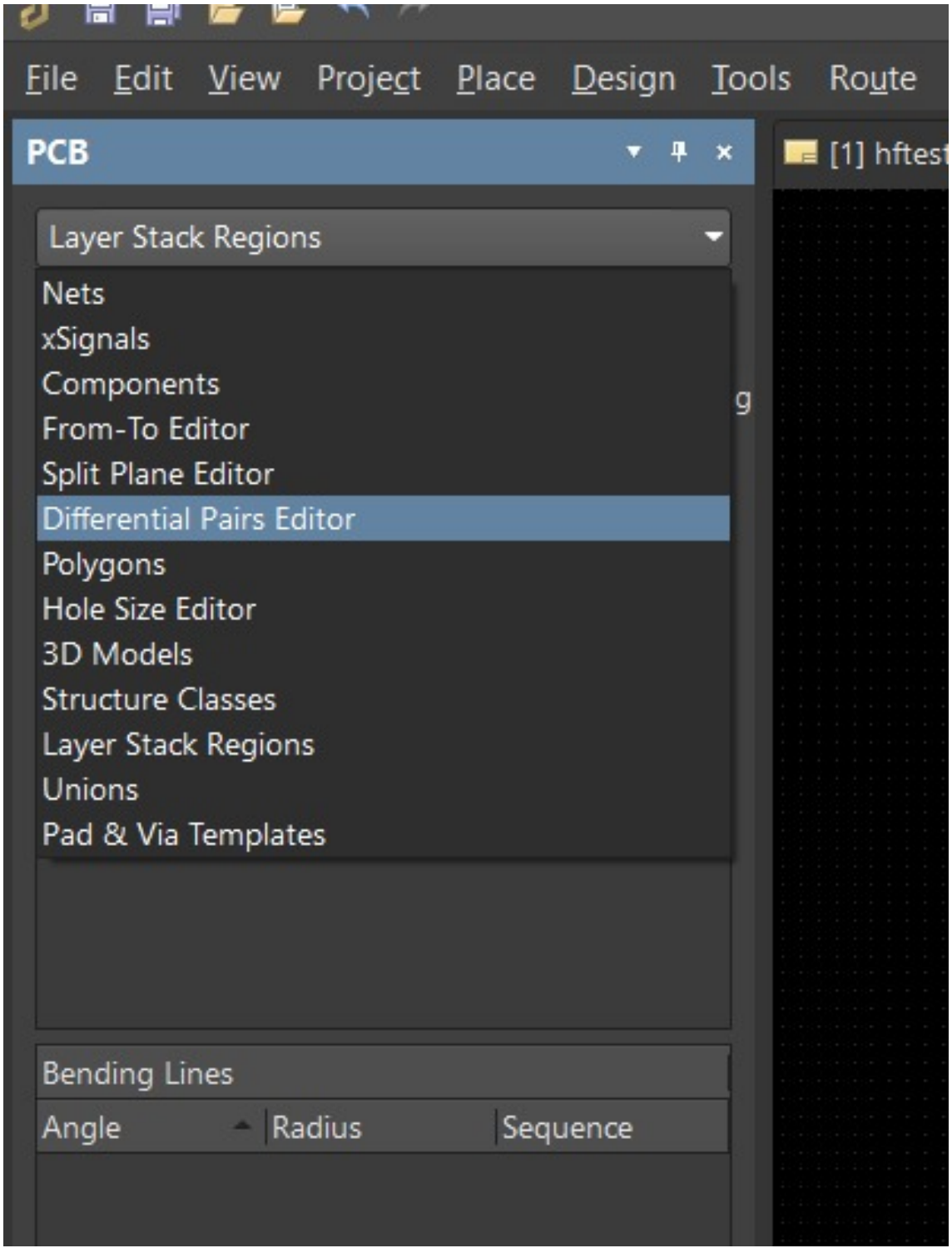

(c) Add a differential pair based on the Nets Given to your IC(i.e BALUN) and save it.

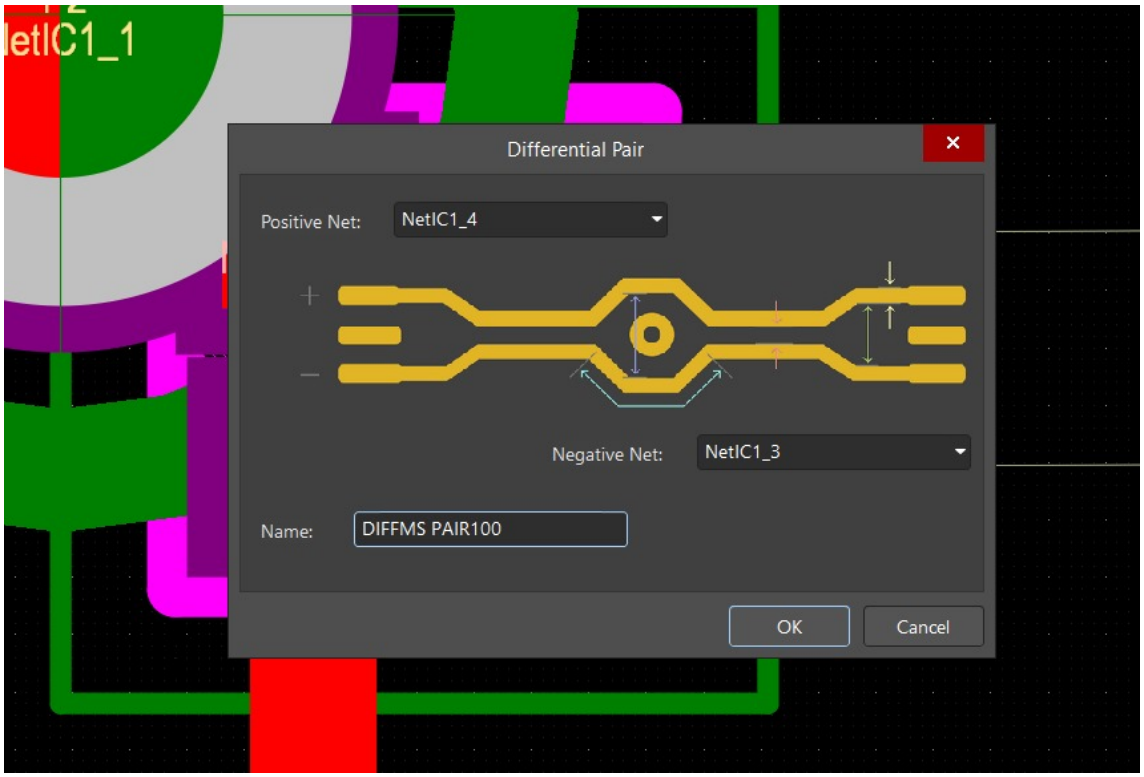

(d) Add differential pair to the differential pair class.

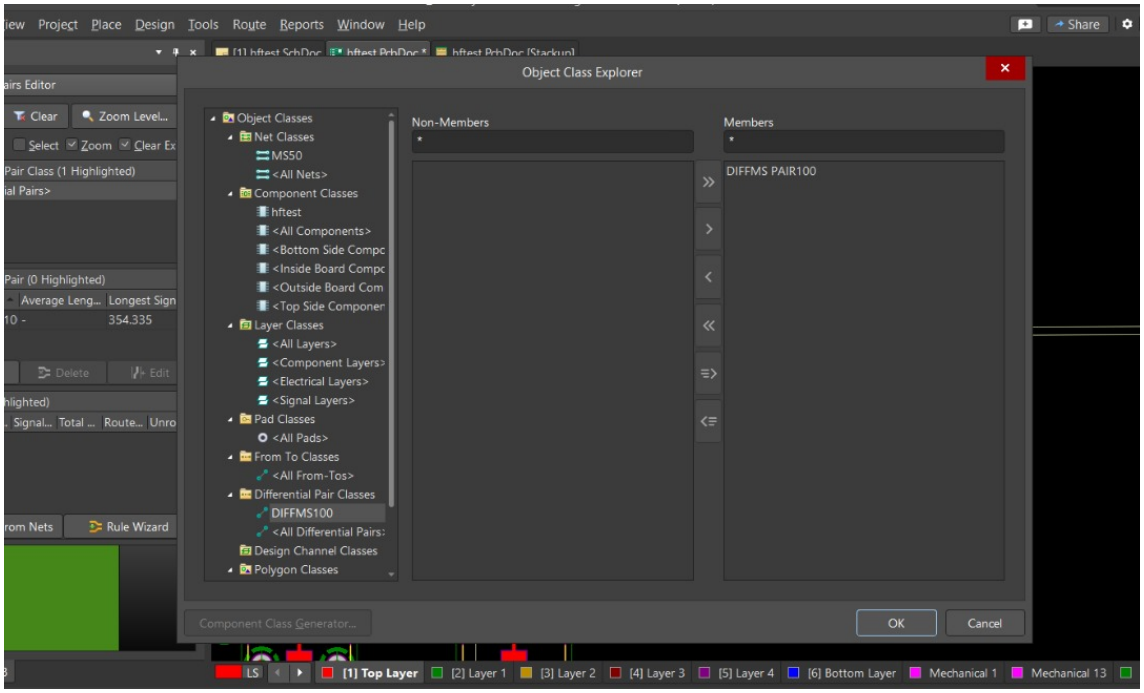

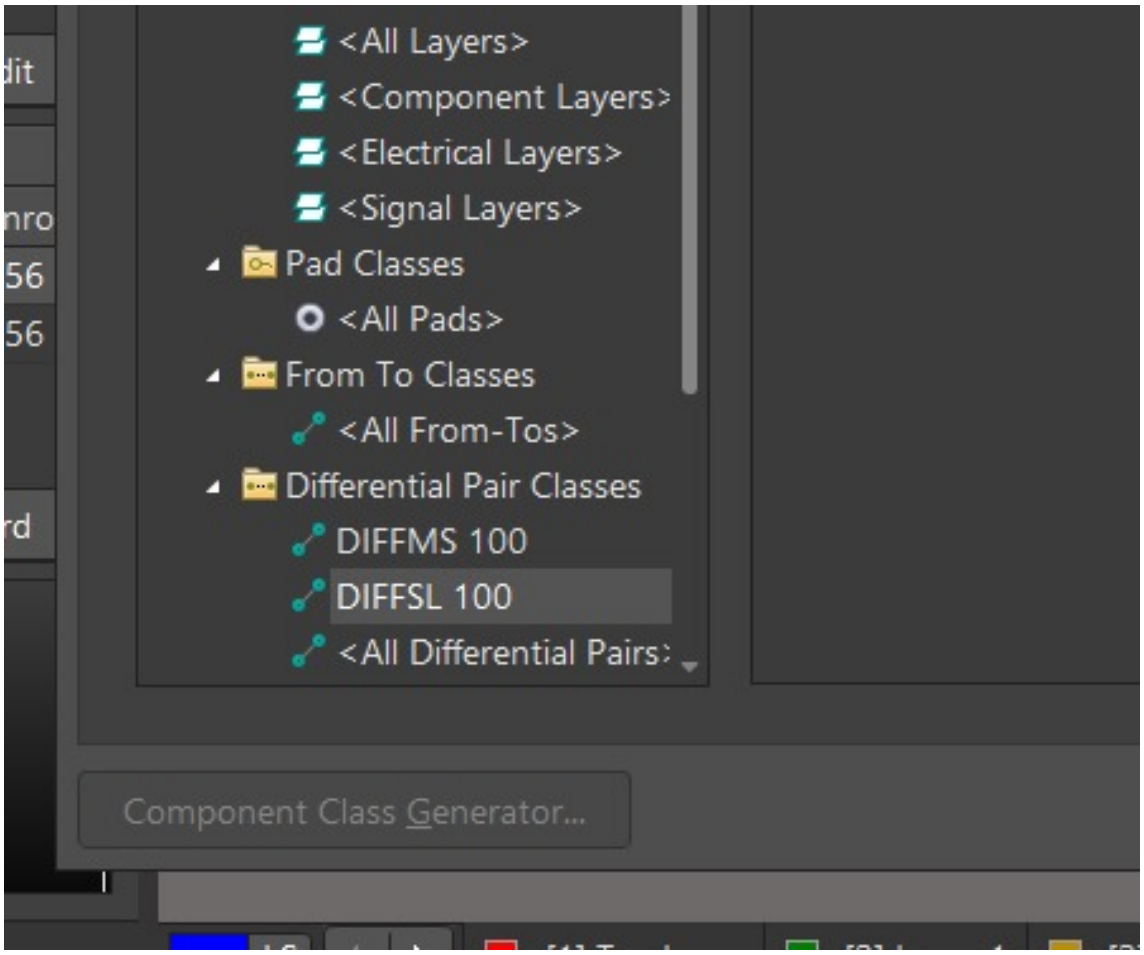

(e) Next, define the differential pair rule in the **Design rules editor**.

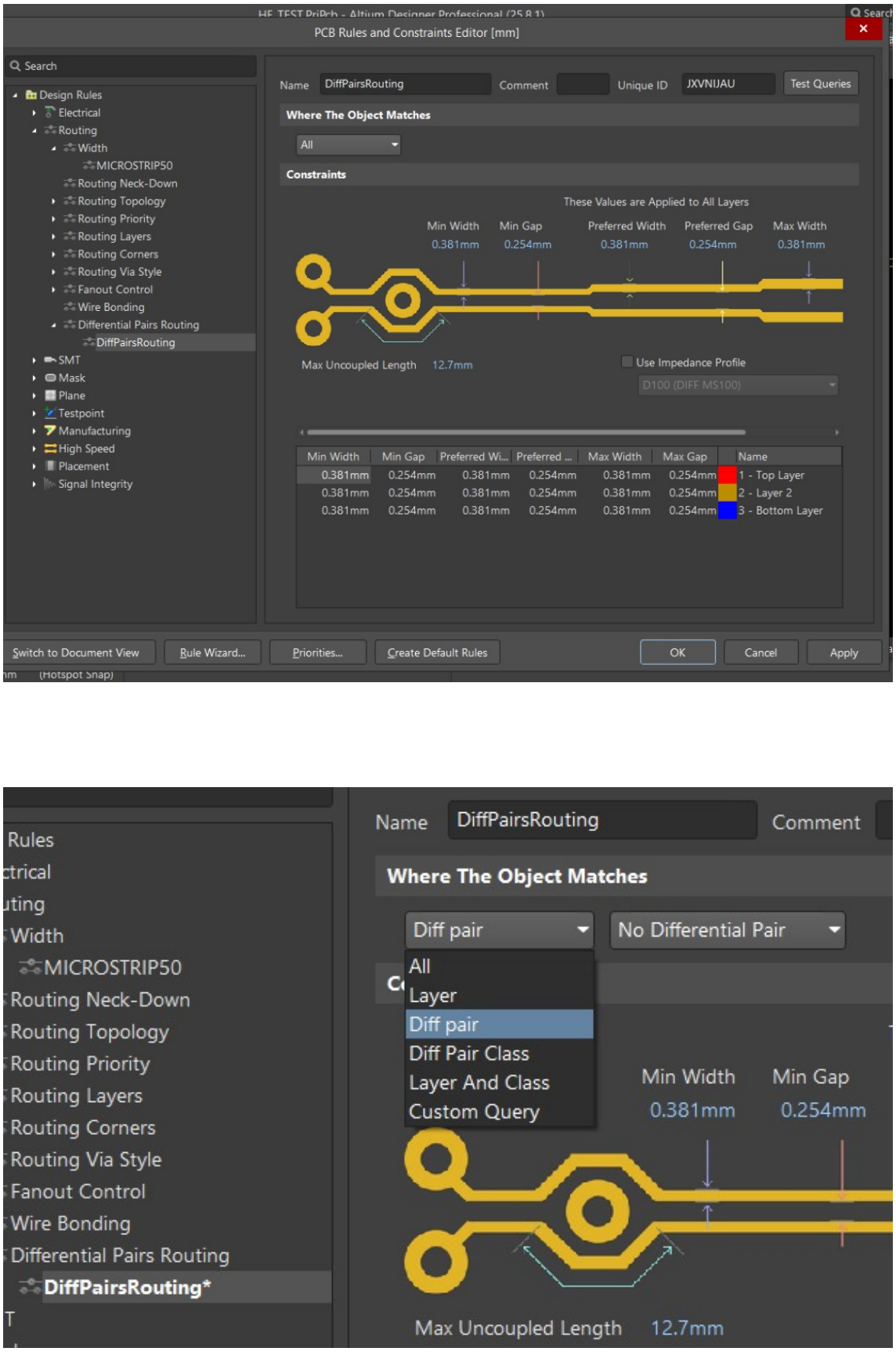

Figure 3.36: Define differential pair rule

(f) Use the impedance profiles to set your required differential pair rule.

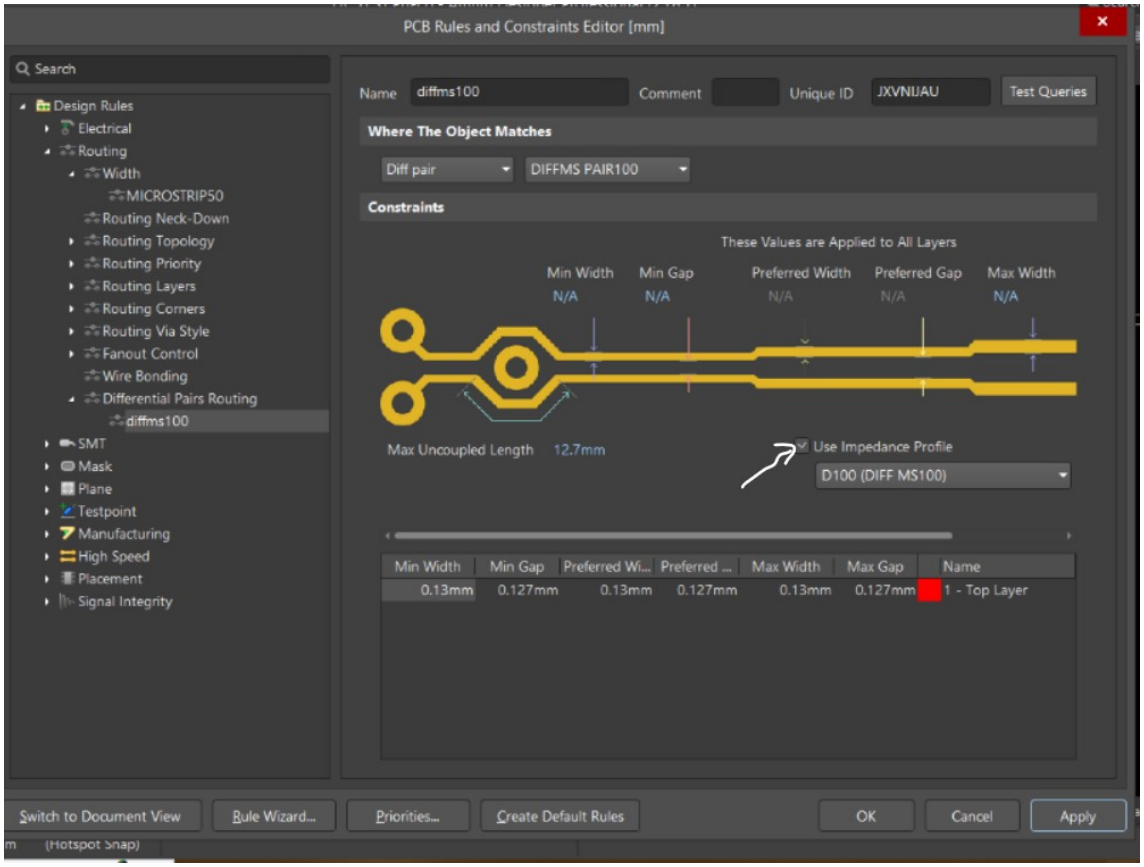

Figure 3.37: 100 Ω differential microsstrip

(g) Next, Put off rules that are not necessary for your design to avoid design rule violations and zero error during design rule check.

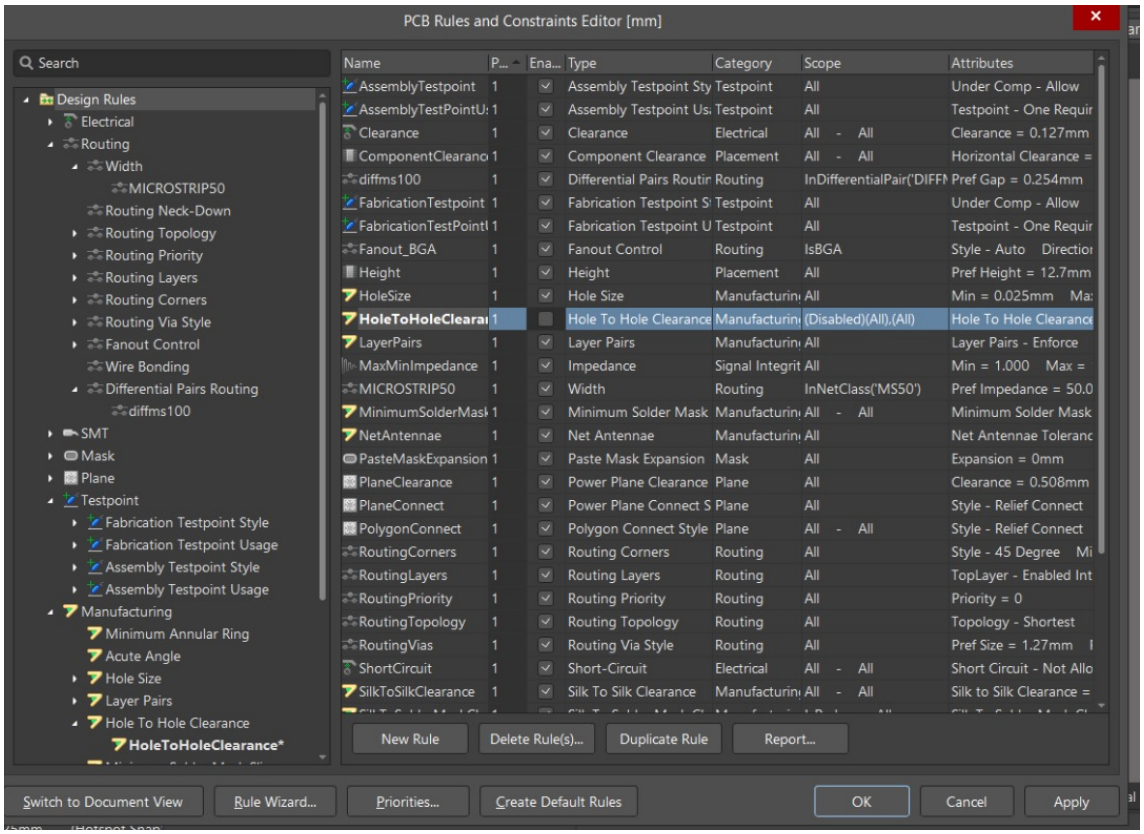

6. **Routing Designs on the PCB**

   (a) Take the SMAs having the same middle nets one after the other into the PCB as a pair to route from one of the SMA to the other.

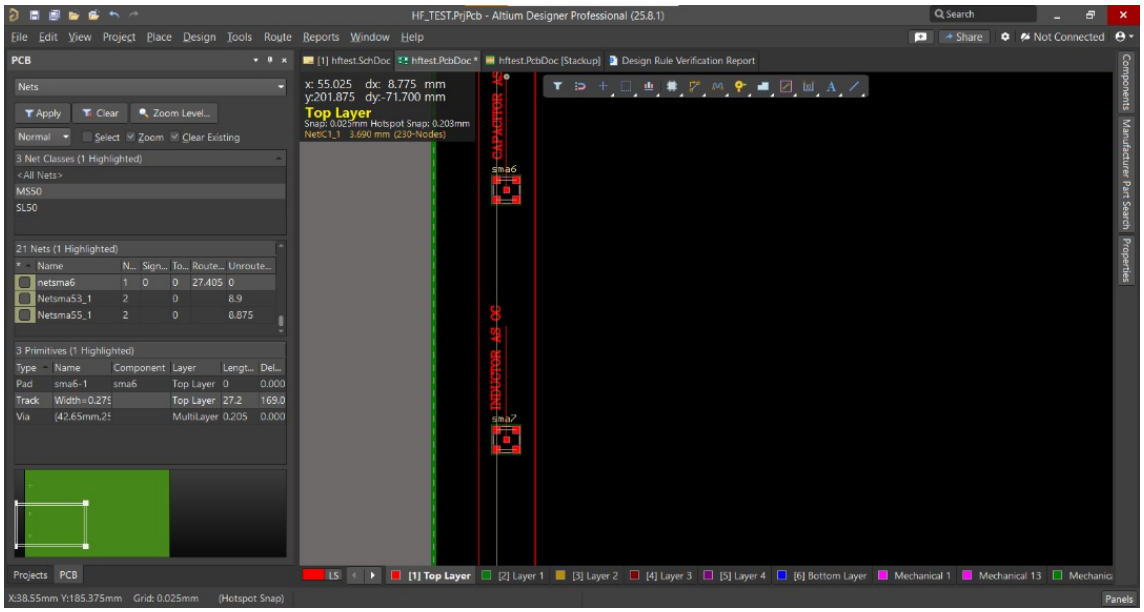

(b) Do the same for every other pairs of SMAs and the single SMAs too (e.g resonant circuits).

(c) Give all the experiments routed on the board names, to specify which experiment is to be carried out on the SMAs.

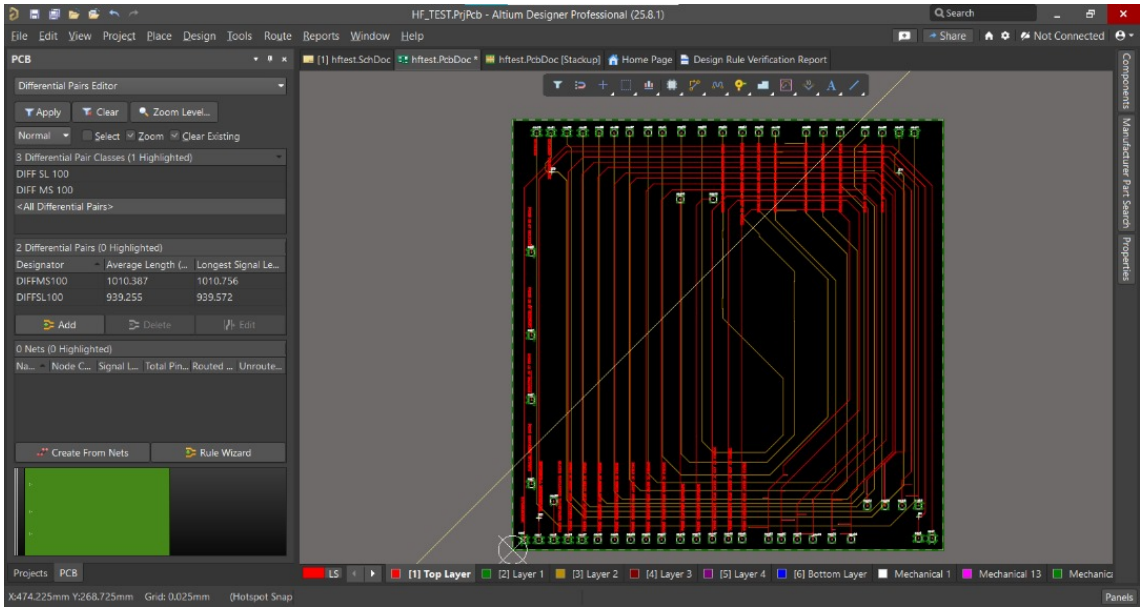

Figure 3.38: All Experiment Connections

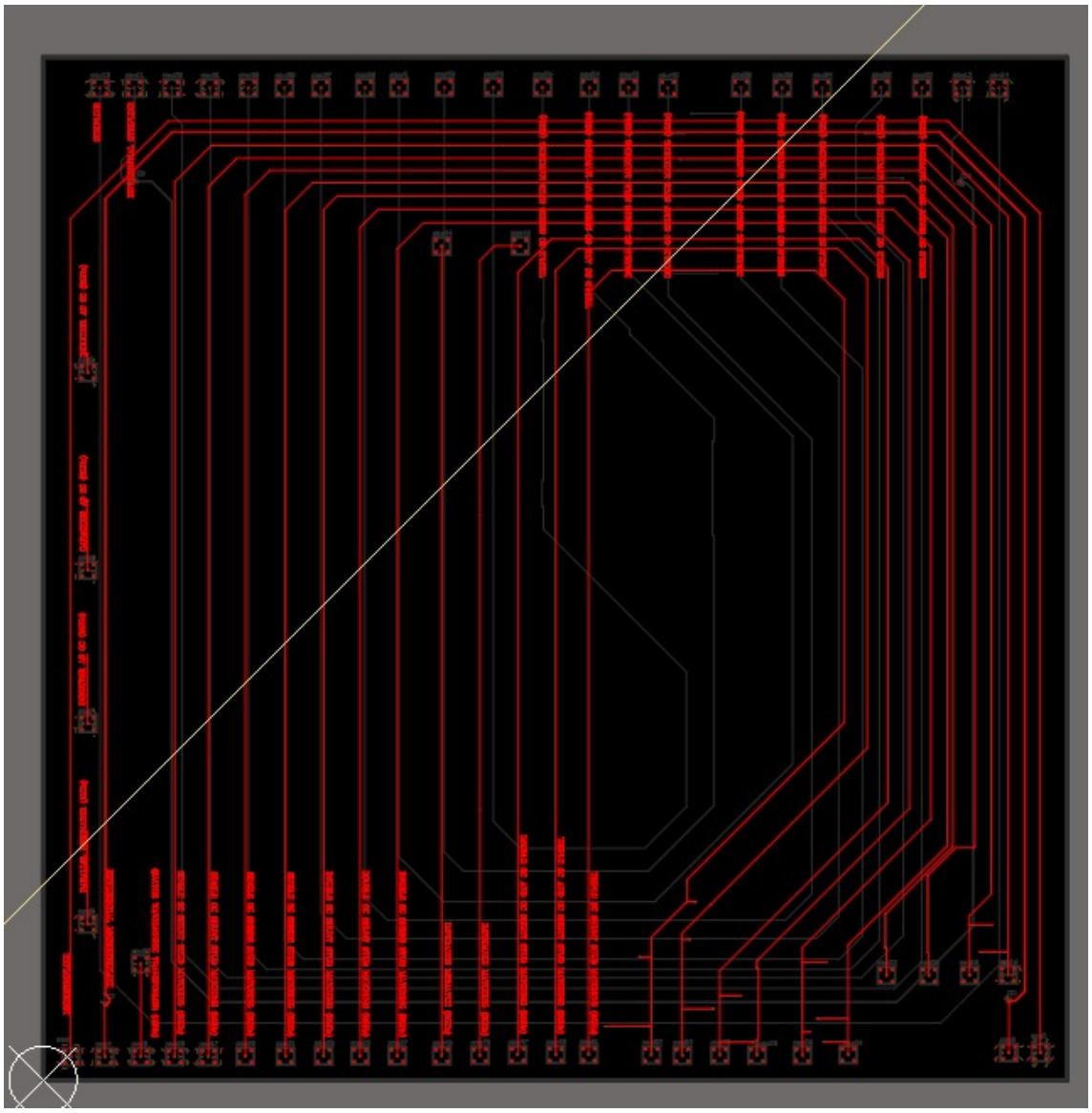

Figure 3.39: All Microstrip Connections

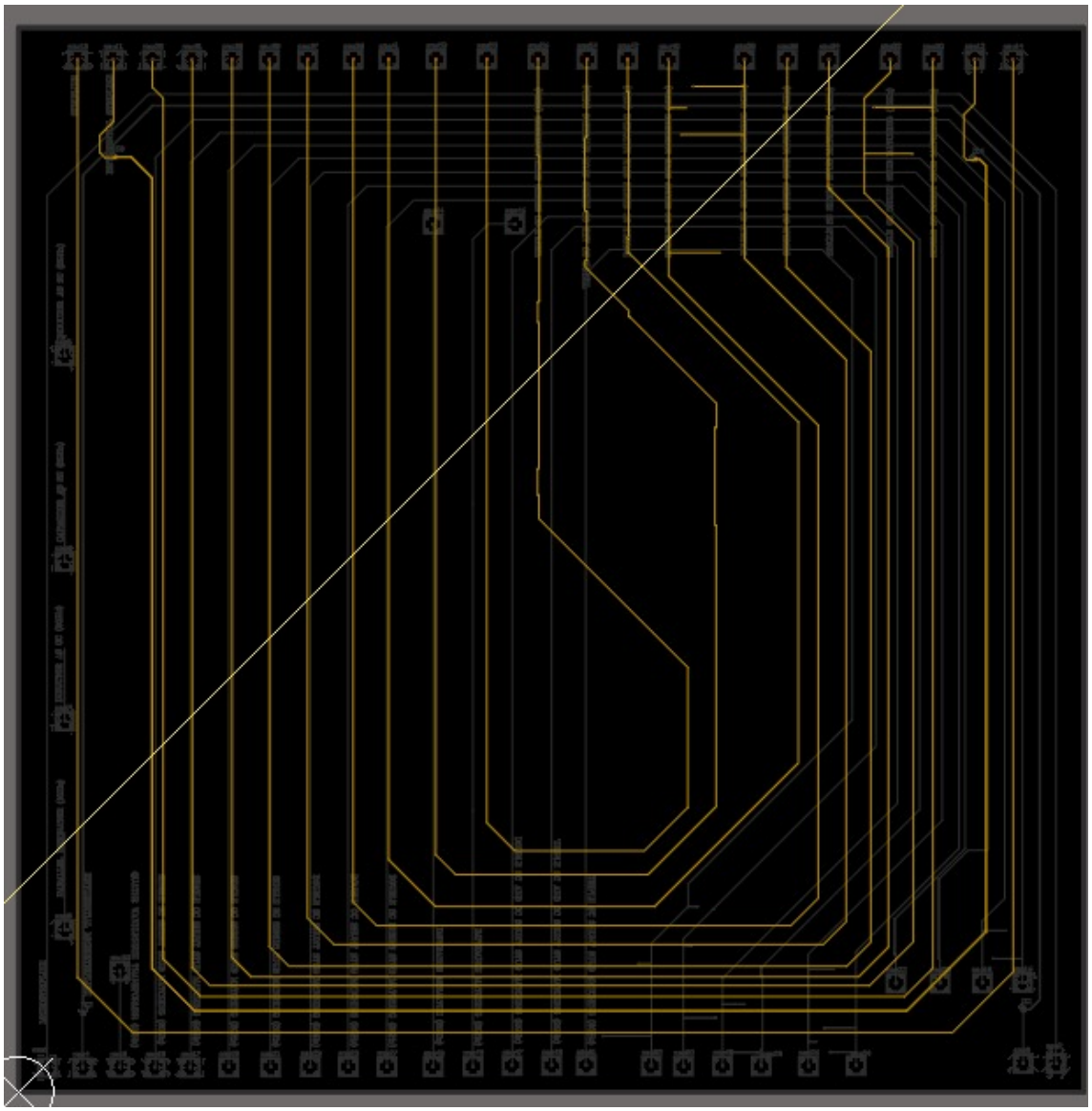

Figure 3.40: All Stripline Connections

(d) **Validate** and **Analyse** the complete **Printed Circuit Board Experiments**

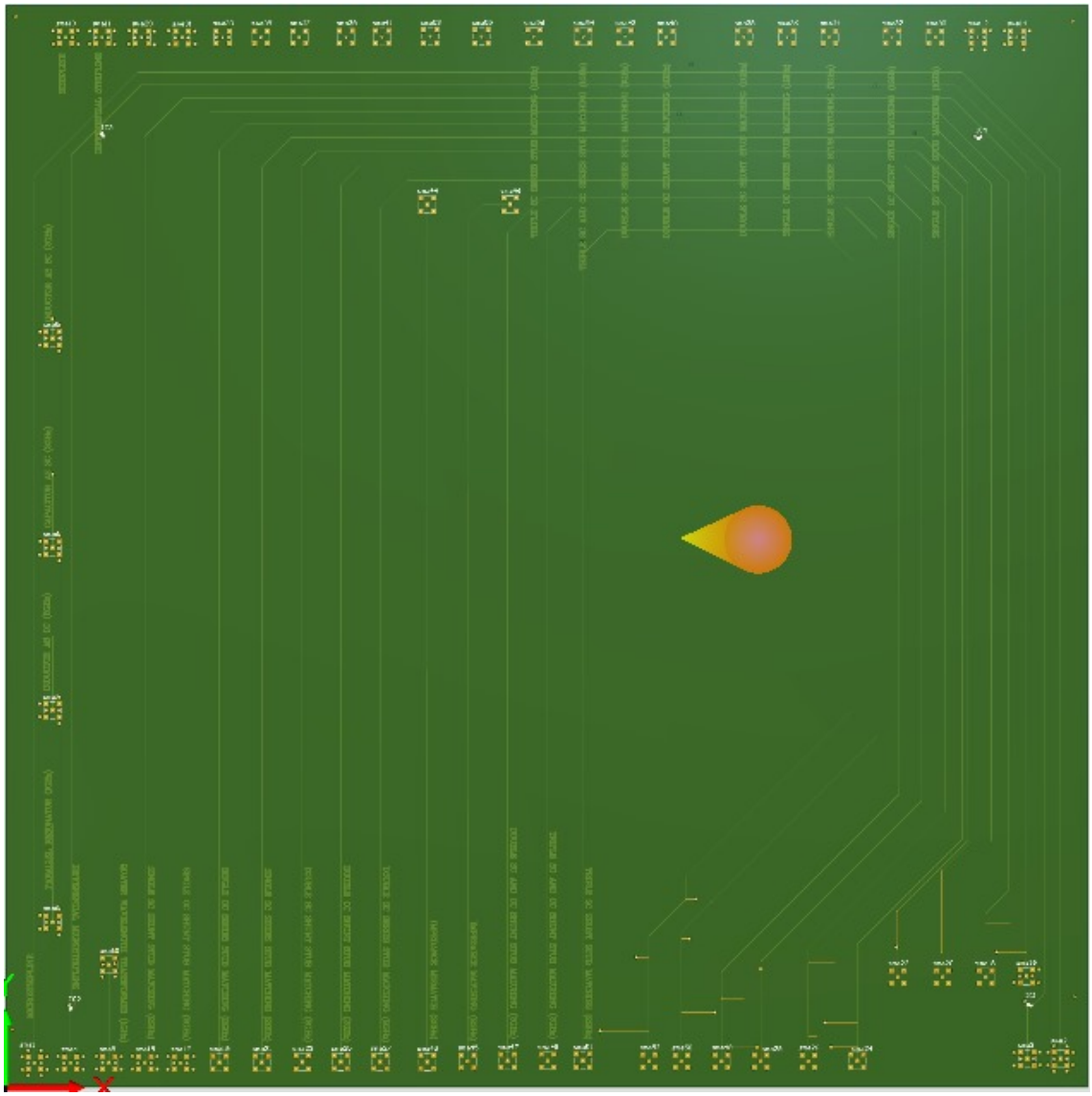

Figure 3.41: Final PCB

Chapter Four

Result and Discussion

4.1 Introduction to the Results

This study evaluates the performance of stripline, microstrip, differential microstrip, and differential stripline configurations on a six-layer printed circuit board, addressing transmission line challenges such as impedance matching, crosstalk, and reflections. A hybrid stack-up is employed, utilizing dielectrics e.g., FR4, to optimize signal integrity across frequencies ranging from below a few MHz to 2 GHz. The results, obtained through Ansys HFSS simulations and theoretical measurements, highlight key performance metrics, including reflection, crosstalk, and S-parameter (Return Loss). These findings provide a comprehensive evaluation of the design's effectiveness for high-speed printed circuit board applications.

4.2 Simulation Result

The electromagnetic (EM) simulation stage was conducted to analyze and validate the high-frequency behaviour of the designed transmission structures under realistic operating conditions. This phase replicated what would have been measured using a vector network analyzer by computing the Return loss, reflection analysis, and transmission responses of the PCB model across sub 2GHz frequency range.

These parameters evaluated reflect how efficiently signals propagate through some stub networks, and how well impedance matching was achieved across the operating frequency range of sub 2GHz.

1. **Reflection Coefficient or return loss** S_{11}

   The reflection coefficient, denoted as S_{11}, represents the ratio of the reflected signal power to the incident power at the input port. It quantifies how much

of the input signal is reflected due to impedance mismatch.

A lower S_{11} value (typically below –10 dB) indicates good impedance matching and minimal signal reflection at the input port. In this project, S_{11} was used to identify resonance frequencies and verify that each transmission line or stub network achieved proper matching conditions.

2. **Voltage Standing Wave Ratio (VSWR)**

   The VSWR expresses the degree of impedance mismatch between the source, transmission line, and load. It is derived from S_{11} and provides an alternative view of matching quality.

   A VSWR value close to 1:1 indicates a perfect match, while values below 2:1 are typically acceptable for most RF systems. Monitoring VSWR helped validate the impedance control achieved through trace geometry and substrate properties.

3. **Crosstalk (Near-End and Far-End)**

   Crosstalk measures the unwanted coupling of signals between adjacent transmission lines. In Altium Designer, this was evaluated by analyzing the voltage response on neighbouring nets when an aggressor line was excited.

   Low crosstalk values confirm proper line spacing and effective ground referencing. This metric was crucial for validating the isolation performance of closely spaced microstrip and differential pairs.

4.2.1 Performance Parameters

Below are the performance parameters for the for the proposed simulations in the table 4.1 below:

Table 4.1: Performance Parameters

parameters	**Single SC shunt stub**	**Double SC shunt stub**	**Triple SC shunt stub**	**Double OC shunt stub**
Physical width(W)	0.313564mm	0.313564mm	0.313564mm	0.261513mm
Physical Length(P)	84.1593mm	84.1593mm	84.1593mm	144.573mm
Effective width	0.279mm	0.279mm	0.279mm	0.179mm
Length of stub(l_s)	$l_{s1} = 12.79$mm	$l_{s1} = 11.193$mm $l_{s2} = 13.802$mm	$l_{s1} = 11.193$mm $l_{s2} = 13.802$mm $l_{s3} = 4.0396$mm	$l_{s1} = 6.5058$mm $l_{s2} = 19.372$mm
Physical Length before stub from load end(l)	$l_1 = 12.79$mm	$l_1 = 15.891$mm $l_2 = 10.5199$mm	$l_1 = 15.891$mm $l_2 = 10.5199$mm $l_2 = 31.5597$mm	$l_1 = 18.072$mm $l_2 = 51.215$mm
Characteristics impedance (z_0)	50Ω	50Ω	50Ω	50Ω
Load(z_L)	$(90 - j25)\Omega$	$(60 - j80)\Omega$	$(60 - j80)\Omega$	$0.3045 + j0.244$ (normalized)
Frequency (GHz)	2	2	2	1

4.3 Return Loss

1. **Return loss for the single sc shunt stub**

   The simulated return loss (S_{11}) characteristic of the single shunt short-circuit stub in the figure 4.1 is presented for the frequency range of 0.50 GHz to 2.50 GHz. From 0.50 GHz to 1.75 GHz, the return loss rises from approximately 0 dB to –20 dB, indicating reduced reflected power. At 2.00 GHz, return loss reaches a minimum of –42 dB, representing optimal matching. Beyond this point, return loss decreases to about –20 dB near 2.25 GHz and continues declining toward 2.50 GHz.

   The sharp dip in the S_{11} curve at 2 GHz indicates that the circuit resonates at this frequency. At resonance, the reactive components of the load and the stub effectively cancel each other, resulting in a purely resistive input impedance close to 50 Ω. This condition ensures maximum power transfer and minimal reflection, confirming that the stub length was accurately tuned for operation at 2 GHz.

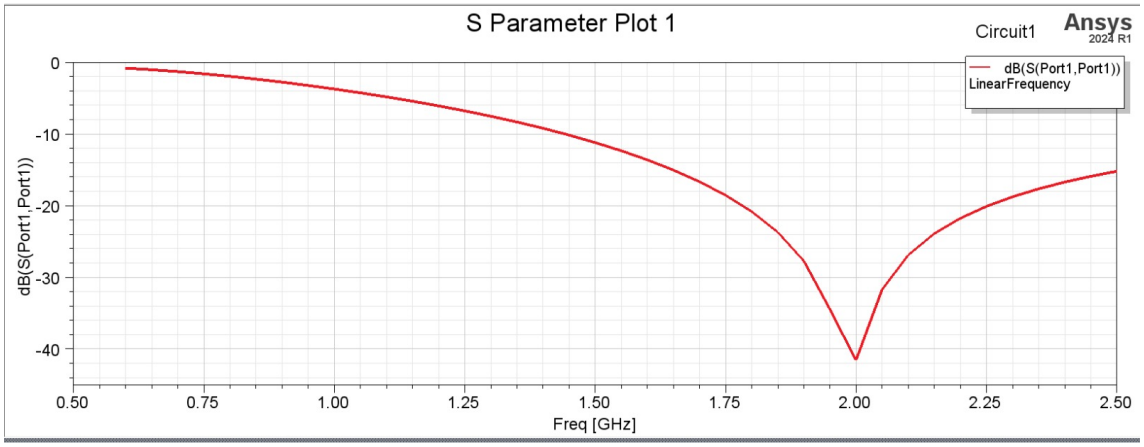

Figure 4.1: Simulated return loss (S_{11}) for single SC shunt stub matching

2. **Return loss for the double sc shunt stub**

   The simulated return loss (S_{11}) characteristic for the double shunt short-circuit stub network in figure 4.2 is presented for the frequency range of 0.50 GHz to 2.50 GHz. The response begins close to 0 dB at 0.50 GHz, indicating poor

impedance matching at lower frequencies. As the frequency increases, the return loss improves gradually, reaching approximately –10 dB near 1.75 GHz. A pronounced dip is then observed at 2.00 GHz, where the return loss attains a minimum value of approximately –34 dB, representing an excellent impedance match and minimal signal reflection. Beyond this frequency, the return loss rises again towards –10 dB between 2.25 GHz and 2.50 GHz, suggesting a gradual decline in matching performance as the circuit moves away from its optimal operating point.

The sharp dip in the S_{11} curve at 2 GHz indicates that the circuit resonates at this frequency. At resonance, the reactive components of the load and the stub effectively cancel each other, resulting in a purely resistive input impedance close to 50 Ω. This condition ensures maximum power transfer and minimal reflection, confirming that the stub length was accurately tuned for operation at 2 GHz.

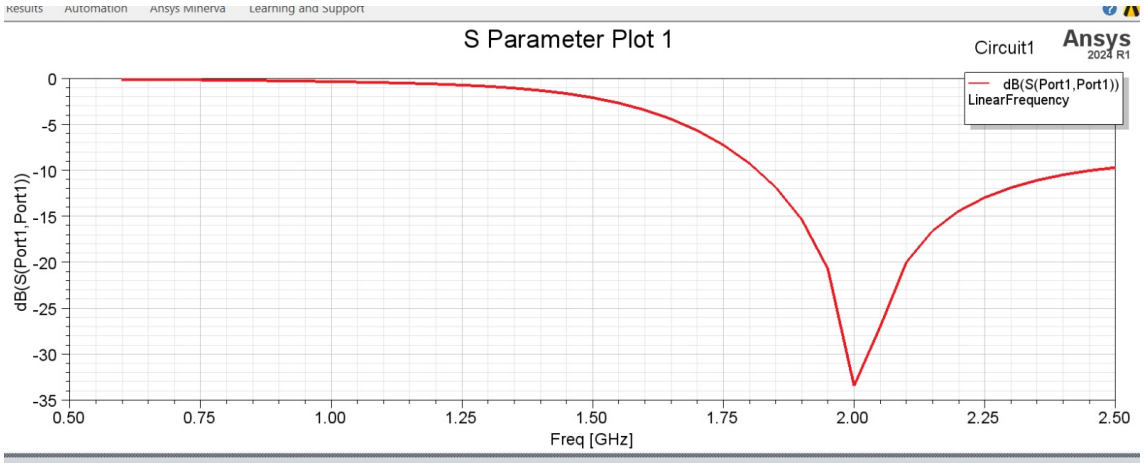

Figure 4.2: Simulated return loss (S_{11}) for double sc shunt stub matching

3. **Return loss for the triple sc shunt stub**

The simulated return loss (S_{11}) characteristic for the triple shunt short-circuit stub network in figure 4.3 is presented for the frequency range of 0.50 GHz to 2.50 GHz. The response remains close to 0 dB between 0.50 GHz and 1.50 GHz, indicating poor impedance matching and a high level of signal reflection within this lower frequency region. As the frequency increases, the return

loss improves significantly, reaching a distinct dip of approximately –23 dB at 2.00 GHz, which corresponds to a strong impedance match at the operating frequency. Beyond this point, the return loss gradually increases, reducing to less than –5 dB as the frequency extends from 2.25 GHz to 2.50 GHz, indicating a decline in matching performance at higher frequencies.

The sharp dip in the S_{11} curve at 2 GHz indicates that the circuit resonates at this frequency. At resonance, the reactive components of the load and the stub effectively cancel each other, resulting in a purely resistive input impedance close to 50 Ω. This condition ensures maximum power transfer and minimal reflection, confirming that the stub length was accurately tuned for operation at 2 GHz.

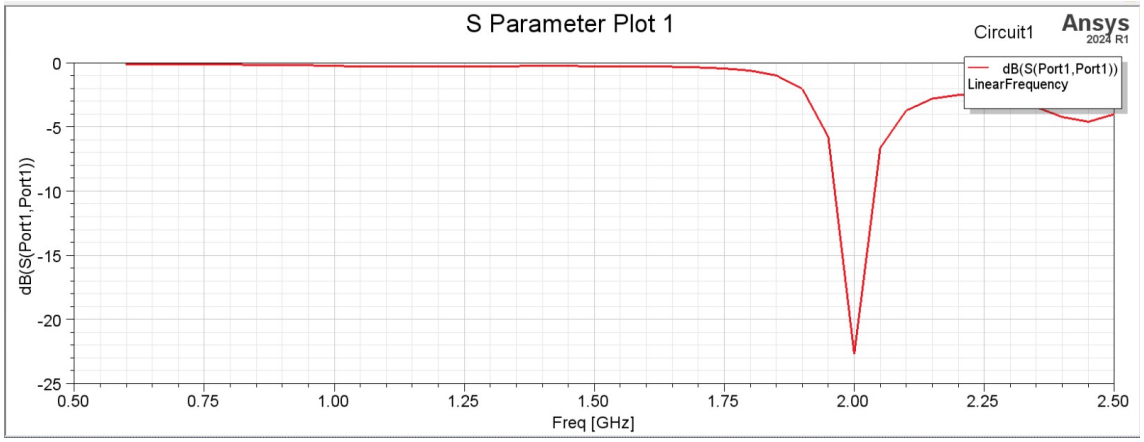

Figure 4.3: Simulated return loss (S_{11}) for triple sc shunt stub matching

4. **Return loss for the double oc shunt stub**

The simulated return loss (S_{11}) characteristic for the double shunt open-circuit stub network in figure 4.4 is presented for the frequency range of 0.60 GHz to 2.50 GHz. The response remains close to 0 dB between 0.50 GHz and 0.8 GHz, indicating poor impedance matching and a high level of signal reflection within this lower frequency region. As the frequency increases, the return loss improves significantly, reaching a distinct dip of approximately –17 dB at 1.00 GHz, which corresponds to a strong impedance match at the operating frequency and slightly above it. Beyond this point, the return loss gradually increases, reducing to less than –5 dB as the frequency extends from 1.15

GHz to 2.50 GHz, indicating a decline in matching performance at higher frequencies.

The sharp dip in the S_{11} curve at 1 GHz indicates that the circuit resonates at this frequency. At resonance, the reactive components of the load and the stub effectively cancel each other, resulting in a purely resistive input impedance close to 50 Ω. This condition ensures maximum power transfer and minimal reflection, confirming that the stub length was accurately tuned for operation at 1 GHz.

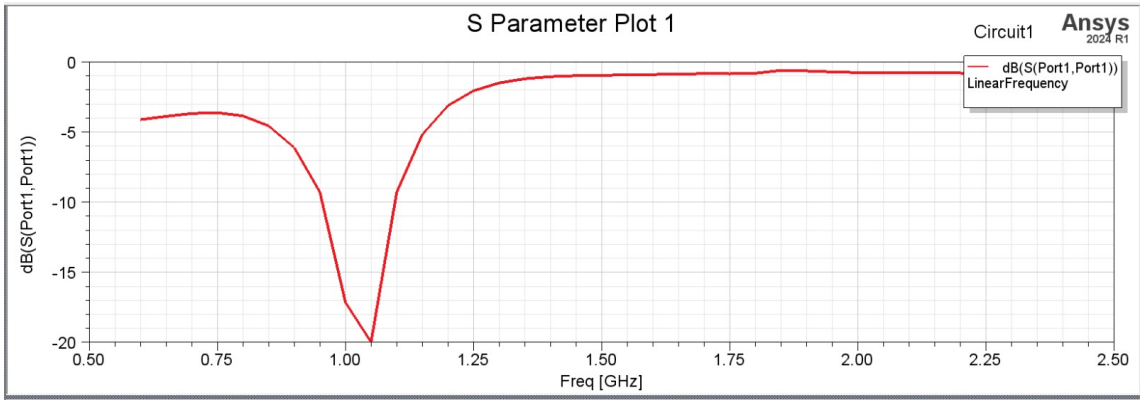

Figure 4.4: Simulated return loss (S_{11}) for double o.c. shunt stub matching

4.4 Voltage Standing Wave Ratio(VSWR)

The VSWR of Double OC shunt is shown in figure 4.8. At the resonant frequency of 1 GHz, the VSWR is approximately 1.32. For Double SC shunt in figure 4.6 at resonance frequency of 2 GHz, the VSWR is approximately 1.04. For Single SC shunt in figure 4.5 at resonance frequency of 2 GHz, the VSWR is approximately 1.02. For Triple SC shunt in figure 4.7 at resonance frequency of 2 GHz, the VSWR is approximately 1.15. All values of which indicates good impedance matching between the feed line and the antenna. This value satisfies the standard condition for efficient power transfer, where VSWR ≤ 2 but ≥ 1.

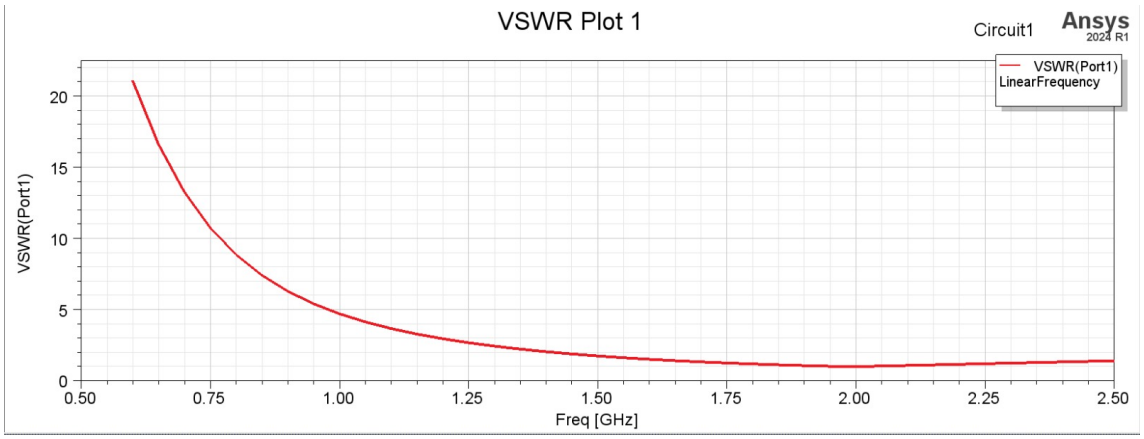

Figure 4.5: Simulated VSWR for Single s.c. shunt stub matching

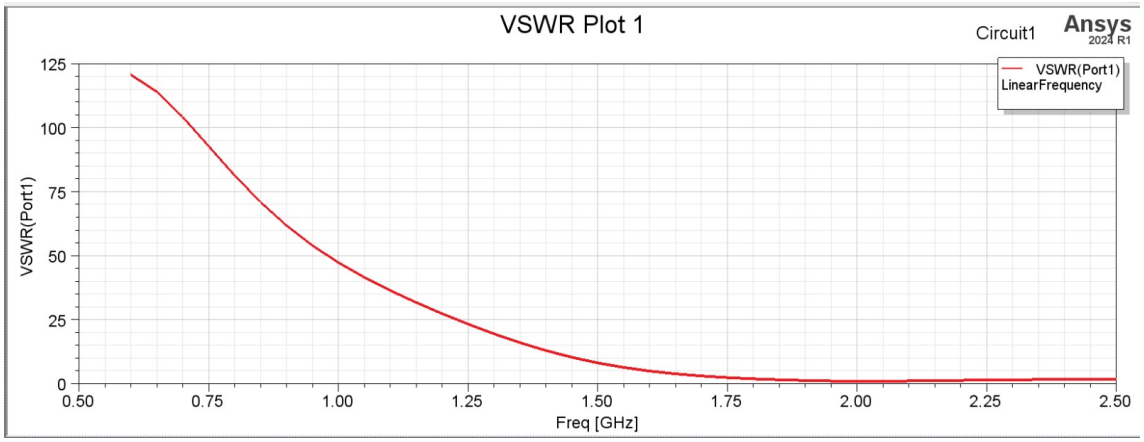

Figure 4.6: Simulated VSWR for double s.c. shunt stub matching

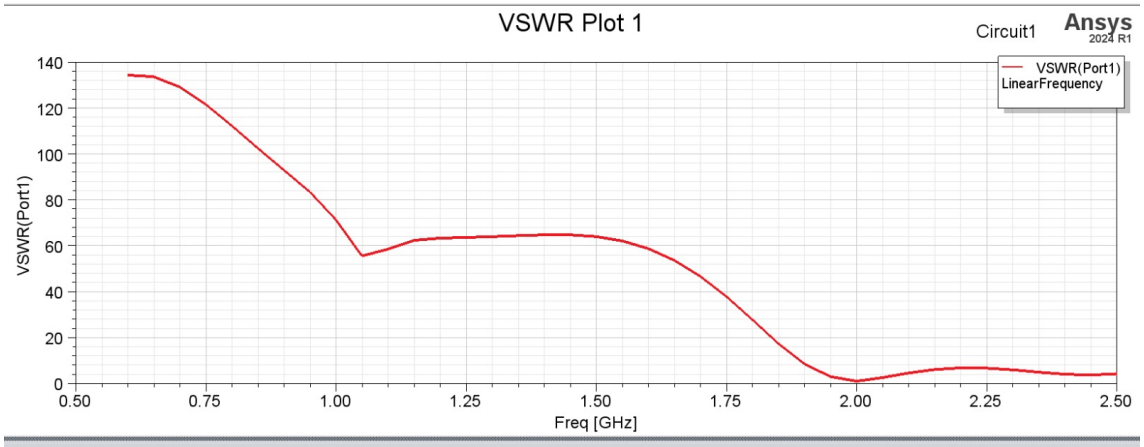

Figure 4.7: Simulated VSWR for triple s.c. shunt stub matching

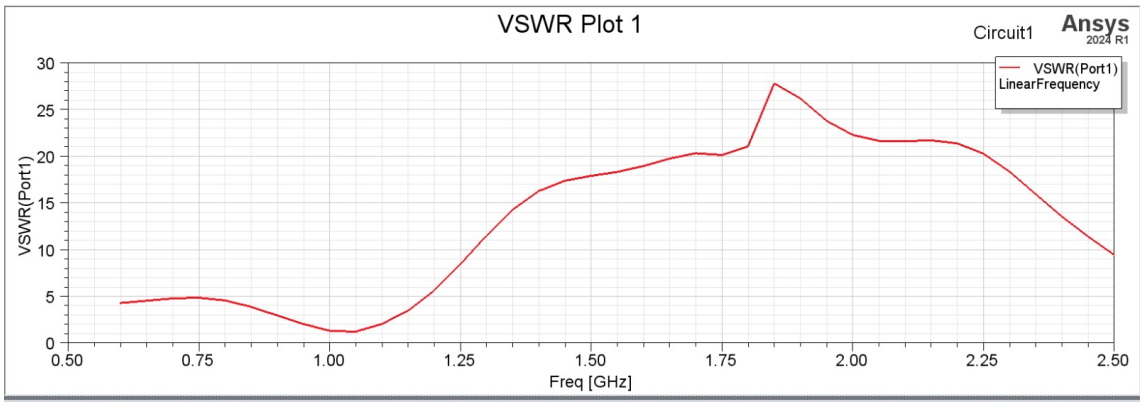

Figure 4.8: Simulated VSWR for double o.c. shunt stub matching

The table 4.3 below shows the key parameters of the simulations and the results that were obtained for each experiment:

Table 4.3: Key Parameters of simulation.

parameters	**Single SC shunt stub**	**Double SC shunt stub**	**Triple SC shunt stub**	**Double OC shunt stub**
Return loss S_{11}	-42dB	-34dB	-23dB	-17dB
VSWR	1.02	1.04	1.15	1.32

4.5 Crosstalk Simulation

The crosstalk behavior for the microstrip transmission lines under different termination conditions is shown in figures 4.9 and 4.10 For the unterminated microstrip line shown in figure 4.9, the induced voltage fluctuation due to crosstalk reaches a peak amplitude of approximately 400 mV, indicating significant signal coupling and reflection along the line. In contrast, the microstrip line with serial resistor termination shown in figure 4.10 exhibits a much lower crosstalk amplitude of about 340 mV, resulting in improved signal stability and reduced overshoot.

The reduction in peak voltage indicates that the series resistor termination (R = 46.67Ω) effectively minimizes reflections and electromagnetic coupling between adjacent traces. Overall, the terminated line demonstrates better signal integrity

and lower crosstalk, satisfying standard design conditions for reliable high-speed interconnects where reflections and interference are required to remain minimal.

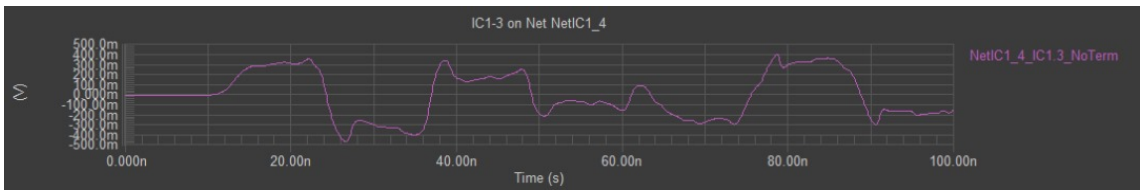

Figure 4.9: Simulated crosstalk for differential microstrip without termination

Figure 4.10: Simulated crosstalk for differential microstrip with serial resistor (46.67Ω) termination

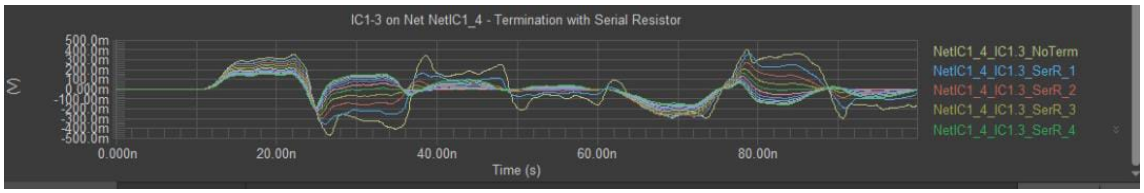

Figure 4.11: Simulated crosstalk for differential microstrip with different serial resistors termination

4.6 Discussion

The simulation results exhibit strong concordance with transmission-line theory. Both microstrip and stripline configurations achieved near-ideal impedance characteristics. This outcome confirms that precise geometrical design and accurate dielectric modeling in Ansys HFSS (High Frequency Structure Simulator) enable the realization of efficient sub-2 GHz structures on FR4 substrates. The stub networks

effectively demonstrated practical impedance matching techniques. The Microstrip differential simulations confirmed that precise conductor spacing and symmetry are essential for achieving high common-mode rejection and stable impedance balance. These findings collectively validate the design principles applied in the HF-TESt project and demonstrate that reliable high-frequency PCB interconnects can be achieved through simulation-driven optimization.

Chapter Five

Conclusion And Recommendations

5.1 Summary of the Work

This study focused on the design and electromagnetic simulation of high-frequency transmission lines using a 6-layer FR4 PCB substrate, aiming to achieve impedance controlled performance for sub-2 GHz applications. The research examined multiple transmission line structures: microstrip, stripline, differential microstrip, and differential stripline alongside stub based impedance matching networks to improve signal transmission and minimize reflections.

The design process was executed using Altium Designer, where the PCB stackup, transmission line geometries, and stub matching networks were developed based on Smith Chart principles. Controlled impedance routing was achieved through careful definition of trace widths, spacing, and dielectric layer thickness.

The completed PCB geometries were then exported into Ansys HFSS for full wave electromagnetic simulation. The tool provided S-parameter analysis, field distribution visualization, and impedance characterization, enabling a clear understanding of how line geometry, dielectric loss, and conductor configuration affect signal integrity and matching.

Comparative simulation results showed that stripline structures offered better shielding and lower crosstalk due to their internal placement between ground planes, while microstrip lines exhibited easier routing and higher radiation losses. Differential pairs demonstrated excellent noise immunity but were sensitive to dielectric inhomogeneity and trace skew. Stub networks, particularly double and triple stub configurations, improved bandwidth and reflection performance compared to single stub designs.

Overall, the combination of Altium Designer for layout design and Ansys HFSS

for electromagnetic simulation provided a comprehensive workflow for analyzing transmission behavior, validating impedance matching, and optimizing line performance for sub-2 GHz systems.

5.2 Conclusion

The project successfully demonstrated that high-frequency transmission lines on a 6-layer FR4 substrate can be accurately designed and simulated to meet impedance and bandwidth requirements for sub-2 GHz applications without the need for physical fabrication. The integration of Altium Designer and Ansys HFSS enabled a seamless transition from circuit layout to electromagnetic verification, allowing precise control of design parameters and realistic prediction of signal performance.

Key conclusions include:

- FR4, despite its dielectric losses at higher frequencies, remains a viable low-cost substrate for sub-2 GHz applications when proper impedance control and stub tuning are implemented.
- Stripline configurations offer superior shielding and impedance uniformity, while microstrip structures provide design simplicity and flexibility.
- Differential transmission lines enhance noise rejection but require tight symmetry and consistent dielectric properties.
- Stub-based impedance matching (especially multi stub networks) effectively minimizes reflection and broadens bandwidth for transmission line applications.
- The methodology provides a reliable digital prototyping framework for RF PCB design, bridging the gap between conceptual transmission line theory and practical implementation.

5.3 Contribution of the Study

This study provides a structured design and simulation methodology for microstrip, stripline, and differential transmission lines on a six-layer FR4 PCB, serving as a

practical reference for sub-2 GHz applications.

By analyzing signal propagation and impedance characteristics across multiple layers, the study contributes valuable insights into how dielectric thickness, copper geometry, and layer arrangement influence performance in complex PCB stack-ups.

The work applies single, double, and triple stub matching techniques to demonstrate how impedance mismatch and reflection can be minimized effectively in both microstrip and stripline structures, reinforcing fundamental transmission line theory with simulation results.

Using Altium Designer's high-frequency analysis tools, the study validates theoretical concepts through visual and quantitative simulation results, eliminating the need for physical fabrication while maintaining accuracy in signal behavior prediction.

The project bridges theoretical electromagnetic principles with practical PCB implementation, offering an educationally relevant resource for students and engineers working on high-frequency signal design, routing, and optimization.

Although fabrication was not part of this phase, the simulation based results provide a solid foundation for future prototype development, measurement, and verification using instruments such as a Vector Network Analyzer (VNA).

5.4 Limitations

Although the design and simulations were performed using professional tools (Altium Designer and Ansys HFSS), no physical fabrication or experimental measurements were conducted to validate the simulated results. Real world factors such as manufacturing tolerances, soldering effects, and connector transitions may introduce discrepancies when implemented practically.

The project employs FR4 substrate, which, despite being cost effective and widely available, exhibits higher dielectric loss and frequency dependent permittivity beyond 2 GHz. These characteristics limit its use for very high-frequency or low-loss applications.

The study focuses on frequencies below 2 GHz, which are adequate for RF communication and control systems, but do not capture ultra high frequency (UHF) or

microwave behaviors that may arise in advanced designs.

The electromagnetic simulations assume ideal boundary conditions and perfect conductor and dielectric models, without considering environmental influences such as temperature variation, mechanical stress, or humidity, which can impact performance in real-world applications.

While HFSS provides accurate frequency domain (S-parameter) analysis, the study does not include time domain reflectometry (TDR) or mixed signal simulations, which are valuable for verifying transient effects and signal integrity in high speed differential lines.

5.5 Recommendations For Future Work

For future research and implementation, the following are recommended:

- Fabricate and experimentally validate the simulated designs using a Vector Network Analyzer (VNA) and Time Domain Reflectometry (TDR) to confirm S-parameter and impedance data.
- Explore higher frequency ranges (>2 GHz) using low loss materials, such as Rogers or Taconic, to compare dielectric performance with FR4.
- Incorporate via transition modeling and connector effects to assess discontinuity losses in multilayer transitions.
- Investigate differential skew compensation techniques and crosstalk mitigation for high density routing in advanced multilayer PCBs.
- Extend the study to filter design and antenna feed networks, using the same modeling principles for more complex RF structures.

5.6 Closing Remark

This project has demonstrated that through proper design methodology and electromagnetic simulation, high frequency transmission lines can be effectively analyzed without physical fabrication. The integration of Altium Designer for precise PCB

layout and Ansys HFSS for field based simulation establishes a reliable workflow for predicting real world signal behavior on multilayer FR4 substrates.

The work bridges the gap between theoretical transmission line concepts and practical RF design, equipping future engineers with tools and insight for efficient sub-2 GHz PCB system development. Though limited to simulation, the study lays a strong foundation for future fabrication, testing, and optimization. The use of high performance RF interconnects in communication and embedded systems.

References

[1] J.L.Knighten, S. Connor, A. Orlandi, and J. Drewniak, "Design methodology for PDN synthesis on multilayer PCBs," 2008 International Symposium on Electromagnetic Compatibility – EMC Europe, Hamburg, Germany, 2008, pp. 1–6.ResearchGate

[2] S. Z. Ali, K. Ahsan, D. ul Khairi, W. Alhalabi M. S. Anwar, "Advancements in FR4 dielectric analysis: Free space approach and measurement validation," PLOS ONE, vol. 19, no. 9, e0305614, Sep 12 2024.https://journals.plos.org/plosone/article?id=10.1371/journal.pone.0305614

[3] Arar, Dr. Steve (2023), "Exploring Single Stub Impedance Matching Through Smith Chart Examples," All About Circuits Technical Article. May 5 2023.https://www.allaboutcircuits.com/technical-articles/learn-about-single-stub-impedance-matching-through-examples/

[4] S. Babic C. Akyel, "An improved analytical method for triple stub matching (Stubs in Parallel)," Global Journal of Engineering and Technology Advances, vol. 7, no. 3, pp. 157–178, June 2021.https://doi.org/10.5281/zenodo.5052386

[5] I. J. Bahl, Lumped Elements for RF and Microwave Circuits. Norwood, MA, USA: Artech House, 2003, pp. 15–20.

[6] T. Becherrawy, Electromagnetism: Maxwell Equations, Wave Propagation and Emission. London, UK: ISTE Ltd., 2013, pp. 112–118.https://www.wiley.com/en-us/Electromagnetism%3A+Maxwell+Equations%2C+Wave+Propagation+and+Emission-p-9781848213555

[7] B. Bhat and S. K. Koul, Stripline-like Transmission Lines for Microwave Integrated Circuits, New Age International, 1989. ISBN 978-81-224-0052-6.https://books.google.co.uk/books/about/Stripline_like_Transmission_Lines_for_Mi.html?id=EDVlt8hXpzAC

[8] I. J. Bahl and D. C. Trivedi, "Design of miniaturized patch antennas for wireless communications," in Handbook of Reflector Antennas and Feed Systems, Vol. 3: Applications of Reflectors, vol. 3, E. F. Knott, Ed. Norwood, MA, USA: Artech House, 2013, ch. 7, pp. 229–258.

[9] B. Bianco, L. Panini, M. Parodi, and S. Ridella, "Some considerations on the characteristic impedance of microstrip lines," IEEE Trans. Microw. Theory Tech., vol. MTT-26, no. 3, pp. 182–186, Mar. 1978.https://ieeexplore.ieee.org/document/1131352

[10] M. Boesch and M. Steffen, "Characterization of FR4-based high-frequency structures using VNA and TDR techniques," in Proc. IEEE Int. Symp. Electromagn. Compat. Signal/Power Integrity (EMCSI), Washington, DC, USA, 2020, pp. 145–150.

[11] E. Bogatin, Signal and Power Integrity - Simplified, 2nd ed. Upper Saddle River, NJ, USA: Prentice Hall, 2009, pp. 245–252.

[12] W. C. Bosshart, Printed Circuit Boards: Design and Technology. New Delhi, India: Tata McGraw-Hill, 1983, pp. 32–40.

[13] S. Bulja D. Mirshekar-Syahkal, “Novel wide-band transition between coplanar waveguide and microstrip line,” IEEE Transactions on Microwave Theory and Techniques, vol. 58, no. 7, pp. 1851-1857, July 2010.https://www.researchgate.net/publication/224142545_Novel_Wideband_Transition_Between_Coplanar_Waveguide_and_Microstrip_Line

[14] J. Carlsson, “Crosstalk on Printed Circuit Boards,” NASA STI/Recon Technical Report N, 1994.https://ntrs.nasa.gov/citations/19940020320

[15] R. H. Caverly, “Use of Low-Cost Vector Network Analyzers in Undergraduate RF and Wireless Circuit Laboratories,” ASEE Peer, 2021.

[16] L. B. Cebik W4RNL, “One Stub Matching: A Review,” antenneX, 2003.https://antenna2.github.io/cebik/content/trans/stub.pdf

[17] C. B. Poole and I. Darwazeh, "Practical transmission lines," in Microwave Active Circuit Analysis and Design, 1st ed. London, UK: Academic Press, 2016, pp.

89–119. doi: 10.1016/B978-0-12-407823-9.00003-2.https://doi.org/10.1016/B978-0-12-407823-9.00003-2

[18] R. E. Collin, Foundations for Microwave Engineering, 2nd ed. Hoboken, NJ, USA: Wiley-IEEE Press, 2001, pp. 1–10, 550–560.)https://www.wiley.com/en-us/Foundations+for+Microwave+Engineering%2C+2nd+Edition-p-9780780360310)

[19] C. F. Coombs, Printed Circuits Handbook, 6th ed. New York, NY, USA: McGraw-Hill, 2008, pp. 1.3–1.10, 5.1–5.20.

[20] F. R. Connor, Wave Transmission. London, UK: Edward Arnold, 1972, pp. 56–62.

[21] S. Connor, B. Archambeault, and M. Mondal, “The impact of common mode currents on signal integrity and EMI in high-speed differential data links,” 2008 IEEE International Symposium on Electromagnetic Compatibility, Detroit, MI, USA, pp. 1–5, 2008.ResearchGate

[22] H. Cory, "Dispersion characteristics of microstrip lines," IEEE Trans. Microw. Theory Tech., vol. MTT-29, no. 1, pp. 59–62, Jan. 1981.url-https://ieeexplore.ieee.org/document/1130278

[23] E. J. Denlinger, "A frequency dependent solution for microstrip transmission lines," IEEE Trans. Microw. Theory Tech., vol. MTT-19, no. 1, pp. 30–39, Jan. 1971.

[24] X. Duan, B. Archambeault, H.-D. Bruens and C. Schuster, “EM emission of differential signals across connected printed circuit boards in the GHz range,” in Proc. 2009 IEEE International Symposium on Electromagnetic Compatibility (EMC), Austin, TX, USA, 2009, pp. 50-55.https://ieeexplore.ieee.org/document/5284616

[25] T. C. Edwards and M. B. Steer, Foundations of Interconnect and Microstrip Design. Chichester, UK: Wiley, 2000, pp. 145–152.

[26] E. Y. Terán-Bahena, S. C. Sejas-García R. Torres-Torres, “Characterization of transmission lines on PCB from S-parameters by determining the dielectric

and conductor losses at the crossover frequency," IEEE Transactions on Components, Packaging and Manufacturing Technology, pp. 1-8, April 2018.https://www.researchgate.net/publication/324766584_Characterization_of_Transmission_Lines_on_PCB_from_S-Parameters_by_Determining_the_Dielectric_and_Conductor_Losses_at_the_Crossover_Frequency

[27] Famoriji, O. J., Shongwe, T. (2022). Transmission line characterization and modeling for electronic circuits and systems design. Indonesian Journal of Electrical Engineering and Computer Science, 30(2), 730–738.https://ijeecs.iaescore.com/index.php/IJEECS/article/view/30771/0

[28] F. De Flaviis, Fundamentals of RF and Microwave Circuit Design. Upper Saddle River, NJ, USA: Prentice Hall, 2004, pp. 89–95.

[29] Y. Gao X. Zhang, "Crosstalk suppression based on mode mismatch between spoof surface plasmon polaritons and conventional transmission lines," Scientific Reports, vol. 7, no. 1, p. 12931, 2017.https://www.semanticscholar.org/paper/Crosstalk-Suppression-Based-on-Mode-Mismatch-Spoof-Gao-Zhang/f2523da7564a998db29e33b9f6d73b97815be23c

[30] A. Gateece, "Transmission line modeling using telegrapher's equations," in Proc. IEEE Int. Conf. Electromagn. Adv. Appl. (ICEAA), Lisbon, Portugal, 2018, pp. 456–460.

[31] Grieg, D. D., Engelmann, H. F. (1952). Microstrip — A new transmission technique for the kilomegacycle range. Proceedings of the IRE, 40(12), 1644–1650.

[32] K. C. Gupta, R. Garg, I. Bahl, and P. Bhartia, Microstrip Lines and Slotlines, 2nd ed. Norwood, MA, USA: Artech House, 1996, pp. 75–82.

[33] W. H. Hayt, Jr., Engineering Electromagnetics, 5th ed. New York, NY, USA: McGraw-Hill, 1989, pp. 392–400.

[34] O. Heaviside, Electrical Papers, Volume 1. London, UK: Macmillan and Co., 1887.https://archive.

org/details/electricalpapers01heavuoft(Publicdomain, accessibleviaInternetArchive)

[35] I. C. Hunter, Theory and Design of Microwave Filters. London, UK: Institution of Electrical Engineers, 2001, pp. 300–320.https://digital-library.theiet.org/content/books/ew/pbew048e

[36] H. A. Hussein, Y. S. Mezaal B. M. Alameri, “Miniaturized Microstrip Diplexer Based on FR4 Substrate for Wireless Communications,” Elektronika Ir Elektrotechnika, vol. 27, no. 5, pp. 34-40, 2021.https://doi.org/10.5755/j02.eie.28942

[37] P. Jarry and J. Beneat, Design and Realizations of Miniaturized Fractal Microwave and RF Filters, John Wiley Sons, 2009. ISBN 978-0-470-48781-5.https://books.google.com/books/about/Design_and_Realizations_of_Miniaturized_Fractal.html?id=RaR9lzeRocIC

[38] H. Johnson and M. Graham, High-Speed Signal Propagation: Advanced Black Magic. Upper Saddle River, NJ, USA: Prentice Hall, 2003, pp. 112–120.

[39] J. Varteresian, "Placement and routing considerations for various circuit designs," in Fabricating Printed Circuit Boards, J. Varteresian, Ed. Burlington, MA, USA: Newnes, 2002, pp. 35–56.https://www.sciencedirect.com/science/article/pii/B9781878707505500046

[40] S. Lai, J. Qiao, N. Rasool, K. Li, H. Zhu, and Y. Yang, “A dynamic impedance matching algorithm of three-stub tuners based on equivalent circuit analysis,” Journal of Microwave Power and Electromagnetic Energy, vol. 54, no. 3, pp. 330–347, 2020.https://www.tandfonline.com/doi/full/10.1080/08327823.2020.1838051

[41] Ladou, J. (2006). Printed circuit board industry. International Journal of Hygiene and Environmental Health, 209(3), 211–219.https://doi.org/10.1016/j.ijheh.2006.02.001

[42] T. H. Lee, The Design of CMOS Radio-Frequency Integrated Circuits, 2nd ed. Cambridge, UK: Cambridge Univ.

Press, 2004, pp. 67–72.https://www.cambridge.org/us/academic/subjects/engineering/rf-and-microwave-engineering/design-cmos-radio-frequency-integrated-circuits-2nd-edition

[43] R. Liu, S. Lai, T. Hong, Z. Zhang, L. Dong, H. Zhu Y. Yang, "A low-reflection tuning strategy for three-stub waveguides," Electronics, vol. 13, no. 7, art. 1304, 2024.https://www.mdpi.com/2079-9292/13/7/1304

[44] S. A. Maas, Nonlinear Microwave and RF Circuits, 2nd ed. Norwood, MA, USA: Artech House, 2014, pp. 23–28.

[45] G. Miano and A. Maffucci, Transmission Lines and Lumped Circuits: Fundamentals and Applications. San Diego, CA, USA: Academic Press, 2001, pp. 45–52.https://www.elsevier.com/books/transmission-lines-and-lumped-circuits/miano/978-0-12-189710-9

[46] M. Mondal, B. Mutnury, P. Patel, S. Connor, B. Archambeault and M. Cases, "Electrical Analysis of Multi-board PCB Systems with Differential Signaling Considering Non-ideal Common Ground Connection," Proc. IEEE Electrical Performance of Electronic Packaging (EPEP), Atlanta, GA, USA, 2007, pp. 37-40.https://www.researchgate.net/publication/4293172_Electrical_Analysis_of_Multi-board_PCB_Systems_with_Differential_Signaling_Considering_Non-ideal_Common_Ground_Connection

[47] S. Monk, Electronics Cookbook: Practical Electronic Recipes with Arduino and Raspberry Pi. Sebastopol, CA, USA: O'Reilly Media, 2017, pp. 45–50.https://www.oreilly.com/library/view/electronics-cookbook/9781491953396/

[48] M. I. Montrose, EMC and the Printed Circuit Board: Design, Theory, and Layout Made Simple. New York, NY, USA: IEEE Press, 2000, pp. 123–130.https://ieeexplore.ieee.org/book/5264125

[49] M. Nawazi, Fundamentals of PCB Design and Layout. Upper Saddle River, NJ, USA: Prentice Hall, 2002, pp. 67–72.

[50] A. A. Oliner, Historical Perspectives on Microwave Field Theory. New York, NY, USA: IEEE Press, 2006, pp. 45–50.

[51] B. Olney, "Differential signaling in PCB design for high-speed applications," EDN Mag., vol. 50, no. 12, pp. 45–52, Jun. 2005.

[52] J. Papapolymerou, K. L. Lange, C. L. Goldsmith, A. Malczewski J. Kleber, "Reconfigurable double-stub tuners using MEMS switches for intelligent RF front-ends," IEEE Trans. Microw. Theory Tech., vol. 51, no. 1, pp. 271-278, Jan. 2003.

[53] R. Paschotta, Encyclopedia of Laser Physics and Technology. Weinheim, Germany: Wiley-VCH, 2011, pp. 1–2. [Online].https://www.rp-photonics.com/propagation_constant.html

[54] S. Prasanna, Advanced PCB Design and Manufacturing: Techniques for High-Density and Dynamic Applications. Norwood, MA, USA: Artech House, 2021, pp. 123–135.

[55] G. E. Ponchak and L. P. B. Katehi, "Open- and short-circuit terminated series stubs in finite-width coplanar waveguide on silicon," IEEE Trans. Microwave Theory Tech., vol. 45, no. 6, pp. 970-976, June 1997.

[56] Pozar, D. M. (2012). Microwave Engineering (4th ed.). Hoboken, NJ: John Wiley Sons. ISBN 978-0-470-63155-2.https://www.wiley.com/en-us/Microwave+Engineering%2C+4th+Edition-p-9780470631553

[57] A. Rahman, M. T. Nielsen A. H. Samuel, "Printed Circuit Board (PCB) Design and Electromagnetic Compatibility (EMC) Issues," Journal of Advanced Electronics and Systems, vol. 17, no. 2, pp. 102–110, May 2025.https://www.researchgate.net/publication/392200304_Printed_Circuit_Board_PCB_Design_and_Electromagnetic_Compatibility_EMC_Issues

[58] Rogers Corporation, High Frequency Circuit Materials: A Comparison of Performance and Cost for High-Speed PCB Design. Rogers Corporation Technical Bulletin, 2019.

[59] D. F. Santavicca and D. E. Prober, "Impedance-matched low-pass stripline filters," Measurement Science and Technology, vol. 19, no. 8, arti-

cle 087001, Aug. 2008.https://proberlab.yale.edu/sites/default/files/mst_filterpaper_2008.pdf

[60] A. Sharma, PCB Design and Manufacturing: A Comprehensive Guide. New York, NY, USA: McGraw-Hill Education, 2013, pp. 78–82.

[61] S. Sim, Y. Lee, H.-L. Kang, K.-Y. Shin, S.-H. Lee J.-M. Kim, "Transmission line printed using silver nanoparticle ink on FR-4 and polyimide substrates," Micro and Nano Systems Letters, vol. 4, Article no. 7, 2016.https://www.springeropen.com/articles/10.1186/s40486-016-0032-8

[62] Smith, P. H. (1969). Electronic Applications of the Smith Chart: In Waveguide, Circuit, and Component Analysis. New York: McGraw-Hill.Archive.orglisting

[63] M. B. Steer, Microwave and RF Design: Transmission Lines, 3rd ed. Raleigh, NC, USA: North Carolina State Univ. Press, 2019, pp. 89–96.

[64] H. Tu, H. Hong, Y. Y. Zhang, L. Zhou X. Li, "Influence of Dielectric Loss on RF Performance of Microstrip Multi-Resonant Circuits," Journal of Sensors, vol. 2022, Article ID 3866692, 9 pages, July 2022.https://www.hindawi.com/journals/js/2022/3866692/

[65] R. K. Ulrich and W. D. Brown, Eds., Advanced Electronic Packaging, 2nd ed. Hoboken, NJ, USA: Wiley-IEEE Press, 2008, pp. 45–60, 87–92.

[66] A. Vasjanov and V. Barzdenas, "Microstrip Impedance Management through Multilayer PCB Stack-Up Discontinuity Compensation with Asymmetric Dielectrics," Symmetry, vol. 13, no. 10, pp. 1771, Sept. 23, 2021.https://www.mdpi.com/2073-8994/13/10/1771

[67] B. C. Wadell, Transmission Line Design Handbook. Norwood, MA, USA: Artech House, 1991, pp. 102–110.

[68] C. H. Walter, Traveling Wave Antennas. New York, NY, USA: McGraw-Hill, 1990, pp. 22–28.

[69] Wu, J. J., Hou, D. J., Liu, K., Shen, L., Tsai, C. A., Wu, C. J., Tsai, D., Yang, T. J. (2014). Differential microstrip lines with reduced crosstalk and common mode effect based on spoof surface plasmon polaritons. Optics Express, 22(22), 26777–26787.https://doi.org/10.1364/OE.22.026777

[70] Xu, X., Gamez, J., Machado, P., Valdes-Garcia, J., Lucyszyn, S. (2014). Microstrip-to-stripline planar transitions on LTCC. International Journal of RF and Microwave Computer-Aided Engineering, 24(4), 447–455.https://doi.org/10.1002/mmce.20856

[71] C. Yeh and F. I. Shimabukuro, The Essence of Dielectric Waveguides. New York, NY, USA: Springer, 2008, pp. 237–245, 301–310.https://link.springer.com/book/10.1007/978-0-387-49799-0

[72] Seulgi Yu Dong-Gun Kam, "Improving Signal Integrity by Reducing Mode Conversion in Differential Pairs on a Meshed Ground in Flexible Printed Circuit Boards," Journal of Electromagnetic Engineering and Science, vol. 22, no. 3, pp. 229–235, May 2022.https://doi.org/10.26866/jees.2022.3.r.81

[73] J. Zhang, M. Y. Koledintseva, G. Antonini, J. L. Drewniak, A. Orlandi, and K. N. Rozanov, "Planar transmission line method for characterization of printed circuit board dielectrics," Progress In Electromagnetics Research, Vol. 102, pp. 267-286, 2010.https://www.jpier.org/PIER/pier.php?paper=10012807

[74] J. Zhang, A. C. Scogna, J. Fan, B. Archambeault, J. L. Drewniak A. Orlandi, "A Hybrid Stack-Up of Printed Circuit Board for High-Speed Networking Systems," Proceedings of the IEEE International Symposium on Electromagnetic Compatibility (EMC), Pittsburgh, PA, USA, Aug. 2012, pp. 554–559.https://scholarsmine.mst.edu/ele_comeng_facwork/2702/

[75] J.-F. Zürcher and F. E. Gardiol, Broadband Patch Antennas. Norwood, MA, USA: Artech House, 1995, pp. 25–30.https://www.artechhouse.com/Broadband-Patch-Antennas/PB9780890065136